Detection of grapevine viral diseases in Australian vineyards using remote sensing and hyperspectral technology

Yeniu (Mickey) Wang

BAgSc, MAgrSc

Thesis submitted for the degree of Doctor of Philosophy

School of Agriculture, Food and Wine

The University of Adelaide

Adelaide, Australia

October 2023

Panel of supervisors

Dr. Vinay Pagay

Senior Lecturer, School of Agriculture, Food and Wine

The University of Adelaide

Dr. Bertram Ostendorf

Associate Professor, School of Biological Sciences

The University of Adelaide

Table of Contents

Declaration

I certify that this work contains no material which has been accepted for the award of any other degree or diploma in my name, in any university or other tertiary institution and, to the best of my knowledge and belief, contains no material previously published or written by another person, except where due reference has been made in the text. In addition, I certify that no part of this work will, in the future, be used in a submission in my name, for any other degree or diploma in any university or other tertiary institution without the prior approval of the University of Adelaide and where applicable, any partner institution responsible for the joint-award of this degree.

I acknowledge that copyright of published works contained within this thesis resides with the copyright holder(s) of those works.

I also give permission for the digital version of my thesis to be made available on the web, via the University's digital research repository, the Library Search and also through web search engines, unless permission has been granted by the University to restrict access for a period of time.

I acknowledge the support I have received for my research through the provision of an Australian Government Research Training Program Scholarship.

26/06/2023

---------- ----------

Yeniu Wang Date

Acknowledgements

I would like to express my heartfelt gratitude to my principal supervisor, Dr. Vinay Pagay, and my co-supervisor, Dr. Bertram Ostendorf, for their exceptional mentorship and patient guidance throughout my PhD journey. I consider myself incredibly fortunate to have been offered this incredible opportunity by Vinay, and I am grateful to both supervisors for providing me with a conducive research environment and the freedom to pursue independent study. Over the course of these four years, my PhD study has been a truly rewarding experience, allowing me to develop extensive knowledge and valuable skills that will benefit me in my future career.

I extend my sincere thanks to all those who have assisted me during my PhD study. I am grateful to Dr. Nuredin Habili for generously sharing his knowledge and experience in plant virology, which greatly contributed to the success of my research. I appreciate the technical support provided by Steven Andriolo from the Unmanned Research Aircraft Facility in troubleshooting drone technology. Special thanks go to Dr. Deepak Gautam for his guidance in spectral calibration and GIS software. I am also grateful to Miaochun Yang, a master's student, for assisting me with fieldwork and sample processing in the laboratory. I would like to acknowledge the valuable support and tutoring in molecular biology lab skills provided by Dr. Dilrukshi Nagahatennafor providing guidance with tissue testing for viruses and general lab assistance.

I express my gratitude to the industry collaborators K1 Wines, Kies Family Wines, and CCW Co-operative Limited. Additionally, I am thankful to all the vineyard owners and managers, including Geoff Hardy, Bronson Kies, Matt, and Omer Najar, for their kindness and willingness to facilitate my research on their properties.

I would like to acknowledge the funding bodies that have supported my research: the South Australian Vine Improvement Association, the Riverland Wine Industry Development Council, and Wine Australia. Furthermore, I am grateful for the support from The University of Adelaide.

Last but certainly not least, I want to express my special thanks to my supportive family: my parents, in-laws, and most importantly, my loving wife, Monica. I consider myself

incredibly fortunate to have such a wonderful wife who not only provided financial support for our family but also took on the major responsibility of caring for our two sons (3 and 6 years old) during my PhD study period. Without the unwavering support from my incredible wife, I would not have been able to accomplish my PhD.

List of Abbreviations

3D	3-dimensional
ACCA	Ant colony clustering algorithm
AR	Augmented reality
BOM	Bureau of Meteorology
cDNA	Complementary Deoxyribonucleic acid
Chl-Fl	Chlorophyll fluorescence
CNN	Convolutional neural networks
CV	Computer vision
CV	Cross validation
DA	Discriminant analysis
DEM	Digital elevation model
DN	Digital number
DNA	Deoxyribonucleic acid
DSM	Digital surface model
ELISA	Enzyme-linked immunosorbent assay
FCM	Flow cytometry
FISH	Fluorescence in situ hybridisation
FN	False negatives
FOV	Field of view
FP	False positives
GAN	Generative adversarial nets
GCP	Ground control point
GDD	Growing degree days
GLD	Grapevine Leafroll Disease
GLRaVs	Grapevine leafroll-associated viruses
GPS	Global positioning system
GSD	Ground sample distance
GVA	Grapevine virus A
GVCV	Grapevine vein clearing virus
IF	Immunofluorescence
IMU	Inertial measurement unit
IPM	Integrated pest management
IR	Infrared
KNN	k-nearest neighbours
LAMP	Loop-mediated isothermal amplification
LDA	Linear discriminant analysis
LFD	Lateral flow device
LIDAR	Light detection and ranging
LV	Latent variable
LWI	Long-wave infrared
MCC	Matthews correlation coefficient
MJT	Mean January temperature
MLC	Maximum likelihood classifier

NB	Naive Bayes
NDVI	Normalized difference vegetation index
NIR	Near-infrared
NMR	Nuclear magnetic resonance
OCT	Optical coherence tomography
PCA	Principal component analysis
PCR	Polymerase chain reaction
PLA	Projected leaf area
PLS	Partial least squares
PLS-DA	Partial least squares-discriminant analysis
Q-DA	Quadratic discriminant analysis
qPCR	Quantitative polymerase chain reaction
RF	Random forest
RGB	Red green blue
RNA	Ribonucleic acid
ROC	Receiver operating characteristic
RT-PCR	Reverse transcription polymerase chain reaction
SA	South Australia
SAM	Spectral angle mapper
SD	Shiraz Disease
SNV	Standard normal variate
SVM	Support vector machines
SWIR	Short-wave infrared
TMV	Tobacco mosaic virus
TN	True negatives
TP	True positives
UAV	Unmanned aerial vehicle
UV	Ultraviolet
VIs	Vegetation indices
VNIR	Visible and near-infrared
VOC	Volatile organic compound

Thesis Summary

Grapevine viral diseases cause substantial productivity and economic losses in the Australian viticulture industry. Two economically significant grapevine viral diseases - Grapevine Leafroll Disease (GLD) and Shiraz Disease (SD) - affect numerous vineyards across major wine regions in Australia. Accurate and quick diagnosis of the virus infection would greatly assist disease management for growers. Current detection methods include visual assessment and laboratory-based tests that are expensive and labour-intensive. Low-cost and rapid alternative methods are desirable in the industry. Recent advances in low-altitude remote sensing platforms such as unmanned aerial vehicles (UAVs or “drones”) in conjunction with high-resolution multi- and hyper-spectral cameras now enable large spatial-scale surveillance of plant stresses. My thesis therefore focuses on developing fast and reliable methods for GLD and SD detection on a vineyard scale using optical sensors including RGB and hyperspectral and low-altitude remote sensing technology.

The thesis is constituted by a review article and three result parts, it begins with a general introduction for the background and is followed by the research goals and significance of the project that is described in **Chapter 1**. In order to be familiar with all possible technologies that can be potentially used for GLD and SD detection, **Chapter 2** includes a comprehensive overview of methodologies for the detection of any plant viruses reviewed from laboratory-based, destructive molecular and serological assays, to state-of-the-art non-destructive methods using optical sensors and machine vision, including use of hyperspectral cameras. A key contribution of the review is that, for the first time, a detailed economic analysis or cost comparison of the various detection methodologies for plant viruses is provided.

In my research, various detection methods with different degrees of complexity were attempted for GLD and SD detection. Firstly, a simple and novel detection method using the projected leaf area (PLA) calculated from UAV RGB images is proposed in **Chapter 3** for the disease symptom that alters the growth of the vine such as SD in Shiraz. The PLA is closely related to the canopy size. There are significant differences in PLA between healthy and SD-infected vines in spring due to retarded growth caused

by SD, which offers a simple, rapid and practical method to detect SD in Shiraz vineyards. However, for diseases that cannot be easily detected by RGB images such as GLD in the white grape cultivars, different approaches are needed.

Hyperspectral technology provides a wide spectrum of light with hundreds of narrow bands compared to RGB sensors. The advanced technology can detect imperceptible spectral changes from the disease and is particularly valuable for asymptomatic disease detection. A new approach using proximal hyperspectral sensing is described in **Chapter 4**. Using a handheld passive (sunlight is the radiation source) hyperspectral sensor to detect GLD in the vineyard presents a simple and rapid measurement method to detect the diseases using the spectral information from the canopy. An assessment was done for the disease's spectral reflectance throughout the grape growing season for both red and white cultivars. The partial least squares-discriminant analysis (PLS-DA) was used to build a classification model to predict the disease. Prediction accuracies of 96% and 76% were achieved for Pinot Noir and Chardonnay, respectively. The proximal hyperspectral sensing technique is readily applicable to a low-altitude remote sensing method to capture high-resolution hyperspectral images for large-scale viral disease surveillance in vineyards. The subsequent study in **Chapter 5** presents an advanced method to quickly detect disease using an UAV carried hyperspectral sensor. The study evaluated the feasibility of UAV-based hyperspectral sensing in the visible and near-infrared (VNIR) spectral bands to detect GLD and SD in four popular wine grapevine cultivars in Australian vineyards. The method combined the spectral and spatial analysis to classify disease for individual pixels from the hyperspectral image. The model predictions for red- and white-berried grapevine cultivars achieved accuracies of 98% and 75%, respectively. For each viral disease, unique spectral regions and optimal detection times during the growing season were identified. The spectral difference between virus-infected and healthy vines closely matched the spectral signal from the proximal sensing method in Chapter 4, which demonstrated the reliability of the low-altitude hyperspectral sensing for grapevine disease detection.

Lastly, a summary of the outcomes and remaining challenges and limitations of the existing technology is discussed in **Chapter 6**, followed by suggestions for further research for further improvement.

Chapter 1

Background and research goals

1.1. Background

Grapevine viral diseases contribute to significant productivity and economic losses to the viticulture and wine industry globally (Alabi et al. 2016; Meng et al. 2017). In Australian vineyards, Grapevine Leafroll Disease (GLD) and Shiraz Disease (SD) are two major viral diseases that concern the industry (Wu et al. 2020).

GLD is widely spread globally and can affect both red and white grapevine cultivars (Chooi et al. 2022; Pietersen et al. 2013). Grapevine leafroll-associated viruses (GLRaVs) including GLRaV-1, -2, -3, GLRaV-4 and its strains and GLRaV-7 are associated with GLD (Habili et al. 2007; Naidu, R et al. 2014). GLD symptoms include rolling leaf edges in red and white cultivars, as well as reddening leaves with green veins in red cultivars during the later stages of growth (Naidu, R et al. 2014). GLD infections can cause significant yield losses of around 30% - 50% and result in a 10% penalty due to poor fruit quality (Atallah et al. 2012). If left uncontrolled, GLD can lead to long-term economic losses (Walker et al. 2004). In Australian vineyards, GLRaV-1, -3, and -4 strains have been more frequently detected than other GLRaV strains (Constable et al. 2014).

SD is another destructive viral disease, initially discovered in South Africa, but later identified in Australian vineyards. (Goszczynski et al. 2012; Habili et al. 2016). SD can delay bud bursts and restrict spring growth, disturb the lignification on canes, and delay senescence in winter, consequently, significantly affecting vine health and reducing the yield (Goszczynski 2007; Habili 2013). However, SD symptoms only appear in a few sensitive cultivars including some popular cultivars like Shiraz and Merlot (Goszczynski et al. 2008). Grapevine virus A (GVA) is associated with SD (Habili et al. 2016; Wu et al. 2020), particularly the GVA Group II variants (Goszczynski et al. 2012; Goszczynski et al. 2003). Co-infection of GVA and GLRaVs is commonly found in grapevines (Blaisdell et al. 2020; Credi 1997; Digiaro et al. 1994; Hommay 2008; Wu et al. 2023).

The transmission of grapevine viruses within and between vineyards is facilitated by insects such as scales and mealybugs, which act as vectors for the viruses (Douglas et al. 2008; Fortusini et al. 1997). These insects can spread the viruses locally within the vineyard by feeding on infected plants and then moving to healthy plants. In addition to insect transmission, the propagation of grapevines plays a significant role in the rapid and widespread spread of viruses (Maree et al. 2013; Wu et al. 2020). If the source materials used for propagation are already infected with a virus, the resulting cuttings or plant material will also be contaminated with the virus. This contaminated material can then be transported over long distances to new regions, introducing the virus to previously uninfected areas. Preventing the introduction and spread of viruses in the nursery industry is a high priority. Nurseries invest significant amounts of money to test the virus status of their plant material.

While nearly all fungal diseases of the grapevine can be managed by spraying organic or synthetic chemicals, viral diseases currently have no effective methods for treating

the vine (Hull 2014). Currently, grapevine viral disease management strategies are preventative, including the control of the vectors such as the insects, rouging (removing) the infected vines, and planting with virus-free materials (Almeida et al. 2013; Ricketts et al. 2015). Although no methods of treatment are currently available for virus infections, early and full-scale disease detection in whole vineyards will allow grape growers to rogue infected vines and replant with virus-free certified planting material, to minimise disease spread within the vineyard. This roguing and replanting strategy has been successfully used in several countries including South Africa and New Zealand to manage the symptomatic disease such as GLRaV-3 infection in red cultivars (Bell et al. 2017).

The most commonly used methods for detecting plant viruses are reverse transcription polymerase chain reaction (RT-PCR) and enzyme-linked immunosorbent assay (ELISA) (Olmos et al. 2007; Sankaran et al. 2010). However, these laboratory-based techniques can be prohibitively expensive, making it impractical to test every single vine in a vineyard. Alternatively, visual assessment by trained individuals based on disease symptoms can be employed for large-scale virus detection. Unfortunately, virus infections do not always manifest visible symptoms, such as in the case of GVA infection in white grape cultivars or early-stage GLRaVs infections. This poses a challenge for visual-based methods.

Advanced optical sensing technologies, such as hyperspectral sensors, offer the capability to measure light beyond the range of human vision. Several previous studies have utilised these sensors for the detection of grapevine viruses in field conditions. For instance, hyperspectral approaches have been employed to detect Grapevine Leafroll Disease (GLD) in red cultivars (Naidu, RA et al. 2009). In a study conducted in California, a surveillance aircraft equipped with a hyperspectral camera

demonstrated a remarkable 94% accuracy in detecting GLRaV-3 in Cabernet Sauvignon (MacDonald et al. 2016). More recently, hyperspectral cameras mounted on grape harvest machines were employed in Germany to detect GLD in both red and white cultivars, achieving notable results (Bendel et al. 2020). These studies demonstrate the feasibility of non-destructive disease detection in vineyards.

However, there is still untapped potential in fully exploring the innovative optical sensing technology for viral disease detection on a larger scale. Recent advancements in remote sensing platforms, such as unmanned aerial vehicles (UAVs or "drones"), coupled with high-resolution multi- and hyperspectral cameras, now allow for extensive surveillance of vineyards, enabling monitoring of both biotic and abiotic stresses in grapevines (Jones 2014; Vanegas et al. 2018). These airborne approaches enable the characterization of vineyards at a broader scale, going beyond individual vines. Moreover, by quantifying the temporal dynamics of the disease, it becomes possible to enhance disease management strategies (Nutter 1997). Leveraging fast and cost-effective detection methods, the temporal spread of diseases across vineyard blocks can be effectively monitored.

1.2. Research goals

My PhD study aimed to achieve rapid and non-destructive detection of GLD and SD in Australian vineyards through the utilisation of various optical sensing technologies and the development of simplified algorithms for hyperspectral datasets. Furthermore, the project aimed to predict the spatial distribution of disease spread within vineyards and enhance the sampling strategy to increase confidence in disease status

assessment and improve disease management practices. To address these objectives, the following specific goals were defined:

- Assessing the suitability of different optical sensing technologies for simple and reliable detection of various viral diseases in vineyards.
- Determining the optimal detection parameters for the sensors, including identifying the best development stage to detect the diseases, determining the optimal time of day for applying the technology, establishing the ideal distance and angle for canopy measurement, and optimizing camera settings.
- Investigating the spectral signals captured by both proximal and drone-mounted hyperspectral cameras to identify significant wavelengths in the visible-near-infrared (VNIR) range for disease identification.
- Analysing and comparing the spectral differences between different locations and seasons to understand the variations in disease signals.
- Developing an effective disease modelling methodology using statistical or machine learning approaches to predict disease presence and spread.
- Validating the prediction results obtained from the newly developed sensing methods by ELISA and RT-PCR tests.
- Generating disease prediction maps that accurately indicate the disease status at the individual vine level.

By pursuing these goals, the study aimed to contribute to the advancement of disease detection and prediction methods, providing valuable insights for the effective management of grapevine viral diseases in Australian vineyards.

1.3. Significance of the project

The rapid and non-destructive detection of virus-infected grapevines through my PhD research will provide grape growers with a cost-effective tool to ensure the productivity and quality of their vineyards. By surveying large vineyards, even with minor virus symptoms, growers can benefit in several ways:

1. Adjusting management practices: The utilisation of predicted disease maps allows growers to modify their management practices and minimise the negative impact on vine stress and grape maturation. This proactive approach is instrumental in maintaining vineyard health and optimizing crop quality.
2. Roguing infected vines: By accurately identifying and removing infected vines, growers can effectively minimise the risk of disease transmission through potential vectors. This proactive step helps prevent the further spread of viruses within the vineyards.
3. Supporting grapevine propagators: This research enables grapevine propagators, including nurseries and vine improvement groups, to conduct cost-effective and efficient surveys of entire source blocks. This comprehensive approach offers additional information on a large spatial scale, thereby ensuring the production of virus-free planting materials.
4. Informing top-working decisions: Prior to grafting or top-working vineyard blocks, knowing the virus infection status is crucial. My research provides growers with a valuable tool for assessing established vineyard blocks, empowering them to make informed decisions, e.g., graft sensitive cultivars like Shiraz to an asymptomatic infection such as GVA-infected white cultivar.

Moreover, the temporal change over time could allow for to prediction of the future spatial patterns of virus spreading in vineyards empowering growers to develop effective risk management plans. By understanding the movement of spreading viruses and controlling known vectors, growers can mitigate the spread of diseases and enhance their financial management.

Overall, this project aims to improve viticultural management strategies for grapevine viral diseases in Australia, offering growers valuable tools for early detection, prevention, and risk management, ultimately enhancing the sustainability and success of the wine industry.

Chapter 2

Plant Viral Disease Detection: From Molecular Diagnosis to Optical Sensing Technology—A Multidisciplinary Review

Wang, Y.M.; Ostendorf, B.; Gautam, D.; Habili, N.; Pagay, V.

Preamble:

This chapter provides an overview of the methodology employed for the detection of plant viral diseases. Encompassing direct and indirect methods, as well as traditional and state-of-the-art non-destructive techniques, this comprehensive review serves as a foundation to inspire subsequent studies conducted during my Ph.D. The inclusion of a financial (cost) comparison between these methods also offers valuable insights for industry professionals, enabling them to evaluate and select the most suitable approach for virus detection. This review article is published in the open journal - *Remote Sensing, MDPI, 2022, 14(7), 1542.*

doi.org/10.3390/rs14071542

Statement of Authorship

Title of Paper	Plant viral disease detection: From molecular diagnosis to optical sensing technology—A multidisciplinary review
Publication Status	☑ Published ☐ Accepted for Publication ☐ Submitted for Publication ☐ Unpublished and Unsubmitted w ork w ritten in manuscript style
Publication Details	Remote Sensing. 2022, 14, 1542. https://doi.org/ 10.3390/rs14071542

Principal Author

Name of Principal Author (Candidate)	Yeniu (Mickey) Wang		
Contribution to the Paper	Conceptualisation Writing – original draft and revision Figures design		
Overall percentage (%)	80%		
Certification:	This paper reports on original research I conducted during the period of my Higher Degree by Research candidature and is not subject to any obligations or contractual agreements with a third party that would constrain its inclusion in this thesis. I am the primary author of this paper.		
Signature		Date	13/06/2023

Co-Author Contributions

By signing the Statement of Authorship, each author certifies that:

i. the candidate's stated contribution to the publication is accurate (as detailed above);

ii. permission is granted for the candidate in include the publication in the thesis; and

iii. the sum of all co-author contributions is equal to 100% less the candidate's stated contribution.

Name of Co-Author	Deepak Gautam		
Contribution to the Paper	Reviewing and editing		
Signature		Date	14/06/2023

Name of Co-Author	Nuredin Habili		
Contribution to the Paper	Reviewing and editing		
Signature		Date	14/06/2023

Name of Co-Author	Bertram Ostendorf		
Contribution to the Paper	Reviewing and editing		
Signature		Date	20/06/2023

Name of Co-Author	Vinay Pagay		
Contribution to the Paper	Reviewing and editing Corresponding author		
Signature		Date	27/06/2023

remote sensing

MDPI

Review

Plant Viral Disease Detection: From Molecular Diagnosis to Optical Sensing Technology—A Multidisciplinary Review

Yeniu Mickey Wang [1], Bertram Ostendorf [2], Deepak Gautam [3], Nuredin Habili [4] and Vinay Pagay [1,*]

[1] School of Agriculture, Food & Wine, Waite Research Institute, University of Adelaide, PMB 1, Glen Osmond, Adelaide, SA 5064, Australia; yeniu.wang@adelaide.edu.au
[2] School of Biological Sciences, The University of Adelaide, Molecular Life Sciences Building, North Terrace Campus, Adelaide, SA 5005, Australia; bertram.ostendorf@adelaide.edu.au
[3] Research Institute for the Environment and Livelihoods, Charles Darwin University, Casuarina, NT 0810, Australia; deepak.gautam@cdu.edu.au
[4] The Australian Wine Research Institute, Glen Osmond, Adelaide, SA 5064, Australia; nuredin.habili@awri.com.au
* Correspondence: vinay.pagay@adelaide.edu.au; Tel.: +61-8-8313-0773

Abstract: Plant viral diseases result in productivity and economic losses to agriculture, necessitating accurate detection for effective control. Lab-based molecular testing is the gold standard for providing reliable and accurate diagnostics; however, these tests are expensive, time-consuming, and labour-intensive, especially at the field-scale with a large number of samples. Recent advances in optical remote sensing offer tremendous potential for non-destructive diagnostics of plant viral diseases at large spatial scales. This review provides an overview of traditional diagnostic methods followed by a comprehensive description of optical sensing technology, including camera systems, platforms, and spectral data analysis to detect plant viral diseases. The paper is organized along six multidisciplinary sections: (1) Impact of plant viral disease on plant physiology and consequent phenotypic changes, (2) direct diagnostic methods, (3) traditional indirect detection methods, (4) optical sensing technologies, (5) data processing techniques and modelling for disease detection, and (6) comparison of the costs. Finally, the current challenges and novel ideas of optical sensing for detecting plant viruses are discussed.

Keywords: plant viruses; remote sensing; hyperspectral imaging; disease prediction modelling; machine learning

Citation: Wang, Y.M.; Ostendorf, B.; Gautam, D.; Habili, N.; Pagay, V. Plant Viral Disease Detection: From Molecular Diagnosis to Optical Sensing Technology—A Multidisciplinary Review. *Remote Sens.* **2022**, *14*, 1542. https://doi.org/10.3390/rs14071542

Academic Editors: Giovanni Avola, Alessandro Matese and Jianxi Huang

Received: 18 February 2022
Accepted: 19 March 2022
Published: 23 March 2022

1. Introduction

Plant diseases have plagued agricultural production since antiquity. It is estimated that 20–40% of crop yield losses worldwide are caused by plant diseases, of which plant viruses are the second most significant contributor [1,2]. Viral diseases affect crop growth, reduce yield, influence the survival of scions, and impact fruit quality, consequently causing significant economic losses [3].

Major crop viral disease incidents and economic consequences have been reported worldwide [4–6]. In 1993–1994, tomato yellow leaf curl virus decreased tomato production by 75% and cost more than USD 10 million in the Dominican Republic [7]. Cotton leaf curl virus caused nearly 30% cotton yield loss worth USD 5 billion in Pakistan between 1992 and 1997 [8]. Rice tungro disease is a devastating viral disease that affects rice production in many countries in southeast Asia; a USD 1.5 billion annually economic loss was estimated due to this disease [5]. For woody perennial crops like fruit trees and grapevines, yield losses are not confined to one season, but multiple seasons. A 14-year field study in New Zealand found that apple tree yield and fruit size decreased gradually over this period due to apple mosaic virus infection, and up to two-thirds of yield loss was observed in the severely infected trees [9]. Atallah et al. [10] reported that Grapevine leafroll disease (GLD)

could have a negative long term economic impact if the viral infection is not managed. The same study estimated that losses of between USD 25,000 and USD 40,000 ha^{-1} could be incurred over 25 years in a vineyard in New York State (USA). In addition, indirect damages contributing to the economic loss include the cost of roguing vines, leaving the vineyard fallow for 3–5 years to remove vectors harbouring in the rhizosphere (e.g., nematodes), and the time between replanting to the recovery to full productivity also needs to be considered [11]. Plant viruses affect not only crop yield but also the quality of downstream products. A study showed that red wine colour intensity is reduced by GLD, which may lower the wine's price and the financial return to the winery [12]. In addition, numerous unreported and undiscovered plant viral infections make the true extent of yield loss difficult to ascertain. Viruses may cause far more significant economic losses than what is usually recognised.

Managing viral disease in the field can be challenging due to its insidious and persistent nature. Unlike other pathogens, plant viruses are incorporated in the plant genome and therefore cannot be eliminated using chemicals [13]. Infected plants are unlikely to be cured; hence they must be removed and destroyed to minimise further spreading. Viruses can be rapidly transmitted between plants in the field by vectors like insects and nematodes or spread through human activities. Insecticides have some degree of control for vectors to limit the spread of viruses; however, it is not a preferred solution due to the cost associated with ecosystem damage and concerns regarding human health risks and the possibility of vectors developing resistance [14,15]. Thus, most viral disease management strategies are preventative, including using certified virus-free planting materials, breaking down the disease cycle by removing infected plants, vector control, and breeding virus-resistant plants [14].

As part of an effective disease control strategy, detection and diagnosis perform vital roles. Traditionally, direct and indirect plant viral disease detection methods have been distinguished. Direct methods are lab-based testing methods that are either based on detecting DNA, RNA, or virus proteins. While these methods are reliable and accurate, they are expensive, time-consuming, and destructive, mandating alternative options [16–18]. Indirect methods, including visual assessment and biological indexing methods, have been used to overcome cost and logistic limitations. However, visual assessment by human eyes is unreliable due to the different levels of experience of the surveyors, whereas biological indexing using indicator plants for viral disease diagnosis is excessively time-consuming [19].

Recent advances in imaging and data processing technologies have accelerated the development of rapid virus detection methods based on remote and proximal optical sensors. It is thus timely and opportune to review recent developments. This paper reviews optical sensing methodologies, data processing, and disease classification modelling methods from a multidisciplinary perspective. A multidisciplinary approach has the advantage that it utilises a diverse array of tools ranging from traditional molecular biology approaches to state-of-the-art sensing and detection methods, providing analysis and insight that would not be possible with any of these tools individually. We believe that this approach has not been thoroughly reviewed in the literature on plant viruses.

We begin by giving a brief overview of how viruses affect plants and then discuss current direct diagnostic techniques and traditional indirect methods. We then describe optical sensing technology and disease prediction modelling methods for virus detection, followed by a comparison of the economics associated with using different sensing methods. We conclude with a discussion of the current challenges and outstanding opportunities for enhancing methods for plant viral disease detection.

2. Detection of Viruses

2.1. Background-Physiological and Phenotypic Changes of Plants Affected by Viruses

Unlike living organisms that possess a cellular structure, viruses only consist of a set of one or more nucleic acid template molecules (DNA or RNA) which are covered by a coat

protein [20]. They lack the protein-coding capacity of living cells and thus need to parasitise a host to utilise the host cells' transcription machinery to replicate [13]. Replication can occur in most cells—mesophyll, epidermis, parenchyma, phloem companion, and bundle sheath [21]. Infections result in various physiological and biochemical changes that can lead to disease. Viral disease has been observed to alter amino acids and phytohormone levels, cause cell structure distortion, degrade chloroplasts to lower leaf photosynthetic capacity, and decrease nutrient uptake to retard plant growth and development [22,23]. These physiological changes can be visualised and detected as disease symptoms. For example, Gutha et al. [24] showed that a typical symptom-reddish-purple colour in red grape cultivars was caused by grapevine leafroll associated virus 3 (GLRaV-3) mainly due to the accumulation of anthocyanin in grape leaves. They also found that chlorophyll and carotenoid content were 20% less in the infected leaves than in the healthy plants, which may enhance the symptoms. Other studies suggested that insect-borne plant viruses could modify the plant pigments level to attract the vectors to spread the viruses [25,26]. Moreover, other phytochemicals that can be influenced by plant viruses include carbohydrates, polyphenols, and oxidative enzymes such as peroxidase, catalase, ascorbate peroxidase, and superoxide dismutase [27]. These chemicals can be indirectly and non-destructively estimated by eyes or optical sensors as an indication of virus infection (Figure 1).

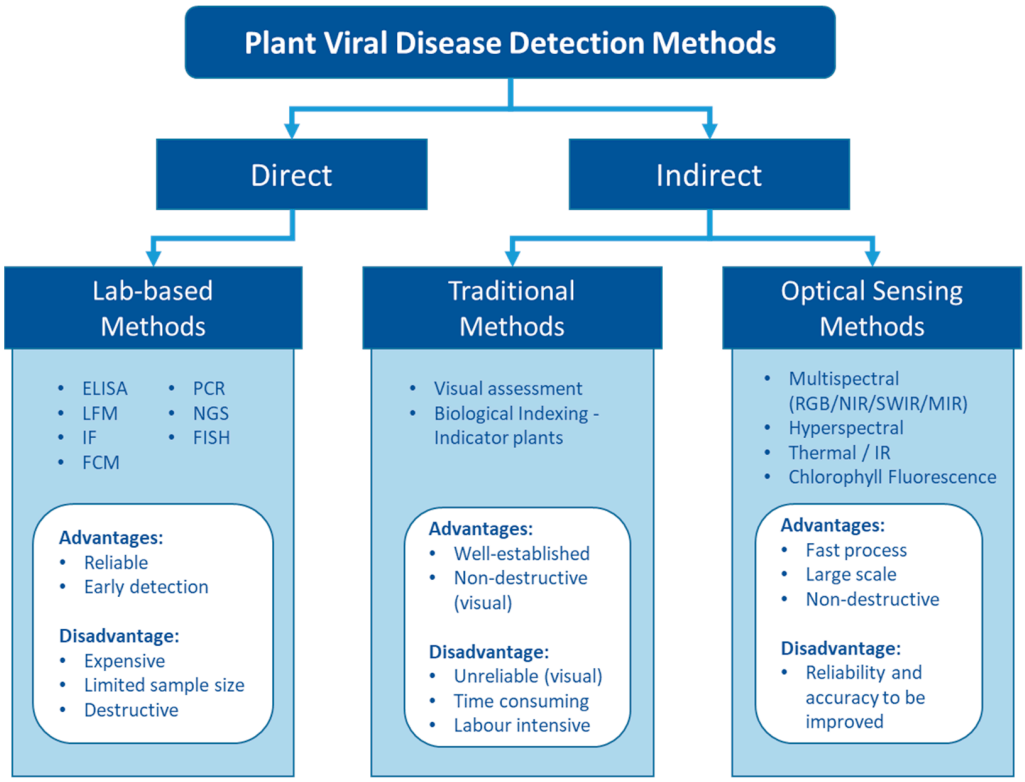

Figure 1. The pros and cons of different types of detection methods for plant viruses.

Fundamentally, plant viruses can be either directly detected by finding their genomic sequence and viral protein or indirectly assessed via the plant phenotypic response to the virus (Figure 1). Numerous plant virus detection methods have been developed to date. The rapid development of molecular and biochemical technologies has ushered in a new era of virus detection over the last few decades. Today, various lab-based diagnosis methods are available for plant virus detection [16,18,28,29]. These methods are generally sensitive and reliable and have been widely used for plant virus diagnostics.

Indirect methods that assess the plant response include traditional methods to detect virus symptoms visually in the field and novel approaches to assess the altered phenotype

using optical sensors. The key advantages of these three major detection methods are related to reliability and the ability to provide efficient sampling (Figure 1).

2.2. Direct Methods

There are two major direct diagnostic methods: serological and nucleic acid. Serological methods developed in the mid-1960s use antibodies produced from an animal's immune system to detect plant viruses [30,31]. The enzyme-labelled antibodies that bind to specific viral proteins (antigens) are readily observable and measurable through spectrophotometry [30,32]. In 1977, using the 'double-antibody sandwich' (DAS) form of enzyme-linked immunosorbent assay (ELISA), Clark and Adams [33] demonstrated the efficiency of the DAS-ELISA method to quantify virus concentration in plants. This method is economical and suitable for a quantity of testing compared to many other lab-based methods and continues to be widely used for plant viral disease detection. Another convenient serological diagnostic tool is the lateral flow device (LFD). It uses the virus antibodies attached to nitrocellulose membrane strip with coloured nanoparticles to produce results [34–36]; it has been used as a rapid, in-field detection method for plant viruses. Immunofluorescence (IF) is a technique commonly used in microbiology. Using fluorescent dye-labelled antibodies to bind the antigens, IF allows for the visualisation of plant viruses via microscopy that provides valuable information on the intracellular distribution of viruses [37,38].

Nucleic acid-based methods have been used for plant virus detection since 1979 and directly target viral DNA or RNA fragments [39]. In 1985, the revolutionary nucleic acid-based polymerase chain reaction (PCR) method was developed by Saiki et al. [40], which significantly improved plant virus diagnosis. After multiple amplification cycles in two hours, PCR can duplicate a single DNA strand up to 10^9-fold, which dramatically increases the sensitivity and effectiveness of the virus detection [41]. Based on PCR, many modifications and improvements were subsequently developed and extensively used in plant virus detection, including reverse transcription PCR (RT-PCR), quantitative PCR (qPCR), and loop-mediated isothermal amplification (LAMP). As most plant viruses are RNA viruses, and RNA degrades rapidly under ambient conditions, it is common to reverse-transcribe unstable RNA to more stable complementary DNA (cDNA), which are then amplified using PCR [42]. Today, RT-PCR is the most used method for plant virus diagnosis due to its capability to detect viruses at low concentrations or titer levels [43,44]. Several studies have shown that RT-PCR is more sensitive than ELISA for plant virus detection, with fewer false-negative results [44–50]. The qPCR, also referred to as real-time PCR, can quantify the virus titre level in the samples by measuring the DNA concentration after each amplification step during the PCR process [51,52]. The loop-mediated isothermal amplification (LAMP) technique is a promising method developed in 2000 by Notomi et al. [53]. Comparing conventional PCR, LAMP does not require a high precision thermocycler to amplify DNA. It is simpler, faster, lower-cost, and has increased popularity in plant virus detection.

Other nucleic acid-based methods have recently been developed to study and detect plant viruses. Next-generation sequencing (NGS), also known as high-throughput sequencing, is a powerful technology that can rapidly sequence the entire viral genome [28,54,55]. NGS provides a comprehensive methodology for detecting and studying plant viruses and has been instrumental in discovering previously unknown viruses and hosts for known viruses [56–58]. Fluorescence in situ hybridisation (FISH) uses fluorescent-labelled probes to detect the target virus nucleic acid [59]. FISH can detect and localise the viruses in plants and vectors tissues, which provides a better understanding of virus epidemiology within plant tissues, therefore potentially implicated for disease management [60,61]. Flow cytometry (FCM) can detect multiple plant viruses simultaneous in a sample [62]. It uses a laser beam to excite the fluorescence-labelled antibodies or nucleic acid probes in a fluid stream. By analysing the pass through fluorescence and scattered laser light, FCM can detect specific viruses and measure genome size and gene expression [63].

Lab-based methods remain the gold standard for the detection of plant viruses. They are highly sensitive, accurate, and reliable. They directly target the virus and do not require

a plant response, and thus, they can be used for early warning of the disease. However, these methods require special attention to plant tissue sampling and sample processing to avoid cross-contamination, which is labour intensive and time-consuming. Several detection methods also require sophisticated equipment and expensive materials [64]. In light of these costs, it is economically unviable for large numbers of plants, and hence, it cannot be used to obtain representative samples of viruses at the scale of large industrial production farms. Instead, a small proportion of plants are sampled randomly, standard field patterns like X or W patterns, or strategically according to visual assessment to represent the overall disease status in a field [65,66]. However, an insufficient test rate could cause hit-and-miss situations; this is especially unacceptable for critical industries such as nurseries.

2.3. Traditional Indirect Methods

Identifying disease symptoms by eye is the simplest indirect method to detect viruses. Due to physiological changes, viruses-infected plants can show typical symptoms such as mosaic patterns on the leaf, yellowing, leaf rolling, ring spots, necrotic tissues, wilting, and nodulating [13]. Accordingly, most names of plant viruses are related to the typical symptom(s) caused to their major host. Visually identifying these typical symptoms is a quick and simple disease detection method. However, the ease of utilising this approach comes with the drawback of low accuracy for reasons that include individual variability of the surveyors, different infection rates, the developmental stage of disease, and complexity of symptoms [67]. Similar symptoms can manifest from various biotic and abiotic stresses such as nutrient deficiency, fungal or bacterial diseases, environmental factors, or mechanical damage to the plants, further reducing the accuracy.

Virus infections do not always produce apparent visual symptoms in the host plants, making accurate disease detection challenging. Biological indexing was a method developed to address this challenge; it relies on specific indicator plants that have been selected to help identify the disease symptoms. The indicator plants are susceptible species or varieties that usually develop typical symptoms once inoculated with the pathogenic viruses [68]. Biological indexing is able to confirm the potential virus that does not produce symptoms in certain plants, discover an unusual host plant for the virus, and quantify the virus [68]. Biological indexing continues to be used as a complementary method to lab-based testing methods [69]. However, the major disadvantage of using indicator plants is the long duration from inoculation to the development of disease symptoms; this process could take several weeks to months [19]. In addition, symptoms of indicator plants may also vary based on environmental conditions. Constable et al. [70] found that rugose wood symptoms on Rupestris St George indicator plants could not be observed in a cold climate, but could be detected in a hot climate. In contrast, the GLD symptoms appeared in Cabernet Franc in a cool climate, but no symptom was found in the hot climate site for the same treatments, limiting the suitability of this variety as an indicator.

Nowadays, various studies use optical sensors instead of traditional detection methods. Such sensing technology has the advantage of detecting a broader range of spectrums than the human eye, and recently, it was mimicked using computer vision to detect disease in the human brain.

2.4. Optical Sensing Technologies in Plant Viral Disease Detection

Optical sensors measure the frequency and intensity of light, both of which can be interpreted as meaningful information using multivariate statistical techniques. The sensing process is similar to that of human vision, but it has the ability to detect wavelengths of light beyond the visible spectrum detectable by the human eye [71]. The different sensors can measure specific regions of the electromagnetic spectrum, from ultraviolet (UV) to long-wave infrared (LWI). Using optical sensing technologies, subtle phenotype changes caused by the disease are detectable. The sensing technology presents rapid and non-destructive alternatives to the molecular techniques of plant disease detection [17,18] and increases

the objectivity of field-based visual assessment. There is a wide variety of optical sensing methods that can be classified by their platforms and associated scale of imagery, as well as by their spectral characteristics [72–76]. Figure 2 illustrates various sensing technologies, their spectral ranges, and platforms that can be used for plant viral disease detection.

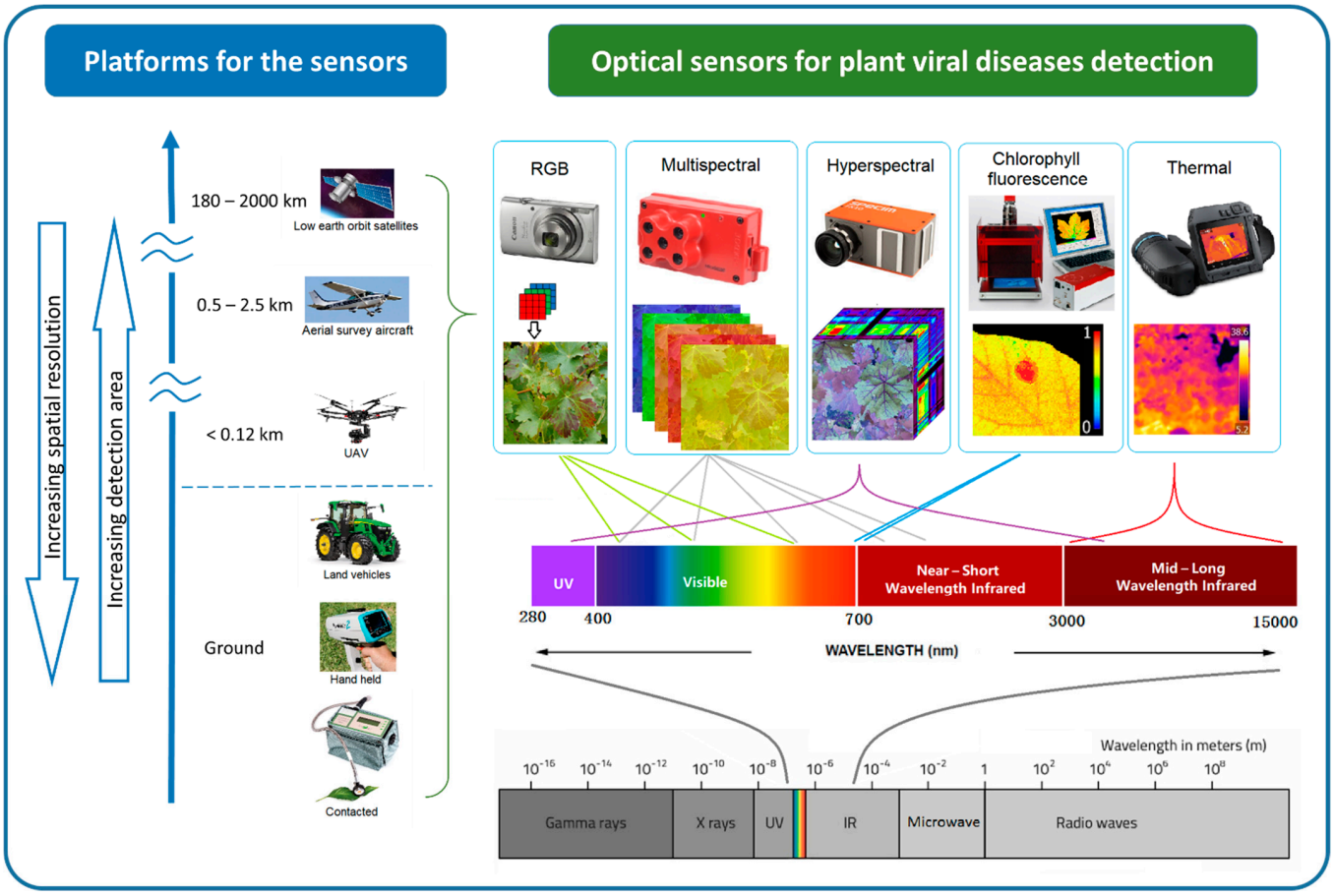

Figure 2. Optical sensing technologies for plant viral disease detection can be classified by their platform and associated spatial resolution and extent. Sensors also vary by band position, the spectral range within the whole electromagnetic spectrum.

At the finest scale, optical sensors can be used directly on contact on leaves, proximally on ground vehicles and hand-held. Some non-imaging sensors like chlorophyll fluorimeter, GreenSeeker, laser thermometer, and spectroradiometer are usually used proximally or directly in contract with the leaf [77]. By increasing the sensing distance, imaging sensors can be used proximally (e.g., mounted on tractors) or remotely (e.g., airborne platforms such as unmanned aerial vehicles (UAV), airplanes, and satellites) to support regional disease management [78]. Generally, increasing sensing distance results in decreasing spatial resolution. Satellite images provide the broadest land coverage but have the lowest spatial resolution. Manned airplanes can capture higher spatial resolution in a moderate area compared to satellite images. UAVs or drones can carry light-weight optical sensors flying as low as a few meters above ground [79–81], potentially providing millimetre spatial resolution images for plant viral disease detection.

In the order of increasing spectral detail, we find the RGB (red, green, and blue), multispectral, and hyperspectral systems. RGB systems have similar sensitivity as the human eye and thus produce images that can be readily interpreted [82]. Modern RGB cameras are user-friendly and readily available to the public, which means they can bring a large number of datasets available for plant disease identification. Community shared databases of plant disease infected images have been used for plant disease identification

in recent studies using computer vision techniques [83,84]. In addition, low altitude, high-resolution aerial photos from UAV have produced a high-popularity in-field plant disease detection [18,85,86].

Multispectral sensors measure specific spectral wavelength regions across the electromagnetic spectrum; different regions or bands can be selected depending on the purpose of usage [87]. Multispectral cameras have been commonly used in remote sensing to explore land use, characterise vegetation, and monitor the environment and urban structures [88]. For agricultural purposes, the spectral bands in multispectral cameras are selected based on the vegetation characteristics of light absorption and reflection at different wavelengths. Typically, RGB, combined with the unique vegetative reflectance regions, red edge (690–740 nm) and near-infrared (NIR) (700–1300 nm) bands, are used in multispectral sensors [89,90]. This information enables the computation of specific vegetation indices (VIs) that can be used to evaluate different characteristics of the vegetation. For example, by contrasting the absorption and reflectance in red and NIR spectral regions, the well-known normalized difference vegetation index (NDVI) can be calculated [91,92].

Hyperspectral sensors capture hundreds of contiguous narrow bands (2–20 nm) across a range of spectra (UV, visible, near-infrared (VNIR) to short-wave infrared (SWIR)) instead of few discrete broad bands as do multispectral sensors [93]. The highest spectral detail is obtained by sensing single point spectroradiometers rather than imaging, for example, ASD FieldSpec 4 and Ocean Optics USB4000. These sensors are mostly used proximally or directly in contract with the plants. Various studies have shown that spectral reflection signals change with plant viral infections and have demonstrated the method's potential for early or asymptomatic stage detection [94–98]. A hyperspectral imaging system provides both spatial and spectral information to produce a 3-dimensional (3D) data cube [99]. Hyperspectral imaging data present a potentially significant advantage in plant disease studies at broader scales. MacDonald et al. [100] were able to detect GLD in vineyards using an aircraft-mounted hyperspectral system. They achieved a prediction accuracy of 94.1% on average compared to visual survey results using specific leaf reflectance spectra using a spectroradiometer reported by Naidu et al. [95]. Wang et al. [101] used proximal sensing hyperspectral images to predict tomato spotted wilt virus infected region on the bell pepper plant. This study achieved 96.2% accuracy on plant level detection by evaluating the healthy and diseased pixel ratio, which demonstrated the potential of the hyperspectral image to predict viral infections on asymptomatic leaves.

Chlorophyll fluorescence (Chl-Fl) and infrared (IR) thermal sensors have also been used for plant virus detection. Chl-Fl is an important parameter for plant health and stress expression [102,103]. Many studies have used Chl-Fl as the laboratory's analysis tool for plant virus infection and demonstrated the likelihood of using Chl-Fl to detect plant virus infection at an early disease stage [104–109]. The passive method that uses solar radiation to measure fluorescence rate (known as solar-induced chlorophyll fluorescence) remotely for vegetation stress has also been attempted for plant stress detection [110–116]. The thermal sensor is predominantly used in precision agriculture to detect and monitor crop biotic and abiotic stress [80,117]. Spatial and temporal thermography patterns have shown potential for the early detection of viral disease. For example, Chaerle et al. [118] demonstrated that a resistant response (cell death) to tobacco mosaic virus (TMV) infection on the tobacco leaves could be detected by thermography rapidly after inoculation, eight hours before visible symptoms were apparent. Similarly, Zhu et al. [119] successfully distinguished the tomato mosaic disease plants five days before the visual symptom appeared using thermal imaging.

Besides those field applicable sensors, other technologies like Raman spectroscopy, Nuclear Magnetic Resonance (NMR) spectroscopy, and optical coherence tomography (OCT) have been used in the lab to detect plant virus diseases. Raman spectroscopy has been used for chemical analysis for decades. Various studies have demonstrated that Raman spectroscopy has the capability to detect plant virus infection at an early stage [120–122]. Some portable Raman spectroscopy is also available for in-field use [123]. NMR spectroscopy is

used to determine the chemical and physical properties of matter. Some studies used NMR spectroscopy to detect plant metabolic changes caused by virus infection [124,125]. An OCT system can see through the material and detect the morphological structure of cells. Various studies have used OCT to detect plant virus infection in leaves and seeds [126–128].

3. Analysis and Modelling Techniques for Optical Sensing Data

The indirect nature of optical sensing technologies in plant viral disease detection implies the need to develop mathematical relationships between sensing information and ground-truthed information (e.g., lab test results or visual assessment). Such disease classification models allow the prediction of diseases from optical sensing data from proximally and remotely sensed spectral data. Model quality is typically validated against reliable ground truth data.

The pipeline for optical disease detection includes data collection, data processing, modelling, and ground-truthing (Figure 3). Different data imply different processing and modelling needs ranging from statistics to machine learning [129,130]. Below, we describe some commonly used methods in plant viral disease modelling.

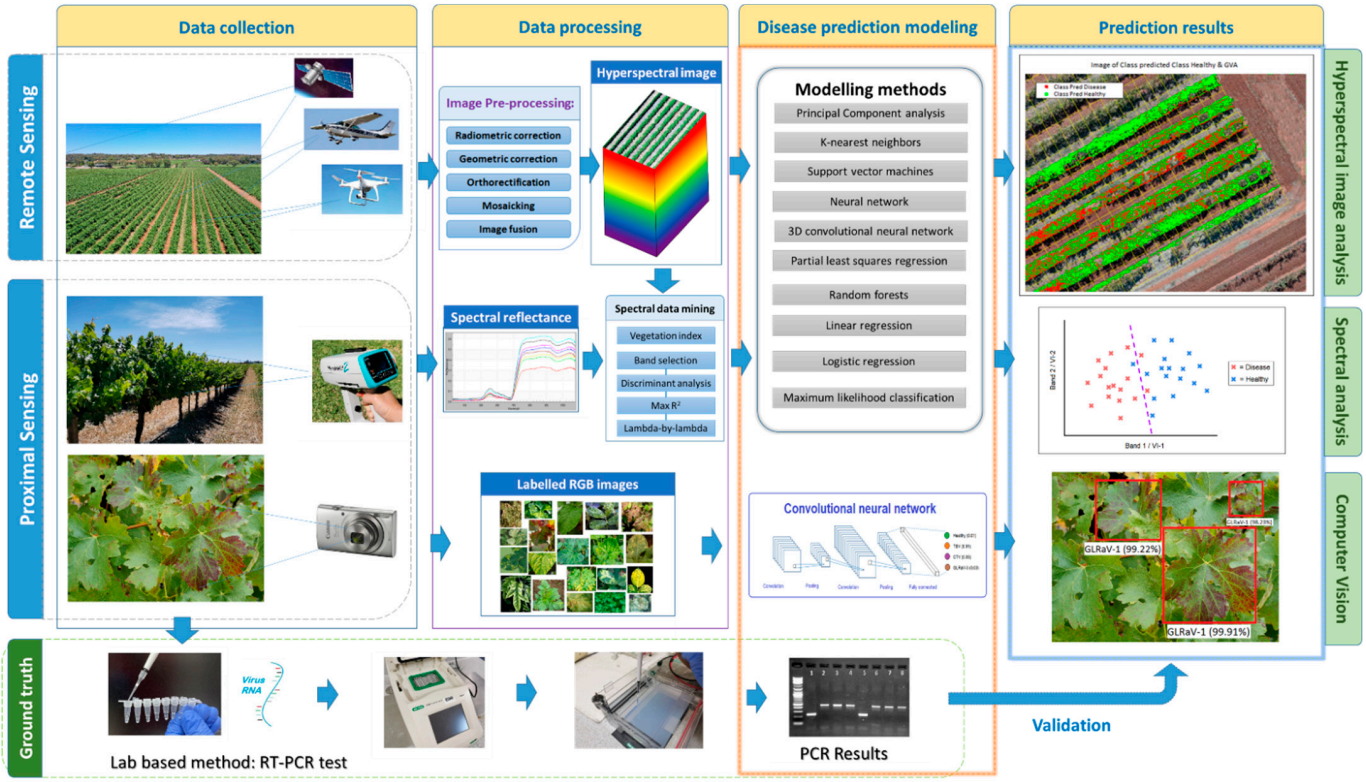

Figure 3. Workflow chart for plant viral disease prediction at different scales. Proximal sensing can obtain detailed spectral information at a point scale or leaf phenotypes at the leaf scale. Airborne remote sensing can be conducted at different spatial and spectral detail to be used for spatial mapping. Different data types involve various classification methods, including object-based methods like computer vision, spectral signal analysis, and pixel-based for multi and hyperspectral images. Indirect methods rely on ground-based information for model development and predictions.

3.1. Using Computer Vision for Leaf-Based Viral Disease Detection

As described in Section 2.1, viruses alter leaf phenotype. This principle has traditionally been used in field-based reconnaissance of viruses. It has also been adopted in computer vision, which has become popular in recent years due to its excellent performance, such as object detection, facial recognition, and medical diagnosis [131–133]. With a large set of training data (annotated images), computer vision systems can rapidly learn and

recognise an object in a new, previously unseen image. This technology has the potential to increase the efficiency of traditional field-based virus detection by examining leaves. Mohanty et al. [83] correctly identified 26 plant diseases across 14 crops by using images from the PlantVillage project dataset [134] of 54,306 leaf images and obtained a prediction accuracy of over 99%. Ferentinos [84] tested five different convolutional neural networks (CNN) architectures (AlexNet, AlexNetOWTBn, GoogLeNet, Overfeat, and VGG). Using 87,848 open database images containing 25 different plants and 58 diseases, the authors reported a prediction accuracy of >99%. Ramcharan et al. [135] used GoogLeNet to detect five major pests and diseases in cassava plants, including cassava mosaic virus and cassava brown streak virus. This study used 13,500 images to train the model and achieved 93% accuracy in 1500 test images. Polder et al. [136] used a pre-trained region-based CNN (R-CNN) model to detect tulip breaking virus from multispectral images. They reported that the deep-learning model could identify 82% of the diseased plants, which favourably compared to the judgement of experienced crop inspectors.

UAV based RGB imaging at high spatial resolution has been the basis for successful virus detection of plants. Gomez Selvaraj et al. [137] used UAV-RGB images to detect Banana bunchy top disease (BBTD) and Xanthomonas wilt of banana disease (BXW). This study collected images at 50–100 m above ground, providing 1–3 cm spatial resolution. By training 2477 annotated images in a CNN architecture RetinaNet, the authors achieved 98% precision. Using a similar method but lower altitude, Sugiura et al. [138] captured imagery at the height of 5–10 m above ground, with 2–4 mm spatial resolution to study potato virus Y infection. Using 1800 training images, the model achieved 96% accuracy for the training and 84% for the test dataset, respectively.

The above examples demonstrate the feasibility of using leaf-level RGB images in the CV framework for plant disease detection. However, training image recognition models requires a large number of annotated images at different times, environments, and locations for reliable prediction. Image annotation requires labour, time, and experience; a paucity of annotated images is one of the limitations of the technique [139,140]. Additional challenges arise from the quality of images used for training the model; poor resolution or inadequate annotation can negatively affect accuracy.

3.2. Use of Multispectral Imagery for Plant Viral Disease Detection

Multispectral imagery is a simple, cheap, readily available method for plant surveillance. It has established methodologies focused on spectral analysis of individual pixels, which is different from object-based detection like CV using entire images or subsets of images. The relationship between spectral reflectance and vegetation properties is well established and is to a large degree based on chlorophyll a and b spectral properties. Absorption bands are around 440 nm and 650 nm for chlorophyll a and b, respectively, with high reflectance in green and near-infrared spectral ranges [141,142]. There are more than 150 published vegetation indices (VI), and different relationships with plant cell structure, biochemistry, physiology, and stress have been established [143,144]. Commonly used VIs for plant stress studies include NDVI, Chlorophyll Index, Water Index, and Red-edge Vegetation Stress Index [145]. Multispectral sensors can focus on these important spectral bands and produce a variety of indices that have been examined for disease detection.

The potential physiological effects of viruses on the photosynthetic apparatus in leaves imply that multispectral images contain information on virus detection. For example, Mirik et al. [146] used Landsat 5 TM satellite multispectral images for wheat streak mosaic virus detection on a broad scale. Six bands were used in the maximum likelihood classifier (MLC) to classify the disease pixels in the study, and they achieved overall accuracies of 96% and 99% and were obtained on two different dates compared to ELISA test results. Another study by Hou et al. [147] generated seven VIs using four bands (R, G, B, and NIR) in a satellite image for GLD detection. All 11 feature vectors (seven VIs and four bands) were fed in a clustering analysis model Ant colony clustering algorithm (ACCA) [148] for disease detection. They achieved 75% accuracy for plants with mild symptoms and 84% for plants

with severe symptoms. A nine-band multispectral field radiometer was used by Steddom et al. [149] to detect beet necrotic yellow vein virus at canopy level (0.75 m diameter field of view). Using a logistic regression algorithm with Vis, the authors obtained an accuracy of 88% for symptomatic plants; however, they could not separate the asymptomatic plants from healthy plants using their model.

3.3. Use of Hyperspectral Sensing

The success of multispectral approaches has encouraged using more spectral detail through hyperspectral imaging. However, the complexity and volume of hyperspectral imagery imply the need for data reduction as part of the workflow [150]. Different approaches either select spectral bands known to change with physiological plant changes or empirically detect spectral ranges that are affected by the disease using data mining [93,151,152]. Band selection is often used as an initial step. It chooses only those that contribute to the accurate prediction of the disease and remove the redundant bands without losing the key information [93]. In most plant diseases detection studies, the optimum bands in hyperspectral data need to be evaluated and determined for each disease case or development stage. Many methods have been suggested to determine the unique bands for the dataset, such as lambda-by-lambda R-squared to assess pairwise band correlations [93], partial least squares (PLS) [153], successive projections algorithm (SPA) [154], and stepwise discriminant analysis (SDA) [155]. Naidu et al. [95] used SDA to separate infected and healthy GLRaV-3 infected grape leaves. They achieved an overall 81% accuracy and 75% for asymptomatic leaves based on a combination of selected bands and VIs. Zhu et al. [156] used successive projections algorithm (SPA) to determine eight effective wavelengths from 434 variables in hyperspectral imaging for TMV detection. Unsupervised machine learning methods like principal component analysis (PCA) also be used for clustering [97] and reducing dimensions for spectral data [157]. A comprehensive review of the various hyperspectral band selection algorithms has been provided by Sun and Du [158].

For viral disease classification modelling, various statistical and machine learning algorithms can be used. Commonly used methods include linear discriminant analysis (LDA), naive Bayes (NB), random forest (RF), support vector machines (SVM), k-nearest neighbours (KNN), partial least square (PLS) and spectral angle mapper (SAM). Grisham et al. [98] used an SD-2000 Ocean Optics spectrometer to measure the change in chlorophylls and carotenoids in asymptomatic sugarcane leaves infected with sugarcane yellow leaf virus. The authors used the LDA model to predict the infected and non-infected plants at 64% and 72% accuracy, respectively. Sinha et al. [96] used a hand-held spectroradiometer to identify GLD. Two statistical algorithms quadratic discriminant analysis (Q-DA) and NB were used for the spectral data analysis. They obtained the results with 93–99% accuracy using Q-DA and 71–99% using NB. Using PLS discriminant analysis, Pagay et al. [159] detected virus infection in three grape varieties (Pinot noir with GLRaV-3, Shiraz with grapevine virus A (GVA) + GLRaV-3, and Riesling with GVA) with 96%, 91%, and 88% accuracy using an ASD FieldSpec-3 spectroradiometer. Polder et al. [160] compared four types of sensors (RGB, spectrophotometer, hyperspectral imaging, and Ch-Fl imaging) versus visual assessment to classify tulip breaking virus infection. Using an LDA classifier, they found the best performance was from the hyperspectral image data, with 73%, 77%, and 87% accuracy in three tulip varieties. Griffel et al. [94] differentiated spectral reflectance curves of Potato Virus Y infected plants. This study used NIR and SWIR bands to achieve an accuracy of approx. 90% taking the visual assessment as a reference. Al-Saddik et al. [161] used two methods discriminant analysis (DA) and SVM to classify grapevine yellows phytoplasma disease with different combinations of VIs. The result showed that SVM had an accuracy of approx. 97%, and this model performed better than DA, which had an accuracy of 95%. Afonso et al. [97] studied asymptomatic citrus tristeza virus infected plants using time series leaf hyperspectral data. They obtained prediction accuracies ranging from 60–90% across four treatments using the KNN algorithm. A study by Bendel et al. [162] evaluated a hyperspectral camera system in both glasshouse and field situations

to detect GLD from symptomatic and asymptomatic plants. In this study, four methods were used for spectral data analysis: LDA, PLS, multi-layer perceptron (MLP), and radial basis function network with relevance (rRBF). Comparison of results showed that MLP had better classification accuracy in the VNIR range (400–1000 nm), and rRBF had better performance in the SWIR range (1000–2500 nm). This study achieved accuracies up to 100% for the symptomatic plants; it also achieved 100% classification accuracy on asymptomatic Aligote variety and 85% on Pinot Noir variety, which demonstrated the potential of using the hyperspectral camera to detect asymptomatic diseases.

Some recent studies in plant viral disease detection used neural networks for hyperspectral image analysis. Zhu et al. [156] compared six different algorithms PLS, SVM, RF, least squares SVM (LS-SVM), extreme learning machine (ELM), and backpropagation neural network (BPNN) for TMV detection. The overall prediction accuracy ranged from 75% to 97%, with the best performance by two machine learning methods, ELM and BPNN, respectively. Another study by Wang et al. [101] aimed to detect tomato spotted wilt virus infection at an early stage with hyperspectral imaging. In this study, a new deep learning algorithm, Outlier removal auxiliary classifier generative adversarial nets (OR-AC-GAN), modified from the GAN network, was used to classify the hyperspectral data. This network was trained to classify three groups healthy, diseased, and background at the pixel level from the hyperspectral image. OR-AC-GAN performed better than 1D-CNN and normal AC-GAN methods with an accuracy of 98%. Moreover, the study showed that this new model was an improvement over classical band selection methods such as maximum variance principal component analysis (MVPCA), fast density-peak-based clustering, and similarity-based unsupervised band selection. The 3D convolutional neural networks (3D CNN) use 3D kernels to produce feature maps that can perform better than traditional classification methods in hyperspectral images [163]. Recently, several studies used 3D CNN algorithms to classify land types based on public satellite hyperspectral data to improve accuracy compared to traditional machine learning methods [164–167]. However, very few studies have been conducted in plant viral disease detection. Nguyen et al. [168] demonstrated that the early detection of grapevine vein-clearing virus could be achieved using a proximal sensing hyperspectral camera, Specim IQ. They compared the conventional 2D CNN to 3D CNN, which utilises the spatial and spectral information simultaneously from the hyperspectral image for modelling and showed that the accuracy of the 3D CNN is higher than the 2D CNN.

Table 1 provides a summary of the studies using optical sensing technologies and the modelling methods for plant viral disease detection.

Table 1. Examples of studies on detecting plant viral disease using different optical sensing technologies and modelling methods.

Sensing System	Platforms/Device	Disease Modelling Methods	Plant Virus	Ground Truthing Methods	Reference
RGB imaging	Handheld/Digital cameras	CNN, SVM, KNN, GoogLeNet	Multiple diseases	Labelled in dataset	[135]
RGB imaging	Handheld/Digital cameras	AlexNet, VGG16net	Multiple diseases	Labelled in dataset	[169]
RGB imaging	A rail system/ Digital cameras	R-CNN	Tulip breaking virus	ELISA	[136]
RGB; Multispectral imaging	UAV/DJI P4, SlantRange 3P	ANN	Tomato yellow leaf curl virus	PCR	[170]

Table 1. *Cont.*

Sensing System	Platforms/Device	Disease Modelling Methods	Plant Virus	Ground Truthing Methods	Reference
RGB; multispectral imaging	UAV and Satellite/DJI P4, Sony QX1, MicaSense RedEdge, WorldView2, PlanetScope, Sentinel 2	RetinaNet, SVM, Random forest	Banana bunchy top virus	Visual assessment	[137]
Multispectral imaging	Satellite/Landsat 5 TM	MLC	Wheat streak mosaic virus	Visual assessment and ELISA	[146]
Multispectral imaging	Satellite/(N/A)	ACCA	Grapevine leafroll-associated virus 3	Visual assessment	[147]
Multispectral; hyperspectral	Handheld/ASD FieldSpec FR	Logistic regression	Beet necrotic yellow vein virus	ELISA	[149]
Hyperspectral	Handheld/ASD Field Spec 3	SDA	Grapevine leafroll-associated virus 3	RT-PCR	[95]
Hyperspectral	Indoor proximal setting/SD-2000 fiber optic	LDA	Sugarcane yellow leaf virus	RT-PCR	[98]
Hyperspectral imaging	Aircraft/Headwall Photonics VNIR E Series	Classification and regression tree (CART)	Grapevine leafroll-associated virus 3	Visual assessment and ELISA and RT-PCR	[100]
Hyperspectral	Handheld/Ocean USB4000	PCA, KNN	Citrus tristeza virus	RT-PCR and qPCR	[97]
Hyperspectral	Handheld/ASD FieldSpec 3	PLS-DA	Grapevine leafroll-associated virus 3, and Grape virus A	RT-PCR	[159]
Hyperspectral	Handheld/ASD FieldSpec 4	SVM	Potato virus Y	Visual assessment and RT-PCR	[94]
Hyperspectral	Handheld/SVC HR–1024i, SVC Spectra Vista	PLSR, SMLR	Grapevine leafroll-associated virus 3	RT-PCR	[96]
Hyperspectral imaging	Indoor proximal setting/V10E Specim ImSpector	OR-AC-GAN, MVPCA, FDPC	Tomato Spotted Wilt Virus	Inoculated virus	[101]
Hyperspectral imaging	Harvest machine mounted/HySpex VNIR & SWIR	LDA, PLS, MLP, rRBF	Grapevine leafroll-associated virus 1, 3	Visual assessment and ELISA and RT-PCR	[162]
Hyperspectral	Handheld/ASD FieldSpec 3	PLS	Grapevine leafroll-associated virus 3	qPCR	[171]
Hyperspectral imaging	Handheld/SPECIM IQ	SVM, RF, 2D CNN, and 3D CNN	Grapevine vein clearing virus	Tested in the previous study	[168]
RGB, Chl-Fl, hyperspectral	Handheld/Nikon D70, ASD FieldSpec Pro FR	LDA	Tulip breaking virus	Visual assessment and ELISA	[160]
Chl-Fl imaging	Indoor proximal setting/Chl-Fl image system	VI: Fm/Fm'-1	Abutilon mosaic virus	Visual assessment	[104]
Chl-Fl imaging	Indoor proximal setting/Customized Chl-Fl imaging	LDA	Pepper mild mottle virus	Inoculated virus	[105]
Chl-Fl, hyperspectral, thermal imaging	Indoor proximal setting and handheld/ ImSpector V10E SPAD-meter VARIOSCAN 3201	LDA, SDA	Cucumber green mottle mosaic virus	Inoculated virus and Visual assessment	[172]

4. Comparison of the Cost for Virus Detection Methods

Costs associated with plant virus testing is a major consideration for growers when selecting detection options for viral disease management. In Table 2, we used a typical Australian vineyard as an example to compare the cost-effectiveness of different existing methods for grapevine virus detection. Detection methods include traditional methods visual and indicator plant assessment; commonly used lab-based methods ELISA and RT-PCR; proximal sensing methods RGB image, Chl-Fl sensor, Thermal image, and spectro-radiometer; remote sensing with multispectral satellite images, manned aircraft that can capture RGB, multispectral and thermal images simultaneously; and, finally, UAV platform RGB, multispectral, hyperspectral, and thermal images.

The assumption is based on single virus detection in a vineyard with 3 m row spacing and 2 m vine spacing, resulting in approx. 1700 vines ha^{-1}. Assuming the block size is 10 ha, there are approx. 17,000 vines in total. The currency is Australian dollars. Due to the extremely high lab costs (a commercial lab charges around AUD 100 per RT-PCR test and AUD 50 per ELISA test) and indicator plant test methods (an estimated cost for one indicator plant is AUD 20 per test, that includes grafting, growing, and biological index assessment), only 1% of vines are randomly sampled for testing. In contrast, the visual assessment and optical sensing technologies measure all vines in the block. The total cost consists of labour for samples or data collection and testing or data processing costs for the 10 ha block. Only operational costs are compared in this scenario; the costs of capital assets, skill training, travelling, disease model development, and other sunk costs are not included. Labour costs are between AUD 40 and AUD 80/hour, depending on skill. The total cost is based on 10 ha (~17,000 vines).

Cost estimates of various virus monitoring techniques shown in Table 2 indicate that lab-based methods are the most expensive, even at the low testing rate of 1%. However, the methods have the highest accuracy and are generally considered "gold standards" of plant disease detection. Satellite images provide the lowest cost option; however, due to the low resolution of the images, their accuracy is also the lowest of the methods considered here. In general, there is a negative correlation between the sensing distance and the accuracy of sensing technology. In terms of the simplicity of the methods, visual assessment is the simplest and least expensive, but the reliability varies between the inspectors and is only feasible on symptomatic plants. Indicator plants provide relatively high accuracy but require a long time from grafting to the development of symptoms. Hyperspectral methods are the most complex, requiring trained operators for both data acquisition and processing. The technique also requires longer data processing times, but it provides more spectral information for disease modelling. In comparing remote and proximal sensing techniques, the major difference is that, although operationally simpler, data collection time and costs are much higher for proximal sensing per hectare for large blocks, which increases the total cost. In terms of data type, RGB (or visible imagery) is the simplest and least expensive, but as in the case of visual assessment, it is unable of detecting asymptomatic diseases directly; indirect assessments through changes in phenotype may be detected, however. It is noteworthy that the reliability of visual assessments can be improved by confirmation of lab tests, and the robustness of the disease models can be enhanced with larger ground truth datasets; however, lab tests cost extra.

Table 2. Cost comparison between detection methods based on a typical Australian vineyard.

Method Type		Reliability	Capability for Asymptomatic Detection	Sensing Resolution	Testing Rate	Sample/Data Collection Cost	Sample/Data Collection Time (Man Hours)	Sample/Data Processing Cost	Sample/Data Processing Time	Total Cost
Traditional	Visual assessment	Low-Medium	No	N/A	100%	AUD 1600	40	0	0	AUD 1600
	Indicator Plants	Medium	Yes	N/A	1%	AUD 320	8	AUD 3400	Months	AUD 3720
Lab-based testing	ELISA	High	Yes	N/A	1%	AUD 320	8	AUD 8500	2–3 days	AUD 8820
	RT-PCR	Very High	Yes	N/A	1%	AUD 320	8	AUD 17,000	2–3 days	AUD 17,320
Proximal sensing	RGB	Low-Medium	No	<Single leaf	100%	AUD 640	16	AUD 1280	2 days	AUD 1920
	Chl-Fl	Low	Yes	Single leaf	100%	AUD 4800	80	AUD 1280	2 days	AUD 6080
	Thermal	Low	Yes	Single leaf	100%	AUD 2400	40	AUD 1280	2 days	AUD 3680
	Hyperspectral	Medium	Yes	Single leaf	100%	AUD 4800	80	AUD 2560	4 days	AUD 7360
Remote sensing (Satellite)	Multispectral	Very Low	Yes	>Single plant	100%	AUD 10/image		AUD 1280	2 days	AUD 1290
Remote sensing (Manned Airplane)	RGB + Multispectral + Thermal	Low	Yes	Single plant	100%	AUD 100	<0.5 h	AUD 1280	2 days	AUD 1380
Remote sensing (UAV)	RGB	Low	No	<Single leaf	100%	AUD 200	2	AUD 1280	2 days	AUD 1480
	Multispectral	Low	Yes	Single leaf	100%	AUD 300	3	AUD 1920	3 days	AUD 2220
	Hyperspectral	Medium	Yes	Single leaf	100%	AUD 400	6	AUD 3200	5 days	AUD 3600
	Thermal	Low	Yes	Single leaf	100%	AUD 300	3	AUD 1280	2 days	AUD 1580

5. Current Challenges and Future Perspectives

5.1. Current Challenges of Plant Viral Disease Detection

Despite significant advances in the detection of plant viral disease, there remain numerous challenges that can be addressed with emerging technologies. Current understanding of plant viruses has increased due to advances in molecular diagnostic methods; however, ascertaining the plant phenotypes resulting from virus infections remains challenging due to the complex interactions between viruses, host genomes, and environmental factors, and symptoms are often not distributed evenly throughout the plant [13]. The viral disease produces variable impacts; some do not produce any symptoms, while others lead to rapid plant decline [56]. Viruses may not necessarily cause disease in the infected plant. Some infected plants have been shown to recover even though the virus remains in the host, suggesting a level of virus tolerance, which has not received much attention to date. All these complexities associated with viruses in plants make disease detection a challenging task.

Viral disease symptoms can be highly variable due to multiple host–pathogen–environment interactions. Multiple pathogens can cause co-infection in plants and make the detection of viruses more difficult. Viral disease symptoms can also be mistaken for other pathogens like fungi, bacteria, nematodes, and viroids; or mislead by abiotic stresses from nutrient deficiencies (e.g., phosphorous or potassium) or water stress. Environmental impacts such as air temperature, soil type, and edge effects also need to be considered. Mechanical and chemical damage such as herbicide injury could cause similar stress responses on plants as the viral disease. These complex combinations of factors could confound the accurate detection of viruses. Thus, a complete understanding of the condition of the plants and continuous monitoring over time is needed to improve the accuracy of viral disease detection.

Building a robust viral disease prediction model with optical sensing technology relies largely on the availability of accurate ground truth data from different times, disease severities, and regions. Acquiring large amounts of data remains a challenge, requiring time, labour, and resources. A simple method like visual assessment can gather sufficient ground truth data for model training. However, its reliability is unsatisfactory as some infected plants do not display visual symptoms and may lead to false negatives. Lab-based testing methods are accurate and essential for ground-truthing; yet, the high cost limits the size of ground truth data, which may reduce the robustness of the model. Nevertheless, none of the diagnostic methods can guarantee 100% accuracy. For example, Pietersen and Harris [173] discovered that even RT-PCR failed to detect GLRaV-3 in the grapevine rootstock-Richter 99 (*V. berlandieri* × *V. rupestris*). In this study, the authors found asymptomatic basal shoots (sucker) grown from the GLRaV-3 symptomatic grapevines from an abandoned vineyard in South Africa. They tested the scion and rootstock materials from the same vines. All scion materials with obvious disease symptoms tested positive, but RT-PCR results of the rootstock tissue tested negative. Therefore, understanding limitations and potential sources of error are critical for any detection method.

5.2. Future Prospects for Optical Sensing Technology in Plant Viral Disease Detection

Speed, coverage, accuracy, and cost determine the choice of viral disease detection methods. The complexity of the host–virus–environment interactions makes optical detection extremely challenging and requires robust models developed using reliable ground truth data. Novel approaches provide improved ground-truthing, sensing data collection, and data processing.

For ground-truthing, various technologies have been developed for virus diagnosis in recent years. The COVID-19 global pandemic (since 2019) has seen an emergence of rapid and novel testing methods, for example, the integration of plasmonic thermocycling and fluorescence detection in a portable device by Cheong et al. [174], a field-effect transistor (FET)-based biosensing devices developed by Seo et al. [175], and a microwave immunosensor cavity resonator developed by Elsheakh et al. [176]. Some of the novel devices may be applicable to plant virus diagnosis for rapid detection. The improved genomic

sequencing and innovative bioinformatics technologies could help rapid identification of previously unknown plant viruses and strains, which can help us better understand the causes of symptomology, as well to build a global database of virus genomes that can better prepare us for future outbreaks of these viruses. Field deployable testing devices are useful for quickly determining viruses on suspected symptoms, which will aid in sample collection efficiency and increase the confidence of visual assessment for adequate and reliable ground-truthing. For example, a portable gene sequencing device developed by Oxford Nanopore Technologies MinION can be used for fast plant virus detection in the field. Various newly developed portable diagnostic tools using LAMP and LFD technology are promising for rapid field testing [177–179].

For optical sensing data collection, understanding the symptomology of viral disease is critical. Establishing optimal crop developmental stages and time of day to capture the optical data, e.g., at a specific incident angle of the sun, are simple approaches to increase detection accuracy. Consistent sensing distance and stabilised sensor movement during the data collection are important for obtaining consistent data. Sensing platforms like autonomous UAVs, ground-based vehicles, and robots are rapidly advancing, offering heavier payload capacities, higher endurance (longer operation duration and range), and high positional accuracy, all of which would help collect quality sensing data while maintaining high consistency. Optical sensors have also steadily improved in resolution, form factor, and weight. Due to the increased demand for low altitude and proximal sensing technology, global manufacturers compete to make higher spatial and spectral resolution optical sensors that are lighter weight and user-friendly. Currently, due to the complexity of the hyperspectral camera system, most high spectral resolution sensors are push-broom type, which requires a very stable condition to operate and needs high positional accuracies, requiring extra processing steps to produce image data. A simple and user-friendly hyperspectral sensor is desirable for disease detection.

In addition to the sensors introduced in Section 2, other types of sensors can be used simultaneously to provide more information to aid in accurate disease detection. For example, a light detection and ranging (LIDAR) sensor has been used with hyperspectral or multispectral systems to reconstruct the image data to aid the accuracy of the positioning. The combination of the sensors can produce a hyperspectral 3D point cloud for plant disease classification [180–182]. A stereoscopic camera uses two or more lenses to capture images from multiple angles in a short distance, which produces the high-resolution 3D structure of the leaf shape and size [183]. Microwave sensors are active sensors that can detect the object at any time of day [184]. Non-optical sensors such as chemical sensors can also be used. For example, volatile organic compounds (VOCs) emitted by plants can be used to indicate a diseased state. The emission of VOCs can be altered due to virus infection. Mauck et al. [185] showed that cucumber mosaic virus infected plants produce about 50% more total volatiles than healthy plants to attract the vectors helping the virus invading other healthy plants. Methyl salicylate volatile emissions were increased in TMV infected tobacco plants to warn neighbouring plants, thereby inducing their defence mechanisms [186]. Although disease detection using VOCs is mainly undertaken on a small scale, such as in growth chambers or small glasshouses, novel technologies can provide early warning in large glasshouses or the field [187,188].

For data processing, novel ML algorithms for band selection and new Vis from hyperspectral data can improve the accuracy of disease detection. Considering that spectral signals change over time at different disease development stages, the disease model should contain large datasets over different periods and be updated regularly to improve the robustness of the models. Optimising the 3D CNN algorithm for hyperspectral image data could improve the model accuracy for hyperspectral data. As computational power increases, onboard mobile devices could speed up data processing, so the analysis occurs on-the-go. The disease information can be provided to growers in near real-time using a combination of miniature sensors and onboard computers on land vehicles or wearable smart devices with augmented reality (AR) technology such as Microsoft Hololens.

Overall, further development of technology in molecular diagnosis, sensors, platforms, and data processing methods will improve plant virus detection, ultimately aiding in the efficient management of plant viral disease.

6. Conclusions

Plant viral diseases have been shown to negatively impact crop health and, consequently, decrease crop yields and global food production. The dearth of control options makes it ever more imperative to utilise a diverse array of tools ranging from molecular detection to optical, non-destructive approaches that provide rapid, spatial scale detection. This combines the scientific rigour of laboratory methods with the spatial representation and detectability of pattern of infections using spatial methods. An ongoing challenge with the use of optical sensing technology is the increased complexity of data; this issue can be addressed by using high-performance computers in conjunction with novel algorithms in data processing to improve disease prediction accuracy. Additional challenges will present themselves including the threat of emerging viruses and their variants, which will require ongoing development of detection methodologies that vary in both cost and accuracy. Our detailed economic analysis suggests that aerial visible imaging is the most cost-effective approach for detection provided that symptoms are manifested on the plant. This information gives a dollar value reference to practitioners to manage viral diseases in their crops.

Author Contributions: Y.M.W. performed the article review and prepared the original draft; N.H., D.G., B.O. and V.P. contributed to reviewing and editing the manuscript. All authors have read and agreed to the published version of the manuscript.

Funding: This research was funded by South Australia Australian Grapevine Foundation Planting Service Inc. (Grant number: DVCR711278), Riverland Wine Industry Development Council (Grant number 194388), and Wine Australia (Grant number: PPA002864). Y.M.W.'s study is supported by the Research Training Program, The University of Adelaide.

Acknowledgments: The authors would like to acknowledge the funding body: South Australian Vine Improvement Association, Riverland Wine, and The University of Adelaide.

Conflicts of Interest: The authors declare no conflict of interest.

References

1. Savary, S.; Willocquet, L.; Pethybridge, S.J.; Esker, P.; McRoberts, N.; Nelson, A. The global burden of pathogens and pests on major food crops. *Nat. Ecol. Evol.* **2019**, *3*, 430–439. [CrossRef] [PubMed]
2. Reddy, D.V.R.; Sudarshana, M.R.; Fuchs, M.; Rao, N.C.; Thottappilly, G. Genetically engineered virus-resistant plants in developing countries: Current status and future prospects. In *Advances in Virus Research*; Loebenstein, G., Carr, J.P., Eds.; Academic Press: Burlington, USA, 2009; Volume 75, pp. 185–220. [CrossRef]
3. Savary, S.; Ficke, A.; Aubertot, J.-N.; Hollier, C. Crop losses due to diseases and their implications for global food production losses and food security. *Food Secur.* **2012**, *4*, 519–537. [CrossRef]
4. Jones, R.A.C. Disease Pandemics and Major Epidemics Arising from New Encounters between Indigenous Viruses and Introduced Crops. *Viruses* **2020**, *12*, 1388. [CrossRef]
5. Jones, R.A.C. Global Plant Virus Disease Pandemics and Epidemics. *Plants* **2021**, *10*, 233. [CrossRef] [PubMed]
6. Sastry, K.S. Impact of virus and viroid diseases on crop yields. In *Plant Virus and Viroid Diseases in the Tropics*; Volume 1: Introduction of Plant Viruses and Sub-Viral Agents, Classification, Assessment of Loss, Transmission and Diagnosis; Springer: Dordrecht, The Netherlands, 2013; pp. 99–159. [CrossRef]
7. Gilbertson, R.L.; Rojas, M.R.; Kon, T.; Jaquez, J. Introduction of Tomato Yellow Leaf Curl Virus into the Dominican Republic: The Development of a Successful Integrated Pest Management Strategy. *Tomato Yellow Leaf Curl Virus Dis.* **2007**, *92*, 487–496. [CrossRef]
8. Briddon, R.W.; Markham, P.G. Cotton leaf curl virus disease. *Virus Res.* **2000**, *71*, 151–159. [CrossRef]
9. Wood, G.A.; Chamberlain, E.E.; Atkinson, J.D.; Hunter, J.A. Field studies with apple mosaic virus. *N. Z. J. Agric. Res.* **1975**, *18*, 399–404. [CrossRef]
10. Atallah, S.S.; Gomez, M.I.; Fuchs, M.F.; Martinson, T.E. Economic Impact of Grapevine Leafroll Disease on Vitis vinifera cv. Cabernet franc in Finger Lakes Vineyards of New York. *Am. J. Enol. Vitic.* **2011**, *63*, 73–79. [CrossRef]
11. Maree, H.J.; Almeida, R.P.P.; Bester, R.; Chooi, K.M.; Cohen, D.; Dolja, V.V.; Fuchs, M.F.; Golino, D.A.; Jooste, A.E.C.; Martelli, G.P.; et al. Grapevine leafroll-associated virus 3. *Front. Microbiol.* **2013**, *4*, 82. [CrossRef]

12. Mannini, F.; Digiaro, M. The effects of viruses and viral diseases on grapes and wine. In *Grapevine Viruses: Molecular Biology, Diagnostics and Management*, 1st ed.; Meng, B., Martelli, G.P., Golino, D.A., Fuchs, M., Eds.; Springer International Publishing: Cham, Switzerland, 2017; pp. 453–482. [CrossRef]
13. Hull, R. *Plant Virology*, 5th ed.; Elsevier: London, UK; Academic Press: London, UK, 2013.
14. Sastry, K.S.; Zitter, T.A. Management of Virus and Viroid Diseases of Crops in the Tropics. In *Plant Virus and Viroid Diseases in the Tropics: Volume 2: Epidemiology and Management*; Springer: Dordrecht, The Netherlands, 2014; pp. 149–480. [CrossRef]
15. Awasthi, L.P. *Recent Advances in the Diagnosis and Management of Plant Diseases*, 1st ed.; Springer: New Delhi, India, 2015; pp. 35–44. [CrossRef]
16. Fang, Y.; Ramasamy, R.P. Current and Prospective Methods for Plant Disease Detection. *Biosensors* **2015**, *5*, 537–561. [CrossRef]
17. Sankaran, S.; Mishra, A.; Ehsani, R.; Davis, C. A review of advanced techniques for detecting plant diseases. *Comput. Electron. Agric.* **2010**, *72*, 1–13. [CrossRef]
18. Martinelli, F.; Scalenghe, R.; Davino, S.; Panno, S.; Scuderi, G.; Ruisi, P.; Villa, P.; Stroppiana, D.; Boschetti, M.; Goulart, R.L.; et al. Advanced methods of plant disease detection: A review. *Agron. Sustain. Dev.* **2015**, *35*, 1–25. [CrossRef]
19. Legrand, P. Biological assays for plant viruses and other graft-transmissible pathogens diagnoses: A review. *EPPO Bull.* **2015**, *45*, 240–251. [CrossRef]
20. Smith, K.M. Introduction. In *Plant Viruses*; Smith, K.M., Ed.; Springer: Dordrecht, The Netherlands, 1977; pp. 1–5. [CrossRef]
21. Hipper, C.; Brault, V.; Ziegler-Graff, V.; Revers, F. Viral and Cellular Factors Involved in Phloem Transport of Plant Viruses. *Front. Plant Sci.* **2013**, *4*, 154. [CrossRef]
22. Mauck, K.E.; De Moraes, C.M.; Mescher, M.C. Biochemical and physiological mechanisms underlying effects ofCucumber mosaic viruson host-plant traits that mediate transmission by aphid vectors. *Plant Cell Environ.* **2014**, *37*, 1427–1439. [CrossRef]
23. Jaime, C.; Muchut, S.E.; Reutemann, A.G.; Gieco, J.O.; Dunger, G. Morphological changes, alteration of photosynthetic parameters and chlorophyll production induced by infection with alfalfa dwarf virus in Medicago sativa plants. *Plant Pathol.* **2019**, *69*, 393–402. [CrossRef]
24. Gutha, L.R.; Casassa, L.F.; Harbertson, J.F.; Naidu, R.A. Modulation of flavonoid biosynthetic pathway genes and anthocyanins due to virus infection in grapevine (*Vitis vinifera* L.) leaves. *BMC Plant Biol.* **2010**, *10*, 187. [CrossRef]
25. Maxwell, D.J.; Partridge, J.C.; Roberts, N.W.; Boonham, N.; Foster, G.D. The Effects of Plant Virus Infection on Polarization Reflection from Leaves. *PLoS ONE* **2016**, *11*, e0152836. [CrossRef]
26. Moeini, P.; Afsharifar, A.; Homayoonzadeh, M.; Hopkins, R.J. Plant virus infection modifies plant pigment and manipulates the host preference behavior of an insect vector. *Èntomol. Exp. Appl.* **2020**, *168*, 599–609. [CrossRef]
27. Bahar, T.; Qureshi, A.M.; Qurashi, F.; Abid, M.; Zahra, M.B.; Haider, M.S. Changes in Phyto-Chemical Status upon Viral Infections in Plant: A Critical Review. *Phyton* **2021**, *90*, 75–86. [CrossRef]
28. Boonham, N.; Kreuze, J.; Winter, S.; van der Vlugt, R.; Bergervoet, J.; Tomlinson, J.; Mumford, R. Methods in virus diagnostics: From ELISA to next generation sequencing. *Virus Res.* **2014**, *186*, 20–31. [CrossRef]
29. Naidu, R.A.; Hughes, J.D.A. Methods for the detection of plant virus diseases. In *Plant Virology in Sub-Saharan Africa: Proceedings of a Conference Organized by IITA: 4–8 June 2001*; International Institute of Tropical Agriculture: Ibadan, Nigeria, 2003; p. 233.
30. Torrance, L.; Jones, R.A.C. Recent developments in serological methods suited for use in routine testing for plant viruses. *Plant Pathol.* **1981**, *30*, 1–24. [CrossRef]
31. Matthews, R.E.F. Serological techniques for plant viruses. In *Methods in Virology*; Maramorosch, K., Koprowski, H., Eds.; Elsevier Science: New York, NY, USA, 1967; Volume 3, pp. 199–241. [CrossRef]
32. Nakane, P.K.; Pierce, G.B. Enzyme-Labeled Antibodies: Preparation and Application for the Localization of Antigens. *J. Histochem. Cytochem.* **1966**, *14*, 929–931. [CrossRef] [PubMed]
33. Clark, M.F.; Adams, A.N.; Graham, F.L.; Smiley, J.; Russell, W.C.; Nairn, R. Characteristics of the Microplate Method of Enzyme-Linked Immunosorbent Assay for the Detection of Plant Viruses. *J. Gen. Virol.* **1977**, *34*, 475–483. [CrossRef]
34. Danks, C.; Barker, I. On-site detection of plant pathogens using lateral-flow devices. *EPPO Bull.* **2000**, *30*, 421–426. [CrossRef]
35. Maheshwari, Y.; Vijayanandraj, S.; Jain, R.K.; Mandal, B. Field-usable lateral flow immunoassay for the rapid detection of a macluravirus, large cardamom chirke virus. *J. Virol. Methods* **2018**, *253*, 43–48. [CrossRef]
36. Selvarajan, R.; Kanichelvam, P.S.; Balasubramanian, V.; Subramanian, S.S. A rapid and sensitive lateral flow immunoassay (LFIA) test for the on-site detection of banana bract mosaic virus in banana plants. *J. Virol. Methods* **2020**, *284*, 113929. [CrossRef]
37. Boine, B.; Kingston, R.L.; Pearson, M.N. Recombinant expression of the coat protein of Botrytis virus X and development of an immunofluorescence detection method to study its intracellular distribution in Botrytis cinerea. *J. Gen. Virol.* **2012**, *93*, 2502–2511. [CrossRef]
38. Kuo, S.-Y.; Lin, Y.-C.; Lai, Y.-C.; Liao, J.-T.; Hsu, Y.-H.; Huang, H.-C.; Hu, C.-C. Production of fluorescent antibody-labeling proteins in plants using a viral vector and the application in the detection of Acidovorax citrulli and Bamboo mosaic virus. *PLoS ONE* **2018**, *13*, e0192455. [CrossRef]
39. Morris, T.J.; Dodds, J. Isolation and analysis of double-stranded RNA from virus-infected plant and fungal tissue. *Phytopathology* **1979**, *69*, 854–858. [CrossRef]
40. Saiki, R.K.; Scharf, S.; Faloona, F.; Mullis, K.B.; Horn, G.T.; Erlich, H.A.; Arnheim, N. Enzymatic amplification of beta-globin genomic sequences and restriction site analysis for diagnosis of sickle cell anemia. *Science* **1985**, *230*, 1350–1354. [CrossRef] [PubMed]

41. Olmos, A.; Capote, N.; Bertolini, E.; Cambra, M. Molecular diagnostic methods for plant viruses. In *Biotechnology and Plant Disease Management*; Punja, Z.K., de Boer, S.H., Sanfaçon, H., Eds.; CAB International: Wallingford, UK, 2007; pp. 227–249. [CrossRef]
42. Farkas, D.H.; Holland, C.A. Overview of molecular diagnostic techniques and instrumentation. In *Cell and Tissue Based Molecular Pathology*; Tubbs, R.R., Stoler, M.H., Eds.; Churchill Livingstone: Philadelphia, CA, USA, 2009; pp. 19–32. [CrossRef]
43. Scagliusi, S.M.; Basu, S.; Gouvêa, J.A.D.; Vega, J. Comparison of two diagnostic methods for evaluation of Sugarcane yellow leaf virus concentration in Brazilian sugarcane cultivars. *Funct. Plant Sci. Biotechnol.* **2009**, *3*, 26–30.
44. Mekuria, G.; Ramesh, S.; Alberts, E.; Bertozzi, T.; Wirthensohn, M.; Collins, G.; Sedgley, M. Comparison of ELISA and RT-PCR for the detection of Prunus necrotic ring spot virus and prune dwarf virus in almond (*Prunus dulcis*). *J. Virol. Methods* **2003**, *114*, 65–69. [CrossRef] [PubMed]
45. Vigne, E.; Garcia, S.; Komar, V.; Lemaire, O.; Hily, J.-M. Comparison of Serological and Molecular Methods With High-Throughput Sequencing for the Detection and Quantification of Grapevine Fanleaf Virus in Vineyard Samples. *Front. Microbiol.* **2018**, *9*, 2726. [CrossRef]
46. McGavin, W.J.; Cock, P.J.A.; Macfarlane, S.A. Partial sequence and RT-PCR diagnostic test for the plant rhabdovirus Raspberry vein chlorosis virus. *Plant Pathol.* **2010**, *60*, 462–467. [CrossRef]
47. Lima, J.A.A.; Nascimento, A.K.Q.; Radaelli, P.; Silva, A.K.F.; Silva, F.R. A Technique Combining Immunoprecipitation and RT-PCR for RNA Plant Virus Detection. *J. Phytopathol.* **2013**, *162*, 426–433. [CrossRef]
48. Rojas, M.R.; Gilbertson, R.J.; Russell, D.R.; Maxwell, D.P. Use of Degenerate Primers in the Polymerase Chain Reaction to Detect Whitefly-Transmitted Geminiviruses. *Plant Dis.* **1993**, *77*, 340–347. [CrossRef]
49. Nakaune, R.; Nakano, M. Efficient methods for sample processing and cDNA synthesis by RT-PCR for the detection of grapevine viruses and viroids. *J. Virol. Methods* **2006**, *134*, 244–249. [CrossRef]
50. Kokkinos, C.D.; Clark, C.A. Real-Time PCR Assays for Detection and Quantification of Sweetpotato Viruses. *Plant Dis.* **2006**, *90*, 783–788. [CrossRef]
51. Taylor, S.; Wakem, M.; Dijkman, G.; Alsarraj, M.; Nguyen, M. A practical approach to RT-qPCR—Publishing data that conform to the MIQE guidelines. *Methods* **2010**, *50*, S1–S5. [CrossRef]
52. Deepak, S.; Kottapalli, K.; Rakwal, R.; Oros, G.; Rangappa, K.; Iwahashi, H.; Masuo, Y.; Agrawal, G. Real-Time PCR: Revolutionizing Detection and Expression Analysis of Genes. *Curr. Genom.* **2007**, *8*, 234–251. [CrossRef] [PubMed]
53. Notomi, T.; Okayama, H.; Masubuchi, H.; Yonekawa, T.; Watanabe, K.; Amino, N.; Hase, T. Loop-mediated isothermal amplification of DNA. *Nucleic Acids Res.* **2000**, *28*, E63. [CrossRef] [PubMed]
54. Adams, I.P.; Glover, R.H.; Monger, W.A.; Mumford, R.; Jackeviciene, E.; Navalinskiene, M.; Samuitiene, M.; Boonham, N. Next-generation sequencing and metagenomic analysis: A universal diagnostic tool in plant virology. *Mol. Plant Pathol.* **2009**, *10*, 537–545. [CrossRef] [PubMed]
55. Barba, M.; Czosnek, H.; Hadidi, A. Historical Perspective, Development and Applications of Next-Generation Sequencing in Plant Virology. *Viruses* **2014**, *6*, 106–136. [CrossRef] [PubMed]
56. Wu, Q.; Habili, N.; Constable, F.; Al Rwahnih, M.A.; Goszczynski, D.E.; Wang, Y.; Pagay, V. Virus Pathogens in Australian Vineyards with an Emphasis on Shiraz Disease. *Viruses* **2020**, *12*, 818. [CrossRef]
57. Pecman, A.; Kutnjak, D.; Gutiérrez-Aguirre, I.; Adams, I.; Fox, A.; Boonham, N.; Ravnikar, M. Next Generation Sequencing for Detection and Discovery of Plant Viruses and Viroids: Comparison of Two Approaches. *Front. Microbiol.* **2017**, *8*, 1998. [CrossRef]
58. Blawid, R.; Silva, J.M.F.; Nagata, T. Discovering and sequencing new plant viral genomes by next-generation sequencing: Description of a practical pipeline. *Ann. Appl. Biol.* **2017**, *170*, 301–314. [CrossRef]
59. Rudkin, G.T.; Stollar, B.D. High resolution detection of DNA–RNA hybrids in situ by indirect immunofluorescence. *Nature* **1977**, *265*, 472–473. [CrossRef]
60. Kliot, A.; Kontsedalov, S.; Lebedev, G.; Brumin, M.; Cathrin, P.B.; Marubayashi, J.M.; Škaljac, M.; Belausov, E.; Czosnek, H.; Ghanim, M. Fluorescence in situ Hybridizations (FISH) for the Localization of Viruses and Endosymbiotic Bacteria in Plant and Insect Tissues. *J. Vis. Exp.* **2014**, *84*, e51030. [CrossRef]
61. Shargil, D.; Zemach, H.; Belausov, E.; Lachman, O.; Kamenetsky, R.; Dombrovsky, A. Development of a fluorescent in situ hybridization (FISH) technique for visualizing CGMMV in plant tissues. *J. Virol. Methods* **2015**, *223*, 55–60. [CrossRef]
62. Iannelli, D.; D'Apice, L.; Cottone, C.; Viscardi, M.; Scala, F.; Zoina, A.; Del Sorbo, G.; Spigno, P.; Capparelli, R. Simultaneous detection of cucumber mosaic virus, tomato mosaic virus and potato virus Y by flow cytometry. *J. Virol. Methods* **1997**, *69*, 137–145. [CrossRef]
63. D'Hondt, L.; Höfte, M.; VAN Bockstaele, E.; Leus, L. Applications of flow cytometry in plant pathology for genome size determination, detection and physiological status. *Mol. Plant Pathol.* **2011**, *12*, 815–828. [CrossRef] [PubMed]
64. Constable, F.E. *A review of Diagnostic Technologies to Benefit the Australian Nursery Industry*; Hort Innovation: North Sydney, Australia, 2019.
65. Luo, W.; Pietravalle, S.; Parnell, S.; van den Bosch, F.; Gottwald, T.R.; Irey, M.S.; Parker, S.R. An improved regulatory sampling method for mapping and representing plant disease from a limited number of samples. *Epidemics* **2012**, *4*, 68–77. [CrossRef] [PubMed]
66. Jones, R.A.C. Control of plant virus diseases. *Adv. Virus Res.* **2006**, *67*, 205–244. [CrossRef]
67. Bock, C.H.; Poole, G.H.; Parker, P.E.; Gottwald, T.R. Plant Disease Severity Estimated Visually, by Digital Photography and Image Analysis, and by Hyperspectral Imaging. *Crit. Rev. Plant Sci.* **2010**, *29*, 59–107. [CrossRef]

68. Smith, K.M. Testing for viruses: Indicator plants. In *Plant Viruses*; Smith, K.M., Ed.; Springer: Dordrecht, The Netherlands, 1977; pp. 175–180. [CrossRef]
69. Wolfenden, R.; Henderson, C.; Dennien, S. *Innovating New Virus Diagnostics and Planting Bed Management in the Australian Sweetpotato Industry*; Hort Innovation: North Sydney, Australia, 2018.
70. Constable, F.E.; Connellan, J.; Nicholas, P.; Rodoni, B.C. The reliability of woody indexing for detection of grapevine virus-associated diseases in three different climatic conditions in Australia. *Aust. J. Grape Wine Res.* **2012**, *19*, 74–80. [CrossRef]
71. Santos, J.L.; Farahi, F. *Handbook of Optical Sensors*; Taylor & Francis: London, UK, 2014; pp. 3–11.
72. Lee, W.S.; Alchanatis, V.; Yang, C.; Hirafuji, M.; Moshou, D.; Li, C. Sensing technologies for precision specialty crop production. *Comput. Electron. Agric.* **2010**, *74*, 2–33. [CrossRef]
73. Mahlein, A.-K.; Oerke, E.-C.; Steiner, U.; Dehne, H.-W. Recent advances in sensing plant diseases for precision crop protection. *Eur. J. Plant Pathol.* **2012**, *133*, 197–209. [CrossRef]
74. Heim, R.H.J.; Carnegie, A.J.; Zarco-Tejada, P.J. Breaking down barriers between remote sensing and plant pathology. *Trop. Plant Pathol.* **2019**, *44*, 398–400. [CrossRef]
75. Thomas, S.; Kuska, M.T.; Bohnenkamp, D.; Brugger, A.; Alisaac, E.; Wahabzada, M.; Behmann, J.; Mahlein, A.-K. Benefits of hyperspectral imaging for plant disease detection and plant protection: A technical perspective. *J. Plant Dis. Prot.* **2017**, *125*, 5–20. [CrossRef]
76. Mahlein, A.-K. Plant Disease Detection by Imaging Sensors—Parallels and Specific Demands for Precision Agriculture and Plant Phenotyping. *Plant Dis.* **2016**, *100*, 241–251. [CrossRef] [PubMed]
77. Oerke, E.-C.; Mahlein, A.-K.; Steiner, U. Proximal Sensing of Plant Diseases. In *Detection and Diagnostics of Plant Pathogens*; Gullino, M.L., Bonants, P.J.M., Eds.; Springer: Dordrecht, The Netherlands, 2014; Volume 5, pp. 55–70. [CrossRef]
78. Jones, R. Trends in plant virus epidemiology: Opportunities from new or improved technologies. *Virus Res.* **2014**, *186*, 3–19. [CrossRef] [PubMed]
79. Adão, T.; Hruška, J.; Pádua, L.; Bessa, J.; Peres, E.; Morais, R.; Sousa, J.J. Hyperspectral imaging: A review on UAV-based sensors, data processing and applications for agriculture and forestry. *Remote Sens.* **2017**, *9*, 1110. [CrossRef]
80. Gautam, D.; Pagay, V. A Review of Current and Potential Applications of Remote Sensing to Study the Water Status of Horticultural Crops. *Agronomy* **2020**, *10*, 140. [CrossRef]
81. Aasen, H.; Honkavaara, E.; Lucieer, A.; Zarco-Tejada, P.J. Quantitative Remote Sensing at Ultra-High Resolution with UAV Spectroscopy: A Review of Sensor Technology, Measurement Procedures, and Data Correction Workflows. *Remote Sens.* **2018**, *10*, 1091. [CrossRef]
82. Hirsch, R. *Exploring Colour Photography: A Complete Guide*; Laurence King: London, UK, 2004.
83. Mohanty, S.P.; Hughes, D.P.; Salathé, M. Using Deep Learning for Image-Based Plant Disease Detection. *Front. Plant Sci.* **2016**, *7*, 1419. [CrossRef]
84. Ferentinos, K.P. Deep learning models for plant disease detection and diagnosis. *Comput. Electron. Agric.* **2018**, *145*, 311–318. [CrossRef]
85. Wiesner-Hanks, T.; Wu, H.; Stewart, E.; DeChant, C.; Kaczmar, N.; Lipson, H.; Gore, M.A.; Nelson, R.J. Millimeter-Level Plant Disease Detection From Aerial Photographs via Deep Learning and Crowdsourced Data. *Front. Plant Sci.* **2019**, *10*, 1550. [CrossRef]
86. Zhou, X.-G.; Zhang, D.; Lin, F. *UAV Remote Sensing: An Innovative Tool for Detection and Management of Rice Diseases*; IntechOpen: London, UK, 2021. [CrossRef]
87. Kang, H.R. Multispectral imaging. In *Computational Color Technology*; Kang, H.R., Ed.; SPIE Press: Bellingham, WC, USA, 2006; pp. 301–324. [CrossRef]
88. Ünsalan, C.; Boyer, K.L. *Multispectral Satellite Image Understanding: From Land Classification to Building and Road Detection*; Springer: London, UK, 2011; pp. 49–119.
89. Curran, P.J.; Windham, W.R.; Gholz, H.L. Exploring the relationship between reflectance red edge and chlorophyll concentration in slash pine leaves. *Tree Physiol.* **1995**, *15*, 203–206. [CrossRef]
90. Mulla, D.J. Twenty five years of remote sensing in precision agriculture: Key advances and remaining knowledge gaps. *Biosyst. Eng.* **2013**, *114*, 358–371. [CrossRef]
91. Rouse, J.W., Jr.; Harlan, J.C.; Haas, R.H.; Schell, J.A.; Deering, D.W. Monitoring the Vernal Advancement and Retrogradation (Green Wave Effect) of Natural Vegetation. NASA/GSFCT Type III Final Report 1974, NASA-CR-144661. Available online: https://ntrs.nasa.gov/citations/19740022555 (accessed on 12 May 2021).
92. Davy, S.H. NDVI from A to Z. In *The Normalized Difference Vegetation Index*; Pettorelli, N., Ed.; OUP Oxford: Oxford, UK, 2013; pp. 30–43.
93. Thenkabail, P.S.; Lyon, J.G.; Huete, A. Advances in hyperspectral remote sensing of vegetation and agricultural croplands. In *Hyperspectral Remote Sensing of Vegetation*; Thenkabail, P.S., Lyon, J.G., Huete, A., Eds.; CRC Press: Boca Raton, FL, USA, 2011; pp. 3–35. [CrossRef]
94. Griffel, L.; Delparte, D.; Edwards, J. Using Support Vector Machines classification to differentiate spectral signatures of potato plants infected with Potato Virus Y. *Comput. Electron. Agric.* **2018**, *153*, 318–324. [CrossRef]
95. Naidu, R.A.; Perry, E.M.; Pierce, F.J.; Mekuria, T. The potential of spectral reflectance technique for the detection of Grapevine leafroll-associated virus-3 in two red-berried wine grape cultivars. *Comput. Electron. Agric.* **2009**, *66*, 38–45. [CrossRef]

96. Sinha, R.; Khot, L.R.; Rathnayake, A.P.; Gao, Z.; Naidu, R.A. Visible-near infrared spectroradiometry-based detection of grapevine leafroll-associated virus 3 in a red-fruited wine grape cultivar. *Comput. Electron. Agric.* **2019**, *162*, 165–173. [CrossRef]
97. Afonso, A.M.; Guerra, R.; Cavaco, A.M.; Pinto, P.; Andrade, A.; Duarte, A.; Power, D.M.; Marques, N.T. Identification of asymptomatic plants infected with Citrus tristeza virus from a time series of leaf spectral characteristics. *Comput. Electron. Agric.* **2017**, *141*, 340–350. [CrossRef]
98. Grisham, M.P.; Johnson, R.M.; Zimba, P.V. Detecting Sugarcane yellow leaf virus infection in asymptomatic leaves with hyperspectral remote sensing and associated leaf pigment changes. *J. Virol. Methods* **2010**, *167*, 140–145. [CrossRef]
99. Qin, J. Hyperspectral imaging instruments. In *Hyperspectral Imaging for Food Quality Analysis and Control*; Sun, D.-W., Ed.; Academic Press: San Diego, CA, USA, 2010; pp. 129–172. [CrossRef]
100. MacDonald, S.L.; Staid, M.; Staid, M.; Cooper, M.L. Remote hyperspectral imaging of grapevine leafroll-associated virus 3 in cabernet sauvignon vineyards. *Comput. Electron. Agric.* **2016**, *130*, 109–117. [CrossRef]
101. Wang, D.; Vinson, R.; Holmes, M.; Seibel, G.; Bechar, A.; Nof, S.; Tao, Y. Early Detection of Tomato Spotted Wilt Virus by Hyperspectral Imaging and Outlier Removal Auxiliary Classifier Generative Adversarial Nets (OR-AC-GAN). *Sci. Rep.* **2019**, *9*, 4377. [CrossRef]
102. Gorbe, E.; Calatayud, A. Applications of chlorophyll fluorescence imaging technique in horticultural research: A review. *Sci. Hortic.* **2012**, *138*, 24–35. [CrossRef]
103. Daley, P.F. Chlorophyll fluorescence analysis and imaging in plant stress and disease. *Can. J. Plant Pathol.* **1995**, *17*, 167–173. [CrossRef]
104. Osmond, C.B.; Daley, P.F.; Badger, M.R.; Lüttge, U. Chlorophyll Fluorescence Quenching During Photosynthetic Induction in Leaves of Abutilon striatum Dicks. Infected with Abutilon Mosaic Virus, Observed with a Field-Portable Imaging System. *Bot. Acta* **1998**, *111*, 390–397. [CrossRef]
105. Pineda, M.; Soukupová, J.; Matouš, K.; Nedbal, L.; Barón, M. Conventional and combinatorial chlorophyll fluorescence imaging of tobamovirus-infected plants. *Photosynthetica* **2008**, *46*, 441–451. [CrossRef]
106. Spoustová, P.; Synková, H.; Valcke, R.; Čeřovská, N. Chlorophyll a fluorescence as a tool for a study of the Potato virus Y effects on photosynthesis of nontransgenic and transgenic Pssu-ipt tobacco. *Photosynthetica* **2013**, *51*, 191–201. [CrossRef]
107. Lei, R.; Jiang, H.; Hu, F.; Yan, J.; Zhu, S. Chlorophyll fluorescence lifetime imaging provides new insight into the chlorosis induced by plant virus infection. *Plant Cell Rep.* **2016**, *36*, 327–341. [CrossRef] [PubMed]
108. Chaerle, L.; Lenk, S.; Hagenbeek, D.; Buschmann, C.; Van Der Straeten, D. Multicolor fluorescence imaging for early detection of the hypersensitive reaction to tobacco mosaic virus. *J. Plant Physiol.* **2007**, *164*, 253–262. [CrossRef]
109. Pérez-Bueno, M.L.; Pineda, M.; Barón, M. Phenotyping Plant Responses to Biotic Stress by Chlorophyll Fluorescence Imaging. *Front. Plant Sci.* **2019**, *10*, 1135. [CrossRef]
110. Fernandez-Jaramillo, A.A.; Duarte-Galvan, C.; Contreras-Medina, L.M.; Torres-Pacheco, I.; Romero-Troncoso, R.D.J.; Guevara-Gonzalez, R.G.; Millan-Almaraz, J.R. Instrumentation in Developing Chlorophyll Fluorescence Biosensing: A Review. *Sensors* **2012**, *12*, 11853–11869. [CrossRef] [PubMed]
111. Ni, Z.; Lu, Q.; Huo, H.; Zhang, H. Estimation of Chlorophyll Fluorescence at Different Scales: A Review. *Sensors* **2019**, *19*, 3000. [CrossRef] [PubMed]
112. Grace, J.; Nichol, C.; Disney, M.; Lewis, P.; Quaife, T.; Bowyer, P. Can we measure terrestrial photosynthesis from space directly, using spectral reflectance and fluorescence? *Glob. Chang. Biol.* **2007**, *13*, 1484–1497. [CrossRef]
113. Zarco-Tejada, P.J.; Jimenez-Berni, J.A.; Suárez, L.; Sepulcre-Cantó, G.; Morales, F.; Miller, J.R. Imaging chlorophyll fluorescence with an airborne narrow-band multispectral camera for vegetation stress detection. *Remote Sens. Environ.* **2009**, *113*, 1262–1275. [CrossRef]
114. MacArthur, A.; Robinson, I.C.; Rossini, M.; Davis, N.; Macdonald, K. A dual-field-of-view spectrometer system for reflectance and fluorescence measurements (Piccolo Doppio) and correction of etaloning. In Proceedings of the Fifth International Workshop on Remote Sensing of Vegetation Fluorescence, Paris, France, 22–24 April 2014.
115. Chang, C.Y.; Zhou, R.; Kira, O.; Marri, S.; Skovira, J.; Gu, L.; Sun, Y. An Unmanned Aerial System (UAS) for concurrent measurements of solar-induced chlorophyll fluorescence and hyperspectral reflectance toward improving crop monitoring. *Agric. For. Meteorol.* **2020**, *294*, 108145. [CrossRef]
116. Vargas, J.Q.; Bendig, J.; Mac Arthur, A.; Burkart, A.; Julitta, T.; Maseyk, K.; Thomas, R.; Siegmann, B.; Rossini, M.; Celesti, M.; et al. Unmanned Aerial Systems (UAS)-Based Methods for Solar Induced Chlorophyll Fluorescence (SIF) Retrieval with Non-Imaging Spectrometers: State of the Art. *Remote Sens.* **2020**, *12*, 1624. [CrossRef]
117. Khanal, S.; Fulton, J.; Shearer, S. An overview of current and potential applications of thermal remote sensing in precision agriculture. *Comput. Electron. Agric.* **2017**, *139*, 22–32. [CrossRef]
118. Chaerle, L.; Van Caeneghem, W.; Messens, E.; Lambers, H.; Van Montagu, M.; Van Der Straeten, D. Presymptomatic visualization of plant–virus interactions by thermography. *Nat. Biotechnol.* **1999**, *17*, 813–816. [CrossRef] [PubMed]
119. Zhu, W.; Chen, H.; Ciechanowska, I.; Spaner, D. Application of infrared thermal imaging for the rapid diagnosis of crop disease. *IFAC-PapersOnLine* **2018**, *51*, 424–430. [CrossRef]
120. Mandrile, L.; Rotunno, S.; Miozzi, L.; Vaira, A.M.; Giovannozzi, A.M.; Rossi, A.M.; Noris, E. Nondestructive Raman Spectroscopy as a Tool for Early Detection and Discrimination of the Infection of Tomato Plants by Two Economically Important Viruses. *Anal. Chem.* **2019**, *91*, 9025–9031. [CrossRef]

121. Farber, C.; Shires, M.; Ong, K.; Byrne, D.; Kurouski, D. Raman spectroscopy as an early detection tool for rose rosette infection. *Planta* **2019**, *250*, 1247–1254. [CrossRef]
122. Rys, M.; Juhász, C.; Surówka, E.; Janeczko, A.; Saja, D.; Tóbiás, I.; Skoczowski, A.; Barna, B.; Gullner, G. Comparison of a compatible and an incompatible pepper-tobamovirus interaction by biochemical and non-invasive techniques: Chlorophyll a fluorescence, isothermal calorimetry and FT-Raman spectroscopy. *Plant Physiol. Biochem.* **2014**, *83*, 267–278. [CrossRef]
123. Yeturu, S.; Jentzsch, P.V.; Ciobotă, V.; Guerrero, R.; Garrido, P.; Ramos, L.A. Handheld Raman spectroscopy for the early detection of plant diseases: *Abutilon mosaic* virus infecting *Abutilon* sp. *Anal. Methods* **2016**, *8*, 3450–3457. [CrossRef]
124. Choi, Y.H.; Kim, H.K.; Linthorst, H.J.M.; Hollander, J.G.; Lefeber, A.W.M.; Erkelens, C.; Nuzillard, A.J.-M.; Verpoorte, R. NMR Metabolomics to Revisit the Tobacco Mosaic Virus Infection in *Nicotiana tabacum* Leaves. *J. Nat. Prod.* **2006**, *69*, 742–748. [CrossRef]
125. López-Gresa, M.P.; Lisón, P.; Kim, H.K.; Choi, Y.H.; Verpoorte, R.; Rodrigo, I.; Conejero, V.; Bellés, J.M. Metabolic fingerprinting of Tomato Mosaic Virus infected *Solanum lycopersicum*. *J. Plant Physiol.* **2012**, *169*, 1586–1596. [CrossRef]
126. Lee, C.; Lee, S.-Y.; Kim, J.-Y.; Jung, H.-Y.; Kim, J. Optical Sensing Method for Screening Disease in Melon Seeds by Using Optical Coherence Tomography. *Sensors* **2011**, *11*, 9467–9477. [CrossRef] [PubMed]
127. Hao, C.T.; Eddie, T.K.-M.; Beng-Koon, N.; Sirajudeen, G.R.; Meng, T.C.; Fatt, C.T.; Tang, P.W. Diagnosis of virus infection in orchid plants with high-resolution optical coherence tomography. *J. Biomed. Opt.* **2009**, *14*, 014006. [CrossRef]
128. Lee, S.-Y.; Lee, C.; Kim, J.; Jung, H.-Y. Application of optical coherence tomography to detect Cucumber green mottle mosaic virus (CGMMV) infected cucumber seed. *Hortic. Environ. Biotechnol.* **2012**, *53*, 428–433. [CrossRef]
129. Ose, K.; Corpetti, T.; Demagistri, L. Multispectral satellite image processing. In *Optical Remote Sensing of Land Surface*; Elsevier: Oxford, UK, 2016; pp. 57–124. [CrossRef]
130. Hastie, T.; Tibshirani, R.; Friedman, J.H. *The Elements of Statistical Learning: Data Mining, Inference, and Prediction*, 2nd ed.; Springer: New York, NY, USA, 2009; pp. 9–42.
131. Sinha, P.; Balas, B.; Ostrovsky, Y.; Russell, R. Face Recognition by Humans: Nineteen Results All Computer Vision Researchers Should Know About. *Proc. IEEE* **2006**, *94*, 1948–1962. [CrossRef]
132. Pathak, A.R.; Pandey, M.; Rautaray, S. Application of deep learning for object detection. *Procedia Comput. Sci.* **2018**, *132*, 1706–1717. [CrossRef]
133. Esteva, A.; Chou, K.; Yeung, S.; Naik, N.; Madani, A.; Mottaghi, A.; Liu, Y.; Topol, E.; Dean, J.; Socher, R. Deep learning-enabled medical computer vision. *npj Digit. Med.* **2021**, *4*, 5. [CrossRef]
134. Hughes, D.P.; Salathe, M. An open access repository of images on plant health to enable the development of mobile disease diagnostics. *arXiv* **2016**, arXiv:1511.08060.
135. Ramcharan, A.; Baranowski, K.; McCloskey, P.; Ahmed, B.; Legg, J.; Hughes, D.P. Deep Learning for Image-Based Cassava Disease Detection. *Front. Plant Sci.* **2017**, *8*, 1852. [CrossRef]
136. Polder, G.; van de Westeringh, N.; Kool, J.; Khan, H.A.; Kootstra, G.; Nieuwenhuizen, A. Automatic Detection of Tulip Breaking Virus (TBV) Using a Deep Convolutional Neural Network. *IFAC-PapersOnLine* **2019**, *52*, 12–17. [CrossRef]
137. Selvaraj, M.G.; Vergara, A.; Montenegro, F.; Ruiz, H.A.; Safari, N.; Raymaekers, D.; Ocimati, W.; Ntamwira, J.; Tits, L.; Omondi, A.B.; et al. Detection of banana plants and their major diseases through aerial images and machine learning methods: A case study in DR Congo and Republic of Benin. *ISPRS J. Photogramm. Remote Sens.* **2020**, *169*, 110–124. [CrossRef]
138. Sugiura, R.; Tsuda, S.; Tsuji, H.; Murakami, N. Virus-infected plant detection in potato seed production field by uav imagery. In Proceedings of the 2018 ASABE Annual International Meeting, Detroit, MI, USA, 29 July–1 August 2018. [CrossRef]
139. Barbedo, J.G.A. Plant disease identification from individual lesions and spots using deep learning. *Biosyst. Eng.* **2019**, *180*, 96–107. [CrossRef]
140. Barbedo, J.G.A. Impact of dataset size and variety on the effectiveness of deep learning and transfer learning for plant disease classification. *Comput. Electron. Agric.* **2018**, *153*, 46–53. [CrossRef]
141. Thenkabail, P.S.; Smith, R.B.; De-Pauw, E. Evaluation of narrowband and broadband vegetation indices for determining optimal hyperspectral wavebands for agricultural crop characterization. *Photogramm. Eng. Remote Sens.* **2002**, *68*, 607–622.
142. Yao, X.; Zhu, Y.; Tian, Y.; Feng, W.; Cao, W. Exploring hyperspectral bands and estimation indices for leaf nitrogen accumulation in wheat. *Int. J. Appl. Earth Obs. Geoinf.* **2010**, *12*, 89–100. [CrossRef]
143. Roberts, D.A.; Roth, K.L.; Perroy, R.L. Hyperspectral vegetation indices. In *Hyperspectral Remote Sensing of Vegetation*; Thenkabail, P.S., Lyon, J.G., Huete, A., Eds.; CRC Press: Boca Raton, FL, USA, 2011. [CrossRef]
144. Tocqueville, A.D. Vegetation indices. In *The Normalized Difference Vegetation Index*; Pettorelli, N., Ed.; OUP Oxford: Oxford, UK, 2013; pp. 18–29.
145. Prabhakar, M.; Prasad, Y.G.; Rao, M.N. Remote sensing of biotic stress in crop plants and its applications for pest management. In *Crop Stress and its Management: Perspectives and Strategies*; Venkateswarlu, B., Shanker, A., Shanker, C., Maheswari, M., Eds.; Springer: Dordrecht, The Netherlands, 2012; pp. 517–545. [CrossRef]
146. Mirik, M.; Jones, D.C.; Price, J.A.; Workneh, F.; Ansley, R.J.; Rush, C.M. Satellite Remote Sensing of Wheat Infected by Wheat streak mosaic virus. *Plant Dis.* **2011**, *95*, 4–12. [CrossRef]
147. Hou, J.; Li, L.; He, J. Detection of grapevine leafroll disease based on 11-index imagery and ant colony clustering algorithm. *Precis. Agric.* **2016**, *17*, 488–505. [CrossRef]
148. Gao, W. Improved Ant Colony Clustering Algorithm and Its Performance Study. *Comput. Intell. Neurosci.* **2015**, *2016*, 1–14. [CrossRef]

149. Steddom, K.; Heidel, G.; Jones, D.; Rush, C.M. Remote Detection of Rhizomania in Sugar Beets. *Phytopathology* **2003**, *93*, 720–726. [CrossRef]
150. Bajwa, S.; Kulkarni, S. Hyperspectral Data Mining. In *Hyperspectral Remote Sensing of Vegetation*; Thenkabail, P.S., Lyon, J.G., Huete, A., Eds.; CRC Press: Boca Raton, FL, USA, 2011; pp. 93–120. [CrossRef]
151. Qi, J.; Inoue, Y.; Wiangwang, N. Hyperspectral remote sensing in global change studies. In *Hyperspectral Remote Sensing of Vegetation*; Thenkabail, P.S., Lyon, J.G., Huete, A., Eds.; CRC Press: Boca Raton, FL, USA, 2011; pp. 69–91. [CrossRef]
152. Cogato, A.; Wu, L.; Jewan, S.Y.Y.; Meggio, F.; Marinello, F.; Sozzi, M.; Pagay, V. Evaluating the Spectral and Physiological Responses of Grapevines (*Vitis vinifera* L.) to Heat and Water Stresses under Different Vineyard Cooling and Irrigation Strategies. *Agronomy* **2021**, *11*, 1940. [CrossRef]
153. Stocchero, M.; De Nardi, M.; Scarpa, B. PLS for classification. *Chemom. Intell. Lab. Syst.* **2021**, *216*, 104374. [CrossRef]
154. Soares, S.F.C.; Gomes, A.D.A.; Araujo, M.C.U.; Filho, A.R.G.; Galvão, A. The successive projections algorithm. *TrAC Trends Anal. Chem.* **2012**, *42*, 84–98. [CrossRef]
155. Yeh, Y.-H.F.; Chung, W.-C.; Liao, J.-Y.; Chung, C.-L.; Kuo, Y.-F.; Lin, T.-T. A Comparison of Machine Learning Methods on Hyperspectral Plant Disease Assessments. *IFAC Proc. Vol.* **2013**, *46*, 361–365. [CrossRef]
156. Zhu, H.; Chu, B.; Zhang, C.; Liu, F.; Jiang, L.; He, Y. Hyperspectral Imaging for Presymptomatic Detection of Tobacco Disease with Successive Projections Algorithm and Machine-learning Classifiers. *Sci. Rep.* **2017**, *7*, 4125. [CrossRef]
157. Bagheri, N.; Mohamadi-Monavar, H.; Azizi, A.; Ghasemi, A. Detection of Fire Blight disease in pear trees by hyperspectral data. *Eur. J. Remote Sens.* **2017**, *51*, 1–10. [CrossRef]
158. Sun, W.; Du, Q. Hyperspectral Band Selection: A Review. *IEEE Geosci. Remote Sens. Mag.* **2019**, *7*, 118–139. [CrossRef]
159. Pagay, V.; Habili, N.; Wu, Q.; Coleman, D. Rapid and non-destructive detection of Shiraz disease and grapevine leafroll disease on asymptomatic grapevines in Australian vineyards. In Proceedings of the 19th Congress of the International Council for the study of Virus and Virus-like Diseases of Grapevine, Santiago, Chile, 9–12 April 2018.
160. Polder, G.; van der Heijden, G.W.A.M.; van Doorn, J.; Clevers, J.G.P.W.; van der Schoor, R.; Baltissen, A.H.M.C. Detection of the tulip breaking virus (TBV) in tulips using optical sensors. *Precis. Agric.* **2010**, *11*, 397–412. [CrossRef]
161. Al-Saddik, H.; Simon, J.C.; Cointault, F. Assessment of the optimal spectral bands for designing a sensor for vineyard disease detection: The case of 'Flavescence dorée'. *Precis. Agric.* **2018**, *20*, 398–422. [CrossRef]
162. Bendel, N.; Kicherer, A.; Backhaus, A.; Köckerling, J.; Maixner, M.; Bleser, E.; Klück, H.-C.; Seiffert, U.; Voegele, R.T.; Töpfer, R.J.R.S. Detection of grapevine leafroll-associated virus 1 and 3 in white and red grapevine cultivars using hyperspectral imaging. *Remote Sens.* **2020**, *12*, 1693. [CrossRef]
163. Audebert, N.; Le Saux, B.; Lefèvre, S. Deep Learning for Classification of Hyperspectral Data: A Comparative Review. *IEEE Geosci. Remote Sens. Mag.* **2019**, *7*, 159–173. [CrossRef]
164. Li, Y.; Zhang, H.; Shen, Q. Spectral–Spatial Classification of Hyperspectral Imagery with 3D Convolutional Neural Network. *Remote Sens.* **2017**, *9*, 67. [CrossRef]
165. Wang, C.; Ma, N.; Ming, Y.; Wang, Q.; Xia, J. Classification of hyperspectral imagery with a 3D convolutional neural network and J-M distance. *Adv. Space Res.* **2019**, *64*, 886–899. [CrossRef]
166. Yang, J.; Zhao, Y.-Q.; Chan, J.C.-W.; Xiao, L. A Multi-Scale Wavelet 3D-CNN for Hyperspectral Image Super-Resolution. *Remote Sens.* **2019**, *11*, 1557. [CrossRef]
167. Yang, X.; Zhang, X.; Ye, Y.; Lau, R.; Lu, S.; Li, X.; Huang, X. Synergistic 2D/3D Convolutional Neural Network for Hyperspectral Image Classification. *Remote Sens.* **2020**, *12*, 2033. [CrossRef]
168. Nguyen, C.; Sagan, V.; Maimaitiyiming, M.; Maimaitijiang, M.; Bhadra, S.; Kwasniewski, M.T. Early Detection of Plant Viral Disease Using Hyperspectral Imaging and Deep Learning. *Sensors* **2021**, *21*, 742. [CrossRef]
169. Rangarajan, A.K.; Purushothaman, R.; Ramesh, A. Tomato crop disease classification using pre-trained deep learning algorithm. *Procedia Comput. Sci.* **2018**, *133*, 1040–1047. [CrossRef]
170. Oh, S.; Ashapure, A.; Marconi, T.G.; Jung, J.; Landivar, J.; Thomasson, J.A.; McKee, M.; Moorhead, R.J. UAS based Tomato yellow leaf curl virus (TYLCV) disease detection system. In Proceedings of the SPIE Defense + Commercial Sensing, Baltimore, MA, USA, 14 May 2019. [CrossRef]
171. Junges, A.H.; Almança, M.A.K.; Fajardo, T.V.M.; Ducati, J.R. Leaf hyperspectral reflectance as a potential tool to detect diseases associated with vineyard decline. *Trop. Plant Pathol.* **2020**, *45*, 522–533. [CrossRef]
172. Berdugo, C.A.; Zito, R.; Paulus, S.; Mahlein, A.-K. Fusion of sensor data for the detection and differentiation of plant diseases in cucumber. *Plant Pathol.* **2014**, *63*, 1344–1356. [CrossRef]
173. Pietersen, G.; Harris, M. Poor detection of grapevine leafroll disease in the rootstock Richter 99 (*Vitis berlandieri* X *Vitis rupestris*). In Proceedings of the 19th Congress of the International Council for the Study of Virus and Virus-Like Diseases of the Grapevine (ICVG), Santiago, Chile, 28–29 April 2018.
174. Cheong, J.; Yu, H.; Lee, C.Y.; Lee, J.-U.; Choi, H.-J.; Lee, J.-H.; Lee, H.; Cheon, J. Fast detection of SARS-CoV-2 RNA via the integration of plasmonic thermocycling and fluorescence detection in a portable device. *Nat. Biomed. Eng.* **2020**, *4*, 1159–1167. [CrossRef]
175. Seo, G.; Lee, G.; Kim, M.J.; Baek, S.-H.; Choi, M.; Ku, K.B.; Lee, C.-S.; Jun, S.; Park, D.; Kim, H.G.; et al. Rapid Detection of COVID-19 Causative Virus (SARS-CoV-2) in Human Nasopharyngeal Swab Specimens Using Field-Effect Transistor-Based Biosensor. *ACS Nano* **2020**, *14*, 5135–5142; Erratum in *ACS Nano* **2020**, *14*, 12257–12258. [CrossRef]

176. Elsheakh, D.M.; Ahmed, M.I.; Elashry, G.M.; Moghannem, S.M.; Elsadek, H.A.; Elmazny, W.N.; Alieldin, N.H.; Abdallah, E.A. Rapid Detection of Coronavirus (COVID-19) Using Microwave Immunosensor Cavity Resonator. *Sensors* **2021**, *21*, 7021. [CrossRef]
177. Papadakis, G.; Pantazis, A.K.; Fikas, N.; Chatziioannidou, S.; Tsiakalou, V.; Michaelidou, K.; Pogka, V.; Megariti, M.; Vardaki, M.; Giarentis, K.; et al. Portable real-time colorimetric LAMP-device for rapid quantitative detection of nucleic acids in crude samples. *Sci. Rep.* **2022**, *12*, 3775. [CrossRef] [PubMed]
178. Liu, X.; Zhang, J.; Cai, Y.; Zhang, S.; Ma, K.; Hua, K.; Cui, Y. A novel DNA methylation biosensor by combination of isothermal amplification and lateral flow device. *Sens. Actuators B Chem.* **2021**, *333*, 129624. [CrossRef]
179. Xun, G.; Lane, S.T.; Petrov, V.A.; Pepa, B.E.; Zhao, H. A rapid, accurate, scalable, and portable testing system for COVID-19 diagnosis. *Nat. Commun.* **2021**, *12*, 2905. [CrossRef] [PubMed]
180. Li, N.; Ho, C.P.; Wang, I.-T.; Pitchappa, P.; Fu, Y.H.; Zhu, Y.; Lee, L.Y.T. Spectral imaging and spectral LIDAR systems: Moving toward compact nanophotonics-based sensing. *Nanophotonics* **2021**, *10*, 1437–1467. [CrossRef]
181. Iseli, C.; Lucieer, A. Tree species classification based on 3D spectral point clouds and orthomosaics acquired by snapshot hyperspectral UAS sensor. In Proceedings of the ISPRS Geospatial Week 2019, Enschede, The Netherlands, 10–14 June 2019; pp. 379–384. [CrossRef]
182. Ounis, A.; Bach, J.; Mahjoub, A.; Daumard, F.; Moya, I.; Goulas, Y. Combined use of LIDAR and hyperspectral measurements for remote sensing of fluorescence and vertical profile of canopies. *Span. Assoc. Remote Sens.* **2016**, *45*, 87–94. [CrossRef]
183. Jin, X.; Zarco-Tejada, P.J.; Schmidhalter, U.; Reynolds, M.P.; Hawkesford, M.J.; Varshney, R.K.; Yang, T.; Nie, C.; Li, Z.; Ming, B.; et al. High-Throughput Estimation of Crop Traits: A Review of Ground and Aerial Phenotyping Platforms. *IEEE Geosci. Remote Sens. Mag.* **2020**, *9*, 200–231. [CrossRef]
184. Singh, D.; Sao, R.; Singh, K. A remote sensing assessment of pest infestation on sorghum. *Adv. Space Res.* **2006**, *39*, 155–163. [CrossRef]
185. Mauck, K.E.; De Moraes, C.M.; Mescher, M.C. Deceptive chemical signals induced by a plant virus attract insect vectors to inferior hosts. *Proc. Natl. Acad. Sci. USA* **2010**, *107*, 3600–3605. [CrossRef]
186. Shulaev, V.; Silverman, P.; Raskin, I. Airborne signalling by methyl salicylate in plant pathogen resistance. *Nature* **1997**, *385*, 718–721. [CrossRef]
187. Brilli, F.; Loreto, F.; Baccelli, I. Exploiting Plant Volatile Organic Compounds (VOCs) in Agriculture to Improve Sustainable Defense Strategies and Productivity of Crops. *Front. Plant Sci.* **2019**, *10*, 624. [CrossRef]
188. Jansen, R.M.; Wildt, J.; Kappers, I.F.; Bouwmeester, H.J.; Hofstee, J.W.; van Henten, E.J. Detection of Diseased Plants by Analysis of Volatile Organic Compound Emission. *Annu. Rev. Phytopathol.* **2011**, *49*, 157–174. [CrossRef] [PubMed]

Chapter 3

Evaluating the potential of high-resolution RGB remote sensing to detect Shiraz Disease in grapevines

Wang, Y.M.; Ostendorf, B.; Pagay, V.

Preamble:

In the last chapter, the review article highlighted the availability of various non-destructive methods for disease detection. Among these methods, a simple approach utilizing small UAVs and high-resolution RGB cameras offers detailed information on grapevines, including size, shape, and colour. This information proves invaluable in the rapid detection of obvious symptoms such as SD in Shiraz. In this chapter, a simple method is described, wherein the high-resolution RGB images are utilised to calculate the size of the projected canopy area for SD detection. The findings from this study have been published in the open journal - *Australian Journal of Grape and Wine Research, Hindawi, 2023, 7376153*.

doi.org/10.1155/2023/7376153

Statement of Authorship

Title of Paper	Evaluating the potential of high-resolution visible remote sensing to detect Shiraz Disease in grapevines
Publication Status	☑ Published ☐ Accepted for Publication ☐ Submitted for Publication ☐ Unpublished and Unsubmitted work written in manuscript style
Publication Details	Hindawi, Australian Journal of Grape and Wine Research, Volume 2023, Article ID 7376153, 9 pages https://doi.org/10.1155/2023/7376153

Principal Author

Name of Principal Author (Candidate)	Yeniu (Mickey) Wang		
Contribution to the Paper	Designed the experiments Carried out the field and lab works to gather data Conducted data processing and analysis Drafted the manuscript and revision		
Overall percentage (%)	80%		
Certification:	This paper reports on original research I conducted during the period of my Higher Degree by Research candidature and is not subject to any obligations or contractual agreements with a third party that would constrain its inclusion in this thesis. I am the primary author of this paper.		
Signature		Date	13/06/2023

Co-Author Contributions

By signing the Statement of Authorship, each author certifies that:

i. the candidate's stated contribution to the publication is accurate (as detailed above);

ii. permission is granted for the candidate in include the publication in the thesis; and

iii. the sum of all co-author contributions is equal to 100% less the candidate's stated contribution.

Name of Co-Author	Bertram Ostendorf		
Contribution to the Paper	Conceptualisation Reviewed and edited the manuscript		
Signature		Date	20/06/2023

Name of Co-Author	Vinay Pagay		
Contribution to the Paper	Conceptualisation Reviewed and edited the manuscript Corresponding author		
Signature		Date	27/06/2023

Hindawi
Australian Journal of Grape and Wine Research
Volume 2023, Article ID 7376153, 9 pages
https://doi.org/10.1155/2023/7376153

AUSTRALIAN SOCIETY OF VITICULTURE AND OENOLOGY | ASVO

Research Article

Evaluating the Potential of High-Resolution Visible Remote Sensing to Detect Shiraz Disease in Grapevines

Yeniu Mickey Wang[1,2] **Bertram Ostendorf**[3] **and Vinay Pagay**[1]

[1]*School of Agriculture, Food & Wine, Waite Research Institute, University of Adelaide, PMB 1, Glen Osmond, SA 5064, Australia*
[2]*CSIRO, Manufacturing, Autonomous Sensors Future Science Platform, 13 Kintore Ave, Adelaide, SA 5000, Australia*
[3]*School of Biological Sciences, The University of Adelaide, Molecular Life Sciences Building, North Terrace Campus, Adelaide, SA 5005, Australia*

Correspondence should be addressed to Vinay Pagay; vinay.pagay@adelaide.edu.au

Received 11 November 2022; Revised 8 December 2022; Accepted 20 March 2023; Published 5 May 2023

Academic Editor: K. J. Evans

Background and Aims. Shiraz disease (SD) is a viral disease associated with *Grapevine virus A* that causes significant yield loss in economically important grape cultivars in Australia such as Shiraz and Merlot. Current diagnostic methods are time-consuming and costly. This study evaluates an alternative methodology using visible remote sensing imagery to detect SD in Shiraz grapevines. *Methods and Results*. High-resolution visible remote sensing images were captured of Shiraz grapevines in two South Australian viticultural regions over two seasons. The projected leaf area (PLA) of individual grapevines was estimated from the images. Virus-infected vines had significantly lower PLA than healthy vines in the early season but fewer difference after veraison. The lower PLA was only observed in grapevines coinfected with grapevine leafroll-associated viruses (GLRaVs) and Grapevine virus A (GVA). Shiraz vines infected with either GLRaVs or GVA had similar PLA to healthy vines. *Conclusions*. High-resolution RGB remote sensing technology has the potential to rapidly estimate SD infection in Shiraz grapevines. Our observations of shoot devigouration only in coinfected vines calls into question the etiology of SD. Further validation of the PLA technique incorporating different regions, seasons, cultivars, and combinations of viruses is needed for improving the robustness of the method. *Significance of the Study*. This preliminary study presents a new rapid and low-cost surveillance method to estimate SD infections in Shiraz vineyards, which could significantly lower the cost for growers who conduct on-ground SD visual assessments or lab-based tissue testing at the vineyard scale.

1. Introduction

Shiraz disease (SD) is a devastating viral disease of grapevines that was first reported on Merlot from South Africa [1]. SD disrupts the physiological development of grapevines and causes significant yield loss in specific cultivars, including Shiraz, Merlot, Malbec, and Sumoll [2]. The symptoms of SD infection in Shiraz include delayed budburst with restricted spring growth, lack of lignification on some canes, and delayed leaf senescence well into the dormant season [3, 4]. SD symptoms are latent (no symptoms) in tolerant cultivars such as Chardonnay and Cabernet Sauvignon; however, the viruses can be transmitted to susceptible cultivars (Shiraz and Melot) by mealybugs and soft scales [5, 6]. *Grapevine virus A* (GVA) group II variants were associated with SD [7, 8]. GVA also causes a rugose wood disease known as "Kober stem grooving" [9]. GVA often coexists with grapevine leafroll-associated viruses (GLRaVs) [6, 10–12], which is a group of viruses that causes Grapevine leaf disease (GLD) [13]. In Australia, GLRaV-1, GLRaV-3, and GLRaV-4 strain 9 (GLRaV-9) are commonly associated with GVA in SD-infected vines [14]. There are only a few effective methods to control grapevine viral diseases including roguing infected vines, replanting with certified, virus-free material, and controlling the vectors to stop the virus from spreading [15, 16]. It is therefore critical to accurately detect the patterns and extent of viral infections in vineyards to stop the virus from spreading further.

Standard detection methods for SD include serological methods, nucleic acid-based methods, and visual assessment [17, 18]. Lab-based methods are costly, thus limiting the number of grapevines tested and, consequently, an underestimation of the true incidence of virus infection in vineyards [17, 19]. Currently, the recommended minimum test rate by commercial diagnostic labs is five vines per thousand (0.5%) across the block [20]. Conducting on-ground visual assessments is labour-intensive, subjective, and sometimes unreliable. Low-altitude airborne remote sensing enables the capture of high detail with greater potential to rapidly survey the vineyards. Various optical sensors including red-green-blue (RGB), multispectral, hyperspectral, and thermal sensors have been used on the ground or platforms like unmanned aerial vehicles (UAVs) and manned fixed-wing aircraft for grapevine disease detection [21–26]. RGB imagery acquired through UAV-based remote sensing was used for the current study due to its relative simplicity compared to multi and hyperspectral images. A vertical projection of the canopy from the aerial image, the projected leaf area (PLA), for each vine was calculated from the image to compare the canopy size between healthy and SD-infected vines. PLA acquired from remote sensing imagery has a positive correlation to the canopy area. For example, Raj et al. [27] achieved an R^2 of 0.84 and RMSE of 0.36 by using PLA calculated from UAV RGB image and compared to leaf area index of maize.

In this study, we used high-resolution RGB remote sensing imagery to systematically assess PLA of individual healthy and diseased vines to predict SD infection in Shiraz grapevines in the field. The specific objectives of this study were: (1) to develop a simple remote sensing methodology that can consistently assess grapevine canopy size (using PLA as a surrogate) as a visual indicator of SD infection; (2) to confirm PLA-based disease status classification with lab-based tissue analysis; (3) to evaluate the time series of remote sensing imagery in order to conduct a spatial-within-season temporal analysis of canopy size differences between healthy and infected vines; and (4) to evaluate the temporal consistency of seasonal patterns of canopy development across multiple growing seasons. Our overarching goal was to develop a rapid and low-cost surveillance platform for SD detection at the vineyard scale.

2. Materials and Methods

2.1. Study Sites and Visual Estimation of Virus Infection. Two virus-infected Shiraz blocks (some vines previously tested positive with GVA and GLRaVs) were selected in different climatic wine regions in South Australia (SA) for this study. The first vineyard was in Monash, located in the warm inland region of Riverland (34°13′28″S, 140°33′01″E). A block of 1.5 ha of Shiraz was selected for the study. The soil type of vineyard was sand over limestone. The block was drip-irrigated with 7.5 ml·ha^{-1} of water per year. Approximate 50 kg ha^{-1} N and 50 kg·ha^{-1} P fertiliser were applied through fertigation annually. The vines were consistently machine spur pruned with a same size box shape each winter. Vineyard management was consistent between seasons. Integrated pest management was as per convention in this region, which generally has low disease pressure due to its warm-to-hot climate. The second vineyard was in the Barossa region, located in Lyndoch, SA (34°35′28″S, 138°53′01″E). A 1.5 ha block was chosen for the study. The soil type of the block was Calcic on red Sodosol. It was drip-irrigated with approximate 1 ml·ha^{-1} water per year. Both solid fertiliser and fertigation were applied at the rate of 130 kg·ha^{-1} N, 55 kg·ha^{-1} P, and 9 kg·ha^{-1} K annually. Shiraz was consistently two-bud spur pruned to 20 buds per m each winter. Details of the study sites (vineyards) are provided in Table 1.

2.2. Virus Testing. Laboratory-based tissue testing was used for ground-truthing (Figure 1(b)). Tissue samples were collected based on visual symptoms for virus testing, of which half the vines were symptomatic and half were asymptomatic. Leaf petioles were sampled near harvest time [28]. The leaves were carefully selected from the base of the shoots to avoid errors associated with sampling from a potential long shoot coming through from a neighbour vine. Four petioles near the base of the shoots (two from each side of the canopy) were sampled and transported with chilled ice packs.

All samples were virus-tested in the lab using an enzyme-linked immunosorbent assay (ELISA) [29]. The ELISA test kits produced by Bioreba (Reinach, Switzerland) were used to test GVA, GLRaV-1, GLRaV-3, and GLRaV-4 strains. 20% of these leaves samples were tested with reverse-transcription polymerase chain reaction (RT-PCR) [17, 30] for confirmation of the ELISA results. The RT-PCR test was conducted by a commercial diagnostics lab that routinely tests for grapevine viruses. Six commonly occurring grapevine viruses in Australia [31] were tested: GVA, GLRaV-1, GLRaV-3, GLRaV-4, GLRaV-4 strain 6, and GLRaV-4 strain 9. The result showed a 100% match between PCR and ELISA, confirming the reliability of the ELISA test. The number of vines in each class is shown in Table 2. Because GLRaV-1, -3, and -4 complexes cause similar GLD symptoms in grapevines, vines infected with either a single or combination of any GLRaVs were treated as a GLRaV infection. In total, there were four classes: (i) healthy, (ii) GVA only, (iii) GLRaVs only, and (iv) GVA + GLRaVs.

2.3. High-Resolution Remote Sensing: Data Collection and Processing. DJI Mavic 2 Pro (SZ DJI Technology Co., Ltd, Shenzhen, China) was used for image collection in this study (Figure 1(a)). The UAV uses a Hasselblad RGB camera with a 28 mm focal length and f/2.8–f/11 aperture. The field of view is approximate 77° and the image size is 5472 × 3648. Flight planning was automated by the Pix4D app (Pix4D S.A., Prilly, Switzerland) with the setting of nadir view, side and forward overlapping at approximate 80%, altitude at 45 m above ground level, and forward flight direction. The calculated spatial resolution of the images was approximate 1 cm pixel^{-1}.

Aerial image data were collected between October to April in S1 and September to April in S2. Data were captured at approximate monthly intervals (one flight per month) based on weather conditions (low wind and sunny) which resulted in six flights in Riverland and ten flights in Barossa (Table 1).

Table 1: Vineyard study sites used in the trial.

Vineyard locations	Planting year	Rootstock	Spacing (row × vine)	Vine density (vines ha^{-1})	Occurrence of symptoms (%)	Flight per season		Images per block
						S1	S2	
Riverland	1998	K51–40	3.5 × 3.5 m	816	5	6	8	288
Barossa	Grafted in 2015	Cabernet sauvignon	3.2 × 1.5 m	2165	15	10	8	290

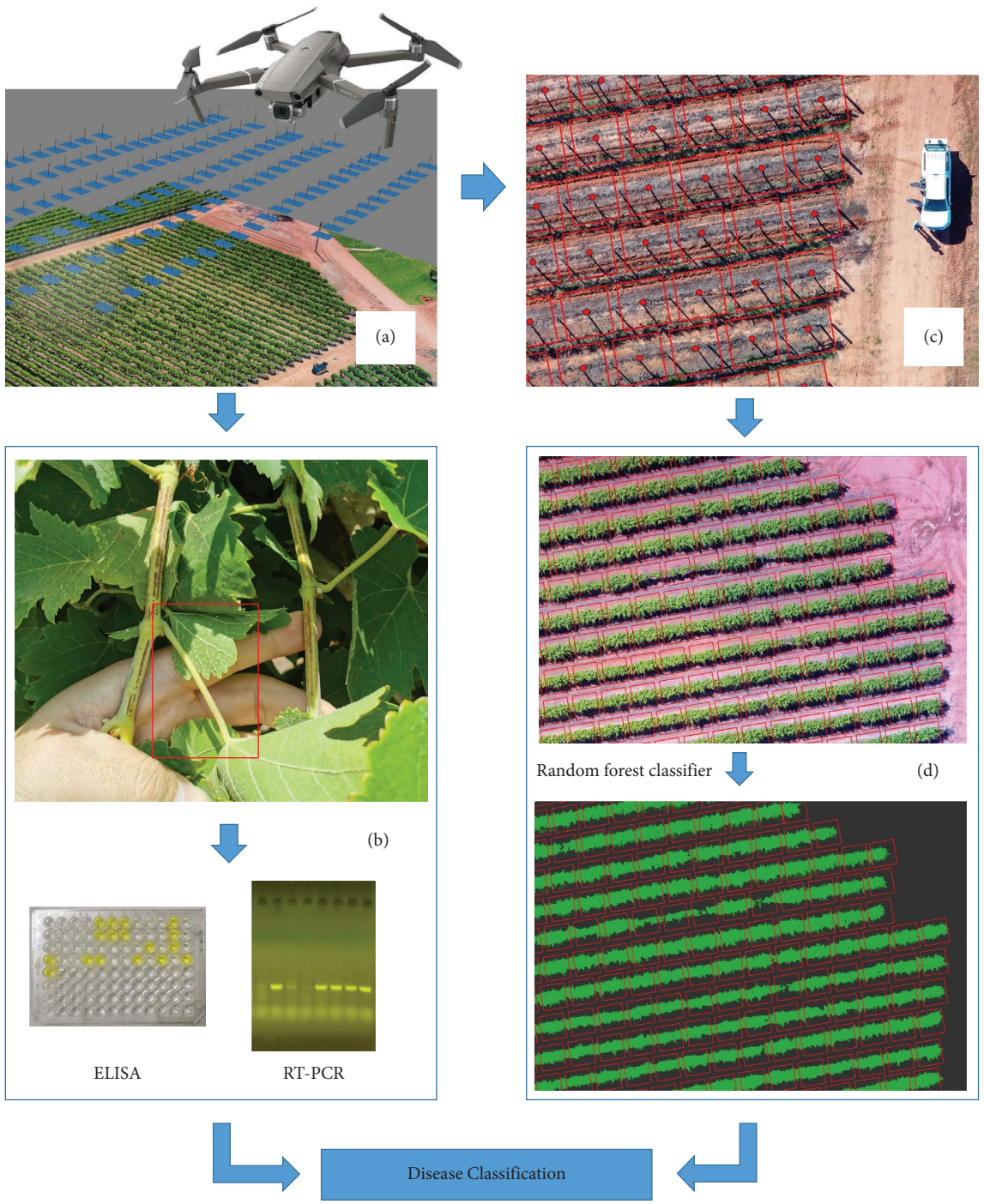

Figure 1: The workflow for disease classification with UAV images. (a) UAV data collection; (b) tissue sampling (petiole) and virus testing; (c) geo-locating and buffer creation for individual vines using the image at dormancy; and (d) grapevine canopy classification using random forest classifier.

All remote sensing imagery was captured under sunny and cloudless conditions between 11:00 to 15:00 h. In each flight, 288 images were taken for the Riverland block and 290 images for the Barossa block.

UAV Image mosaicking was conducted with Agisoft Metashape Professional, Version 1.6.2. (Agisoft LLC, St. Petersburg, Russia) to generate projected images with geo-information for each vineyard at each time point. Based on flight altitude and the resolution of the DJI Mavic 2 Pro camera, the mosaicked images produced a 1 cm pixel^{-1} ground sampling distance. The image geo-processing was conducted with ArcGIS Pro V2.8 (Esri, Redlands, California, US). Individual vines were geolocated using the image at dormancy when the shadow of vine trunks was clearly visible. Grapevine locations were manually digitised, and square buffers were created along with the orientation of row lines (Figure 1(c)). The size of the buffer was adjusted to about 90% of vine spacing to avoid the overlapping area

Table 2: The ELISA test results. Samples classified as "healthy" tested negative for GVA, GLRaV-1, -3, and -4; GVA only is grapevine virus A positive (single infection) but GLRaVs negative; GLRaVs only is single or any combination of grapevine leafroll-associated virus-1, -3, or -4 positive but GVA negative; GVA + GLRaVs is coinfection of both GVA and one or more GLRaV-1, -3 or -4.

	Healthy	GVA only	GLRaVs only	GVA + GLRaVs	Total
Riverland	23	3	0	16	42
Barossa	19	7	6	14	46

between vines. The vine spacing was larger in the Riverland Shiraz block (3.5 × 3.5 m vine and row spacing) compared to Barossa and Adelaide Hills vineyards (spacing 1.5 × 3.0 m), which results in a larger canopy therefore a larger buffer area per vine. Orthomosaics from each date were georeferenced to the dormancy image in order to accurately coalign vines.

The grapevine canopy was mapped using a supervised random forest classifier [32] (also called the random tree method in ArcGIS Pro). We used the ArcGIS Pro V2.8 random trees method with a maximum number of trees of 30 and a maximum tree depth of 15. Pixels in the image were classified as "Grapevine," "Soil," "Shadow," and Weeds." We manually labelled 5–7 training polygons in each training class and found the training data was sufficient to train Random Tree for classifying all pixels in the images. The "Soil," " Shadow," and "Weeds" classes were combined into a "non-grapevine" class to obtain a binary image for canopy area calculation (Figure 1(d)). To improve classification accuracy, different training data sets were created for early, middle, and later seasons as changing colour in the canopy over time. As undervine weeds were well controlled in all blocks, the grapevine was visually clearly distinguishable from the nongrapevine. The classification results were visually assessed by comparing the RGB and classified images, and results were consistent in all images, thus quantitative accuracy assessment of classification results was not required.

The projected leaf area (PLA) per individual vine was calculated as the sum of pixels that classified to "Grapevine" within square reference areas that were adapted to the vine and row spacing of the different vineyards. We used a square area of 3 × 3 m in Riverland, and 1.4 × 1.4 m in Barossa.

2.4. Statistical Analysis. Two-way ANOVA was used for statistical analysis using GraphPad Prism v9.0.0 (San Diego, CA, US). The PLA value of all virus-tested vines was used for analysis. Mean PLA values between each class (healthy, GVA only, GLRaVs only, and GVA + GLRaVs) at each time point were compared. Tukey's multiple comparisons test was used as a post hoc test ($p < 0.05$).

3. Results and Discussion

3.1. Symptoms of Shiraz Disease. The ground visual observations showed that SD-infected Shiraz vines had delayed budburst by approximate 15–20 days and smaller canopies in spring as indicated visually (Figure 2(a)). However, by midsummer (approximate fruitset stage), healthy and infected vines had indistinguishable canopies (Figure 2(b)). However, the canes of infected vines showed a lack of lignification, as shown in Figure 2(c). SD-infected vines were clearly identified in winter due to delayed leaf fall (delay approximate 15–20 days), which shows red leaves attached to the vine, while healthy vines had no leaves (Figure 2(d)). The SD symptoms consistently showed in two seasons and locations, this matched with observations in other studies [2, 4, 33].

3.2. PLA Difference between SD Symptomatic and Asymptomatic Canopy. The average PLA was calculated for each class (healthy, GVA only, GLRaVs only, and GVA + GLRaVs) in both blocks and seasons at each time point (Figure 3). In Riverland, the average size of coinfected (GVA + GLRaVs) vines was consistently approximate 1 m^2 smaller than healthy vines at 25 days after budburst (2.24 m^2 for healthy and 1.32 m^2 for coinfected vines) and flowering stage (4.42 m^2 for healthy and 3.62 m^2 for coinfected vines) in S1 (Figure 3(a)). The statistical analysis showed the GVA + GLRaVs classes were significantly ($p < 0.0001$) different from healthy in the early season. However, the difference in PLA between the two classes decreased after flowering. Figure 3(b) shows PLA of coinfected vines was approximate 1.3 m^2 smaller than healthy vines at 24 days after budburst (1.92 m^2 for healthy and 0.72 m^2 for coinfected vines) and flowering stage (4.26 m^2 for healthy and 2.82 m^2 for coinfected vines) in S2. Similar to S1, the difference in S2 between healthy and coinfected vines decreased after flowering; however, it still has a significant difference before veraison (with $p < 0.0001$).

In the Barossa vineyard, the PLA of coinfected Shiraz was also significantly smaller than that of healthy in the early season, especially at the flowering stage. In S1, the average PLA of the healthy and coinfected vines at the flowering stage was approximate 1.5 m^2 and 1.0 m^2 ($p < 0.0001$), respectively, thus coinfection resulted in 33% smaller PLA (Figure 3(c)). However, the difference between the two classes started to decrease at veraison and no significant differences were observed in PLA in the latter part of the growing season. The PLA difference between diseased and healthy vines was reduced by veraison although still significant ($p = 0.0307$). The p-values for the difference between healthy and coinfected vines were more significant around the flowering stage than at other times in both seasons.

The results indicated the symptomatic SD infection in Shiraz could be predicted using PLA calculated from RGB remote sensing images. The PLA of healthy and SD-infected vines had the highest difference between 20 and 70 days after bud burst, which unveils the optimum time window for SD detection as symptoms could be easily identified due to the significantly smaller PLA of the diseased vines. The PLA of SD-infected vines were 30%–70% smaller than the average healthy vines. We suggest setting a PLA threshold of 70% in healthy vines to classify as an SD infection in Shiraz. Therefore, PLA values at or less than 70% are classified as being SD infected. This threshold works between 15–45 days

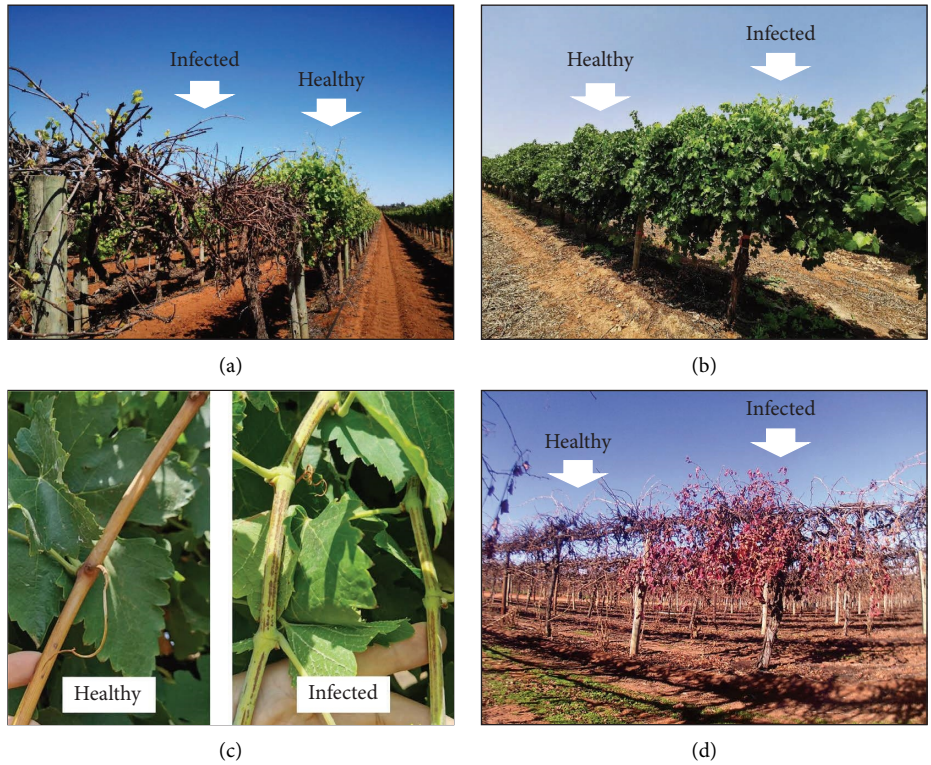

FIGURE 2: Symptoms of SD-infected Shiraz. (a) Restricted spring growth with delayed bud burst in Shiraz; (b) Shiraz canopies fully developed in midsummer at fruit set (EL-27); (c) canes of infected Shiraz show a lack of lignification at véraison (EL-35); and (d) red leaves remain on infected Shiraz vines while healthy vines drop all leaves during the dormant season.

after the budburst in the Riverland region and between 30–60 days after the budburst in the Barossa region. From veraison onwards, this method appeared to be less effective as canopy size differences between infected and healthy vines become smaller. However, our early PLA results could not distinguish SD from Grapevine trunk disease (GTD), a debilitating fungal disease that affects grapevines worldwide, causing devigourated shoots, and sometimes dead cordons [34]. The PLA of GTD-infected vines would likely remain low throughout the season since dieback results in very few growing shoots and death of the cordons [35, 36]. In contrast, SD-infected vines appear similar in growth to GTD-infected vines, but in contrast to GTD vines, have fully-developed canopies by the veraison stage; this key difference can be used to differentiate SD infection from GTD or dead vines. The PLA of SD-infected vines were 5%–15% smaller than the average healthy vines at this stage. Thus, we suggest that an 85% PLA threshold be used at the veraison stage to distinguish between SD-and GTD-infected or dead vines. Therefore, if the PLA is at or below 85% of the PLA of healthy vines between 90–120 days after budburst, the vine could possibly have GTD or be dead. Therefore, a minimum of two data collection timepoints are suggested per season, one in the early season and one in the mid-to-late season for determining SD using remote sensing. However, as the technique is an indirect detection method, which measures the canopy response to the virus, we cannot exclude the possibility that various other factors could be altering the phenotype. For example, other biotic stresses (fungal diseases), abiotic stresses (drought, salinity, heat stress, and mechanical damage), and virus strains and coinfections could influence vegetative growth and alter PLA [37]. Therefore, this remote sensing technique is indicative but not a conclusive method for SD infection. The current results were based on two study sites and years, the further assessments and virus testing validations are needed for the different regions, years, the age of vines, and cultivars. As additional information is acquired, different recommendations of the PLA threshold can be used for vineyards that have similar conditions.

If validated, this method can potentially be scaled to larger regions using RGB imaging from manned aircraft, or even satellite imagery in the future as their camera resolutions continue to increase.

3.3. Difference between Coinfection and Single Infections. Canopy development of coinfected vines (GVA + GLRaVs) lagged behind healthy vines due to delayed budburst in spring. This pattern was consistent in both vineyards and seasons (Figure 3). In comparison, the development of GVA and GLRaV (single infection) infected vines had no significant difference from healthy vines in both blocks or seasons. Despite previous studies showing that GVA and its variants are associated with SD [8], there is little systematic information between coinfection and SD symptoms. As the coinfection of GLRaVs and GVA is commonly found in vines, it is important to

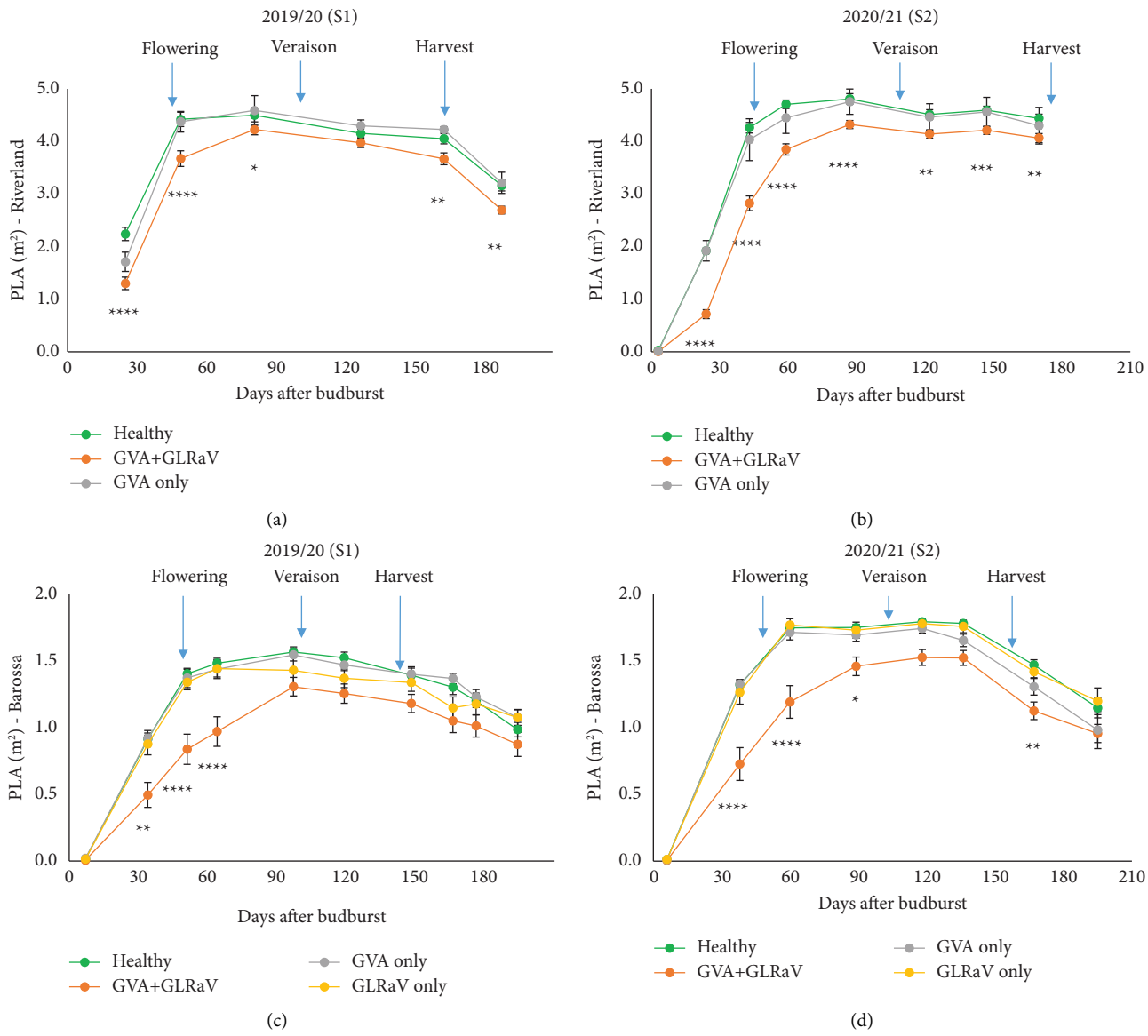

FIGURE 3: Average PLA for each lab-tested class at different times for both seasons in two vineyards. The p-value of healthy vs GVA + GLRaV shows in the graph, with $^{*}p \leq 0.05$, $^{**}p \leq 0.01$, $^{***}p \leq 0.001$, $^{****}p \leq 0.0001$, and nonsignificant with a blank. (a, b) Riverland Shiraz in S1 and S2; (c, d) Barossa Shiraz in S1 and S2.

consider both coinfection as well as environmental factors when studying disease symptoms.

The study found that SD symptoms in both Shiraz blocks only occur in vines that are coinfected with GVA and one or more GLRaVs, which in the vineyards we surveyed, were found to be mostly GLRaV-1 or GLRaV-4 strain 9 (GLRaV-9). We did not observe any typical SD symptoms when Shiraz vines were infected with GVA only (i.e., without GLRaVs). Similarly, Goszczynski and Habili [8] reported that SD symptoms in Shiraz were always associated with GVA group II and GLRaV-3 in South Africa. Consistent with the results of the present study, the same authors also observed that some vines did not exhibit any SD symptoms when infected with GVA group II alone; however, only visual evidence, but no quantitative evidence, was provided. GVA variants of group II have been closely associated with SD, but not groups I and III [3]. As the ELISA serological method is unable to discriminate between virus variants, the asymptomatic GVA-infected vines in our study could belong to group I and/or III. A previous study also reported that the variant GTR1-2 in GVA group II did not produce SD symptoms in Shiraz; however, other group II variants (BMO32-1, KWVMo4-1, and P163M5) produced SD symptoms in both Shiraz and Merlot [33]. The GVA variants in our study were unknown because the GVA primers used for the RT-PCR test in our study were not variant-specific. However, if the GVA variants in the present study did not belong to either group I or III, or the GTR1-2 variant (in group II), we could then infer that coinfection of GVA and GLRaVs is a requisite for SD symptoms in Shiraz. We are

unaware of any systematic studies that have been done to understand the relationship between SD symptoms and the combination of various viruses and their variants. This hypothesis requires a comprehensive investigation, potentially by using next-generation sequencing techniques to screen all GVA and GLRaVs strains in the samples.

4. Conclusion

Reliable detection of grapevine viruses in the field remains challenging due to varying symptomology. This study systematically compared the canopy growth response of SD-infected vines to healthy vines and proposed a rapid method to predict the SD infection in the Shiraz blocks using visible remote sensing technology. This technique has the potential to rapidly detect SD in the field, thereby providing prompt guidance for sampling locations for tissue testing of viruses as well as vineyard management. Further validation studies including various sites, seasons, cultivars, and virus strains are needed for this emerging technology. An additional, but important finding was that coinfection of GVA and GLRaVs results in significant vine devigoration in Shiraz, which does not occur with GVA or GLRaV alone. This observation was consistent across different soils and seasons under different weather conditions.

Data Availability

The raw and processed data used to support the study are available from the corresponding author upon request.

Conflicts of Interest

The authors declare that there are no conflicts of interest regarding publication of this work.

Acknowledgments

The authors gratefully acknowledged funding from South Australian Vine Improvement Association and Riverland Wine. We appreciate the top-up scholarship supported by Wine Australia. Special thanks to the industry collaborators: Kies Family Wines, and Mr Omer Najar from CCW Co-operative Limited.

References

[1] M. K. Corbett and J. Wiid, "Closterovirus-like particles in extracts from diseased grapevines," *Phytopathologia Mediterranea*, vol. 24, pp. 91–100, 1985.

[2] Q. Wu, N. Habili, F. Constable et al., "Virus pathogens in Australian vineyards with an emphasis on Shiraz Disease," *Viruses*, vol. 12, no. 8, p. 818, 2020.

[3] D. E. Goszczynski, "Single-strand conformation polymorphism (SSCP), cloning and sequencing reveal a close association between related molecular variants of Grapevine virus A (GVA) and Shiraz disease in South Africa," *Plant Pathology*, vol. 56, no. 5, pp. 755–762, 2007.

[4] N. Habili, "Australian shiraz disease: an emerging virus disease of *Vitis vinifera* cv. Shiraz," *Wine and Viticulture Journal*, vol. 28, no. 1, pp. 59–61, 2013.

[5] J. Charles, K. Froud, R. Van Den Brink, and D. Allan, "Mealybugs and the spread of grapevine leafroll-associated virus 3 (GLRaV-3) in a New Zealand vineyard," *Australasian Plant Pathology*, vol. 38, no. 6, pp. 576–583, 2009.

[6] G. Hommay, V. Komar, O. Lemaire, and E. Herrbach, "Grapevine virus A transmission by larvae of *Parthenolecanium corni*," *European Journal of Plant Pathology*, vol. 121, no. 2, pp. 185–188, 2008.

[7] D. E. Goszczynski and A. E. C. Jooste, "Identification of divergent variants of Grapevine virus A," *European Journal of Plant Pathology*, vol. 109, no. 4, pp. 397–403, 2003.

[8] D. E. Goszczynski and N. Habili, "Grapevine virus A variants of group II associated with Shiraz disease in South Africa are present in plants affected by Australian Shiraz disease, and have also been detected in the USA," *Plant Pathology*, vol. 61, no. 1, pp. 205–214, 2012.

[9] S. Chevalier, C. Greif, and P. Bass, B. Walter, Investigation on the aetiology of kober stem grooving disease," in *Proceedings of the 11th Meeting ICVG*, Montreux, Switzerland, September, 1993.

[10] R. Credi, "Characterization of grapevine rugose wood disease sources from Italy," *Plant Disease*, vol. 81, no. 11, pp. 1288–1292, 1997.

[11] M. Digiaro, M. P. Bedzrob, A. M. D'Onghia, D. Boscia, and V. N. Savino, "On the correlation between grapevine virus A and rugose wood," *Phytopathologia Mediterranea*, vol. 33, pp. 187–193, 1994.

[12] G. K. Blaisdell, S. Zhang, A. Rowhani et al., "Trends in vector-borne transmission efficiency from coinfected hosts: grapevine leafroll-associated virus-3 and Grapevine virus A," *European Journal of Plant Pathology*, vol. 156, no. 4, pp. 1163–1167, 2020.

[13] R. Naidu, A. Rowhani, M. Fuchs, D. Golino, and G. P. Martelli, "Grapevine leafroll: a complex viral disease affecting a high-value fruit crop," *Plant Disease*, vol. 98, no. 9, pp. 1172–1185, 2014.

[14] N. Habili, Q. Wu, and V. Pagay, "Virus-associated Shiraz Disease may lead Shiraz to become an endangered variety in Australia," *Wine and Viticulture Journal*, vol. 31, pp. 47–50, 2016.

[15] R. Almeida, K. Daane, V. Bell et al., "Ecology and management of grapevine leafroll disease," *Frontiers in Microbiology*, vol. 4, pp. 94–13, 2013.

[16] K. D. Ricketts, M. I. Gomez, S. S. Atallah et al., "Reducing the economic impact of Grapevine leafroll disease in California: identifying optimal disease management strategies," *American Journal of Enology and Viticulture*, vol. 66, no. 2, pp. 138–147, 2015.

[17] A. V. Zherdev, S. V. Vinogradova, N. A. Byzova, E. V. Porotikova, A. M. Kamionskaya, and B. B. Dzantiev, "Methods for the diagnosis of grapevine viral infections: a review," *Agriculture*, vol. 8, no. 12, p. 195, 2018.

[18] E. Rubinson, N. Galiakparov, S. Radian, I. Sela, E. Tanne, and R. Gafny, "Serological detection of grapevine virus A using antiserum to a nonstructural protein, the putative movement protein," *Phytopathology*, vol. 87, no. 10, pp. 1041–1045, 1997.

[19] R. R. Martin, K. C. Eastwell, A. Wagner, S. Lamprecht, and I. E. Tzanetakis, "Survey for viruses of grapevine in Oregon and Washington," *Plant Disease*, vol. 89, no. 7, pp. 763–766, 2005.

[20] Affinitylabs, "Virus testing [Online]," 2022, https://affinitylabs.com.au/virus-testing/.

[21] J. Albetis, S. Duthoit, F. Guttler et al., "Detection of Flavescence dorée Grapevine Disease using unmanned aerial

vehicle (UAV) multispectral imagery," *Remote Sensing*, vol. 9, no. 4, pp. 308–328, 2017.
[22] F. Vanegas, D. Bratanov, K. Powell, J. Weiss, and F. Gonzalez, "A novel methodology for improving plant pest surveillance in vineyards and crops using UAV-based hyperspectral and spatial data," *Sensors*, vol. 18, no. 1, p. 260, 2018.
[23] J. Ouyang, R. De Bei, and C. Collins, "Assessment of canopy size using UAV-based point cloud analysis to detect the severity and spatial distribution of canopy decline," *OENO One*, vol. 55, no. 1, 2021.
[24] S. L. Macdonald, M. Staid, M. Staid, and M. L. Cooper, "Remote hyperspectral imaging of grapevine leafroll-associated virus 3 in Cabernet Sauvignon vineyards," *Computers and Electronics in Agriculture*, vol. 130, pp. 109–117, 2016.
[25] S. Zia-Khan, M. Kleb, N. Merkt, S. Schock, and J. Müller, "Application of infrared imaging for early detection of Downy Mildew (*Plasmopara viticola*) in grapevine," *Agriculture*, vol. 12, no. 5, p. 617, Agriculture, 2022.
[26] Y. M. Wang, B. Ostendorf, D. Gautam, N. Habili, and V. Pagay, "Plant viral disease detection: from molecular diagnosis to optical sensing technology—a multidisciplinary review," *Remote Sensing*, vol. 14, no. 7, p. 1542, 2022.
[27] R. Raj, J. P. Walker, R. Pingale, R. Nandan, B. Naik, and A. Jagarlapudi, "Leaf area index estimation using top-of-canopy airborne RGB images," *International Journal of Applied Earth Observation and Geoinformation*, vol. 96, Article ID 102282, 2021.
[28] J. Monis and R. K. Bestwick, "Detection and localization of Grapevine Leafroll Associated Closteroviruses in greenhouse and tissue culture grown plants," *American Journal of Enology and Viticulture*, vol. 47, no. 2, pp. 199–205, 1996.
[29] E. Engvall and P. Perlmann, "Enzyme-linked immunosorbent assay, elisa," *The Journal of Immunology*, vol. 109, no. 1, pp. 129–135, 1972.
[30] G. Gambino, "Multiplex RT-PCR method for the simultaneous detection of nine grapevine viruses," *Methods in Molecular Biology*, vol. 1236, pp. 39–47, 2015.
[31] F. E. Constable and B. C. Rodoni, *Grapevine Leafroll-Associated Viruses*, Wine Australia, Adelaide, Australia, 2014.
[32] L. Breiman, "Random forests," *Machine Learning*, vol. 45, no. 1, pp. 5–32, 2001.
[33] D. E. Goszczynski, J. Du Preez, and J. T. Burger, "Molecular divergence of Grapevine virus A (GVA) variants associated with Shiraz disease in South Africa," *Virus Research*, vol. 138, no. 1-2, pp. 105–110, 2008.
[34] F. Fontaine, D. Gramaje, J. Armengol et al., *Grapevine Trunk Diseases. A Review*, OIV Publications, Paris, france, 2016.
[35] C. Bertsch, M. Ramírez-Suero, M. Magnin-Robert et al., "Grapevine trunk diseases: complex and still poorly understood," *Plant Pathology*, vol. 62, no. 2, pp. 243–265, 2013.
[36] D. Gramaje, J. R. Úrbez-Torres, and M. R. Sosnowski, "Managing grapevine trunk diseases with respect to etiology and epidemiology: current strategies and future prospects," *Plant Disease*, vol. 102, no. 1, pp. 12–39, 2018.
[37] G. P. Martelli, "Grapevine virology highlights 2006–2009," in *Proceedings of the 16th Meeting of the International Council for the Study of Virus and Virus-like Diseases of the Grapevine*, Dijon, France, September, 2009.

Chapter 4

Detecting grapevine virus infections in red and white winegrape canopies using proximal hyperspectral sensing

Wang, Y.M.; Ostendorf, B.; Pagay, V.

Preamble:

Grapevine viral diseases often do not exhibit readily noticeable symptoms on the leaves, particularly in the case of white cultivars, which poses limitations on the detectability by RGB sensors. However, hyperspectral technology offers a solution by providing detailed spectral information that extends beyond the RGB spectral range of wavelengths. In this chapter, a ground-based approach was implemented, employing a proximal sensing method by using a handheld NIR spectroradiometer for the detection of GLD in both red and white cultivars. The findings of this study have been published in the open journal - *Sensors, MDPI, 2023, 23(5), 2851*.

doi.org/10.3390/s23052851

Statement of Authorship

Title of Paper	Detecting grapevine virus infections in red and white winegrape canopies using proximal hyperspectral sensing
Publication Status	☑ Published ☐ Accepted for Publication ☐ Submitted for Publication ☐ Unpublished and Unsubmitted work written in manuscript style
Publication Details	MDPI, Sensors 2023, 23, 2851. https://doi.org/10.3390/ s23052851

Principal Author

Name of Principal Author (Candidate)	Yeniu (Mickey) Wang		
Contribution to the Paper	Designed the experiments Carried out the field and lab works to gather data Conducted data processing and analysis Drafted the manuscript and revision		
Overall percentage (%)	80%		
Certification:	This paper reports on original research I conducted during the period of my Higher Degree by Research candidature and is not subject to any obligations or contractual agreements with a third party that would constrain its inclusion in this thesis. I am the primary author of this paper.		
Signature		Date	13/06/2023

Co-Author Contributions

By signing the Statement of Authorship, each author certifies that:

i. the candidate's stated contribution to the publication is accurate (as detailed above);

ii. permission is granted for the candidate in include the publication in the thesis; and

iii. the sum of all co-author contributions is equal to 100% less the candidate's stated contribution.

Name of Co-Author	Bertram Ostendorf		
Contribution to the Paper	Conceptualisation Reviewed and edited the manuscript		
Signature		Date	20/06/2023

Name of Co-Author	Vinay Pagay		
Contribution to the Paper	Conceptualisation Reviewed and edited the manuscript		
Signature		Date	27/06/2023

sensors

MDPI

Article

Detecting Grapevine Virus Infections in Red and White Winegrape Canopies Using Proximal Hyperspectral Sensing

Yeniu Mickey Wang [1,2], Bertram Ostendorf [3] and Vinay Pagay [1,*]

[1] School of Agriculture, Food & Wine, Waite Research Institute, The University of Adelaide, PMB 1, Glen Osmond, SA 5064, Australia
[2] CSIRO Manufacturing, 13 Kintore Ave, Adelaide, SA 5000, Australia
[3] School of Biological Sciences, The University of Adelaide, Molecular Life Sciences Building, North Terrace Campus, Adelaide, SA 5005, Australia
* Correspondence: vinay.pagay@adelaide.edu.au; Tel.: +61-8-8313-0773

Abstract: Grapevine virus-associated disease such as grapevine leafroll disease (GLD) affects grapevine health worldwide. Current diagnostic methods are either highly costly (laboratory-based diagnostics) or can be unreliable (visual assessments). Hyperspectral sensing technology is capable of measuring leaf reflectance spectra that can be used for the non-destructive and rapid detection of plant diseases. The present study used proximal hyperspectral sensing to detect virus infection in Pinot Noir (red-berried winegrape cultivar) and Chardonnay (white-berried winegrape cultivar) grapevines. Spectral data were collected throughout the grape growing season at six timepoints per cultivar. Partial least squares-discriminant analysis (PLS-DA) was used to build a predictive model of the presence or absence of GLD. The temporal change of canopy spectral reflectance showed that the harvest timepoint had the best prediction result. Prediction accuracies of 96% and 76% were achieved for Pinot Noir and Chardonnay, respectively. Our results provide valuable information on the optimal time for GLD detection. This hyperspectral method can also be deployed on mobile platforms including ground-based vehicles and unmanned aerial vehicles (UAV) for large-scale disease surveillance in vineyards.

Keywords: GLRaV-1; GVA; GLD; disease detection; proximal sensing; spectroradiometer; PLS-DA

Citation: Wang, Y.M.; Ostendorf, B.; Pagay, V. Detecting Grapevine Virus Infections in Red and White Winegrape Canopies Using Proximal Hyperspectral Sensing. *Sensors* **2023**, *23*, 2851. https://doi.org/10.3390/s23052851

Academic Editor: Jiyul Chang

Received: 13 January 2023
Revised: 21 February 2023
Accepted: 1 March 2023
Published: 6 March 2023

1. Introduction

Virus-associated disease such as grapevine leafroll disease (GLD) affects grapevine health worldwide [1]. GLD has native impacts on both grape quality and yield, for example, lower anthocyanin accumulation rate resulting in poor colour development in red berries, fewer total soluble solids leading to lower °Brix, and smaller cluster size resulting in low yield [1–4]. This viral disease is vectored by sap-feeding insects including mealybugs and soft scales in vineyards [5,6] and causes long-term economic loss if left uncontrolled [4,7,8].

Grapevine leafroll-associated viruses (GLRaVs) such as GLRaV-1, -2, -3, -4, and -7 cause GLD in grapevines [9]. In Australian vineyards, GLRaV-1, -3, and -4 have been frequently found [10]. Co-infection could also happen in an individual vine such as infection with multiple GLRaVs (e.g., GLRaV-1 and GLRaV-3), different strains or variants of one GLRaV, or with multiple grapevine viruses. As an example of the latter, grapevine virus A (GVA) is often found to co-exist with GLRaV in vines, as GLRaVs act as a helper virus for GVA transmission by insect vectors [11]. In certain cultivars including Shiraz, Merlot, and Malbec, the co-infection of GLRaVs and GVA could lead to another devastating disease—Shiraz disease [12].

As there is no cure for virus-infected vines, preventive disease management methods such as quarantine, pest control, and roguing infected vines are the only effective methods to control viral diseases in vineyards [13,14]. However, roguing requires accurate diagnostic results for guidance. Laboratory-based diagnostic methods including the serological

method—enzyme-linked immunosorbent assay (ELISA)—and molecular method—reverse transcription polymerase chain reaction (RT-PCR)—often provide accurate results for virus detection; however, testing rates are hampered by their high costs. Visual assessment is a phenotypic detection method relying on the disease symptoms, which can be an alternative detection method and relatively cost-effective. For example, GLD in red-berried cultivars shows symptoms of reddening on leaves with green veins and rolling leaf edges, while in white cultivars, the same virus shows symptoms of leaf rolling at the edge, and subtle leaf rolling, which is not consistent and more difficult to detect visually compared to red-berried cultivars [15]. Thus, symptom-based detection of GLD is only relatively reliable for red cultivars and for specific leafroll viruses such as GLRaV-3 [16]. The variable reliability of the visual method stems from the varying levels of experience of the surveyors [17].

Hyperspectral technology has the proven capability of detecting plant diseases and, in some cases, even on asymptomatic leaves, as it measures spectra beyond those of human vision [18]. Various studies have used the proximal hyperspectral sensing method for GLD detection directly in contact with grapevine leaves or under a controlled environment in a laboratory [19–23]. However, these studies used active sensors, which rely on artificial illumination [24]. The benefit of active sensors is their consistent incident light levels and spectra that are unaffected by the external light environment. The drawback of using these types of sensors is that they can be time-consuming, as only a small portion of single leaves are measured in the field or leaf samples have to be taken to the laboratory for measurements. To address the speed limit of traditional proximal hyperspectral sensors, Bendel et al. [25] used an over-the-row grape harvester equipped with an active hyperspectral sensor for GLD detection in a vineyard. This method of detection was relatively quick; however, the setup of the system was complicated and impractical for growers to use on a routine basis without significant technical expertise.

In contrast to active sensors, passive sensors use natural light (solar radiation) for the illumination of leaves to measure their reflectance spectra. The detection area is generally larger in size depending on the measure distance, and the measurement can be relatively fast and simple to handle in practice [26]. However, very few studies have used passive hyperspectral sensors to detect grapevine viral disease at a canopy scale. Nguyen et al. [27] used a proximal sensing hyperspectral camera—Specim IQ—to detect grapevine vein clearing virus (GVCV) infections; however, the camera was a line scanner imaging sensor that required a fixed position and ca. 0.5 min for each hyperspectral image collection, which was time-consuming.

Various machine-learning algorithms have been used for disease classification in hyperspectral data, such as partial least squares (PLS), support vector machines, random forests, convolutional neural networks, and more recently deep learning algorithms [27–29]. PLS is the gold standard for binary classification; it is computationally inexpensive compared to other algorithms [30]. The principle of PLS is similar to principle component analysis, but it is a supervised method that uses the known information as input to train the model [31]. PLS relates two data matrices X (spectral dataset for all samples) and Y (disease status for all samples) to maximise the co-variance between components from the two data sets [32,33]. The output of PLS analysis is a linear model that is used for discrimination problems, also called partial least squares-discriminant analysis (PLS-DA) [34]. Various studies have used the PLD-DA method to analyse spectral data for plant disease classification [35–39].

The present study used a hand-held passive spectroradiometer for the proximal detection of virus infection in grapevines, and PLS-DA was used for modelling. Our aim was to (1) evaluate the potential of passive proximal hyperspectral sensors to detect virus infection on both red- and white-berried grape canopies in field conditions; (2) optimise the hyperspectral data processing workflow to produce a robust modelling method for disease prediction using the PLS-DA algorithm; and (3) determine the optimal growth stage for disease detection using this approach. This study could provide valuable guidance for using proximal sensing such as detection time, measuring direction, appropriate environmental

conditions, and measurement distance. Moreover, this method is readily applicable to both ground-based mobile platforms as well as low-altitude remote sensing platforms such as unmanned aerial vehicles (UAV) and airplanes for large-area disease surveillance.

2. Materials and Methods

2.1. Experimental Site and Plant Virus Testing

This study was conducted in a commercial vineyard located in the Adelaide Hills wine region—Kuitpo, SA, Australia (35°13′ S, 138°39′ E). Spectral data collection and plant tissue sampling were performed in the growing season 2020/21, from September 2020 to April 2021. Two grape cultivars—Pinot Noir (red cultivar) and Chardonnay (white cultivar) were selected for the study. Both cultivars were planted in 1988, own-rooted, on a podsol soil type. The vineyard was drip irrigated at 1.8 ML per hectare per season. Vines were spur pruned to 26 buds per metre, and the canopy was uniform in size in the block. Two sulphur sprays per season to control the pest were based on recommendations by a local viticulture consultant. The grapevines did not have any visible symptoms of nutrient deficiencies or diseases other than GLD. A ground-based visual inspection for GLD symptoms (leaf reddening on Pinot Noir and leaf rolling on Chardonnay) was conducted during the previous growing season, 2019/20, which showed a ca. 40% infection rate in the Pinot Noir block, and ca. 60% infection rate in the adjacent Chardonnay block.

Two rows of vines of each grape cultivar were selected for measurement for a total of 173 Pinot Noir and 174 Chardonnay vines. Each vine was tested with ELISA for ground truthing (presence or absence of leafroll virus). The leaf petiole tissue was sampled as suggested by Monis and Bestwick [40] at the harvest stage (March 2021). Virus testing was conducted with the DAS-ELISA (double antibody sandwich-enzyme-linked immunosorbent assay) test kits produced by Bioreba (Reinach, Switzerland). The test method strictly followed the procedure produced by Bioreba [41]. Four viruses (GLRaV-1, -3, -4, and GVA) were tested for each sample as per the manufacturer's instructions. To confirm the accuracy of ELISA results, 10 of the ELISA-tested positive samples and 20 negative samples were tested with RT-PCR (GLRaV-1, -3, -4, -4 strain 6, -4 strain 9, and GVA) in a NATA-accredited commercial laboratory—Affinity Labs (Adelaide, SA, Australia). The RT-PCR results matched all ELISA-tested results. Based on the test results, the samples were grouped into two classes: disease (GLRaV-1 + GVA positive) and healthy (tested negative for GLRaV-1, -3, -4, and GVA).

2.2. Spectral Data Collection

Leaf spectral reflectance data were collected using a portable hand-held spectroradiometer (ASD FieldSpec® HandHeld 2, Malvern Panalytical Ltd., Malvern, UK). The instrument is a silicon array-based sensor that measures light spectra between 325–1075 nm at 1 nm spectral resolution. The optical input has a 25° conical field of view (FOV). Data collection was conducted under sunny conditions at each timepoint. A Labsphere Spectralon® white reference panel (Halma plc, Amersham, UK) was used as the calibration target. The spectroradiometer was calibrated with the white reference (reflectance = 1) immediately before the measurement and was re-calibrated every 10 min to account for the changing illumination due to the sun angle. The instrument was held horizontally (parallel to the ground plane) and pointed to the centre of the canopy, perpendicular to the vertical canopy wall, as shown in Figure 1. The measurement distance was approx. 0.5 m from the canopy, which represented a ca. 20 cm diameter circle on the canopy (approx. three to four fully expanded and mature leaves).

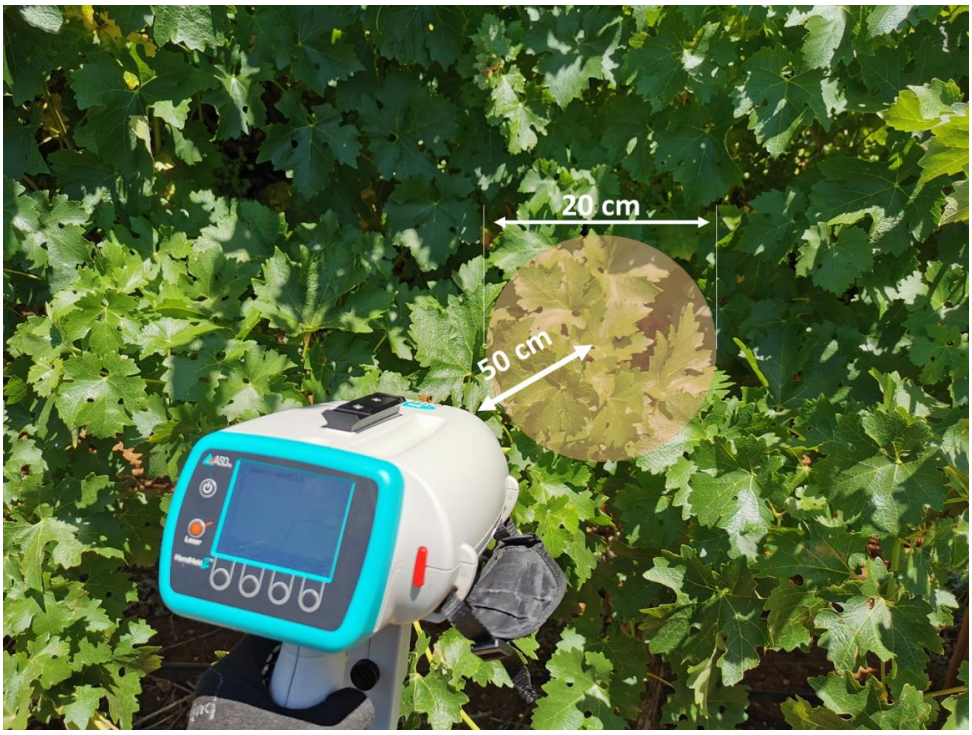

Figure 1. Spectral data measurement. The yellow shaded area shows the circular field of view of diameter of approx. 20 cm based on the approx. 0.5 m horizontal measurement distance.

Since the measurement used solar radiation as the light source, consistency in incident light was critical. Different instrument positions relative to the canopy were tested at the beginning of the season, including holding the sensor vertically and horizontally to measure the top and side of the canopy as well as the sunlit and sunshade sides of the canopy. After several test measurements, we determined that the horizontal position (perpendicular to the canopy wall) at the sunlit side of the canopy provided the most consistent results. All vines in each of the two rows were measured within the time window of 12:00–14:00 h. One spectrum measurement per vine was collected at a monthly interval between the months of November and April. The measurements started from the flowering development stage (EL-23) in November until post-harvest (April), which resulted in six timepoints.

2.3. Data Processing and Modelling

The spectral data processing and modelling were performed as described below using the PLS_Toolbox software plugin (v.9.0, Eigenvector Research, Inc., Manson, WA, USA) within the MATLAB R2021b (The MathWorks Inc., Natick, MA, USA) software environment.

2.3.1. Spectral Data Pre-Processing

To compensate for variations in the leaf angle, sun angle, and instrument holding position during field measurement, the raw spectral data was pre-processed. Pre-processing allows for noise removal, light scattering correction, spectral deviation compensation, and scale optimisation [42,43]. The transformed spectral data improved the prediction model and increased robustness.

Pre-processing in this study included three steps: smoothing, normalisation, and scaling. Firstly, the raw data were smoothed using a Savitzky-Golay Filter (SavGol) [44] with the filter width w = 7. The high-frequency noise was smoothed from the raw data, especially for the wavelengths below 400 nm and above 900 nm, due to the sensitivity of the sensor being lower in these regions. Secondly, the smoothed spectral data were normalised with the standard normal variate (SNV) method [45]. The normalised data overcomes multiplicative and baseline effects caused by a difference in leaf angles, measurement

distance and angles. Thirdly, the data were scaled using the mean centre method [46], which brought all wavelengths to the same magnitude and improved the models in the current study. Figure 2 demonstrates an example of pre-processing for 173 spectral data derived from Pinot Noir vines.

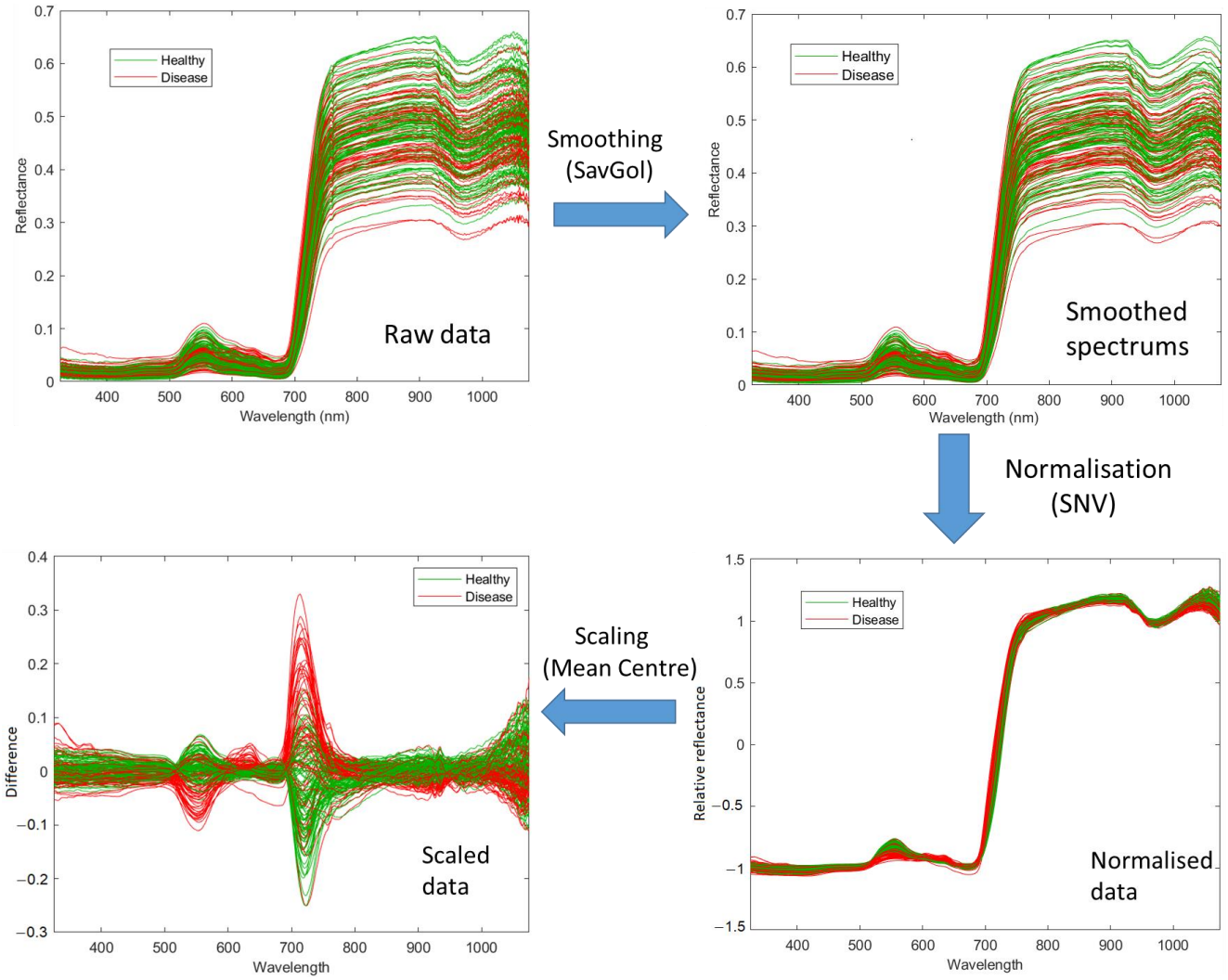

Figure 2. Spectral data pre-processing steps for Pinot Noir at the February 2021 timepoint. The raw spectral data is smoothed using the SavGol algorithm with seven bandwidths, then normalised using the standard normal variate algorithm and, lastly, scaled using the Mean Centring algorithm for 750 bands.

2.3.2. Outlier Removal

The grapevine canopy wall sometimes has gaps and holes that can cause outliers in the dataset. An outlier removal step is necessary, as the outliers could significantly influence the model when the sample number is not large. The Hotelling's T^2 and Q residuals plot was used for outlier identification [47]. The abnormally high values in either Hotelling's T^2 or Q residuals were considered outliers and were removed from the dataset; for example, either the Hotelling's T^2 value or Q residual values larger than 10 were considered outliers in the data set, which resulted in two outliers being removed from the April 2021 timepoint from the Chardonnay data set and one outlier being removed from the April 2021 timepoint from the Pinot Noir data set.

2.3.3. Cross-Validation

Cross-validation (CV) is a practical method for assessing the performance of the model, particularly for small sample sizes such as in this study [48]. The Venetian blinds method was used for the CV method [49]. The data was split into 10 divisions (blinds), and one sample per blind was taken for validation. Thus, the model was built with 90% of the data and validated with 10% of the data. The process was repeated 10 times to cover all data in the training data.

2.3.4. Modelling

PLS-DA was used for the classification modelling in this study due to its simplicity and its computationally efficient and interpretable results [50]. Similar to the components in principle component analysis, latent variables (LVs) represent the linear combination of variables in PLS-DA models [51]. The number of LVs selected for the PLS-DA model could affect the performance of the model. Typically, increasing the number of LVs in a model results in lower prediction error (Equation (1)). However, redundant LVs could result in overfitting, thus the CV error was considered in determining the appropriate number of LVs to use in the model. The sum of error in CV was calculated for selected LVs; this procedure is known as Wold's R criterion [52]. To build a robust model, additional LVs should be selected only when the CV error decreases significantly, which may not necessarily occur at the lowest error. A scree plot of the calibration and CV errors aids the LVs selection.

$$\text{Error} = \frac{\text{FP} + \text{FN}}{\text{FP} + \text{FN} + \text{TP} + \text{TN}} \tag{1}$$

where FP is the number of false positives (healthy that were incorrectly classified disease), FN is the number of false negatives (disease that was incorrectly classified as healthy), TP is the number of true positives (disease that was correctly identified), and TN is the number of true negatives (healthy that were classified correctly).

The PLS-DA model used LVs to calculate each data point (one spectral measurement) and project the result to a linear model—PLS predicted value (disease). The higher the value, the more likely the sample was to be in the predicted (disease) class. Then, a threshold was calculated to discriminate between the two classes. The threshold was based on a balance between sensitivity (Equation (2)) and specificity (Equation (3)) to minimise the error. The receiver operating characteristic (ROC) curve was used to determine the threshold, and the PLS-predicted value at the intersection of sensitivity and specificity was selected as the threshold (Figure 3a). Figure 3b visually illustrates the prediction for the Chardonnay model at the March 2021 timepoint. The samples that lie above the threshold were predicted as 'Disease' while samples below the threshold were predicted as 'Healthy'.

$$\text{Sensitivity} = \frac{\text{TP}}{\text{TP} + \text{FN}} \tag{2}$$

$$\text{Specificity} = \frac{\text{TN}}{\text{TN} + \text{FP}} \tag{3}$$

The PLA-DA models were developed for each cultivar from spectral data collected at each timepoint. The performance of each model was evaluated based on the binary confusion matrix of calibration and CV results (TP, TN, FP, and FN); the sensitivity and F1 score (Equation (4)); the accuracy (Equation (5)), and Matthews correlation coefficient (MCC) [53] (Equation (6)).

$$\text{F1 score} = \frac{2 \cdot \text{TP}}{2 \cdot \text{TP} + \text{FP} + \text{FN}} \tag{4}$$

$$\text{Accuracy} = \frac{\text{TP} + \text{TN}}{\text{TP} + \text{TN} + \text{FP} + \text{FN}} = 1 - \text{Error} \tag{5}$$

$$\text{MCC} = \frac{\text{TP} \cdot \text{TN} - \text{FP} \cdot \text{FN}}{\sqrt{(\text{TP} + \text{FP}) \cdot (\text{TP} + \text{FN}) \cdot (\text{TN} + \text{FP}) \cdot (\text{TN} + \text{FN})}} \tag{6}$$

A regression vector plot for each model was generated to identify the important wavelengths required for modelling. Lastly, each model was used for predicting the data from other timepoints for each cultivar.

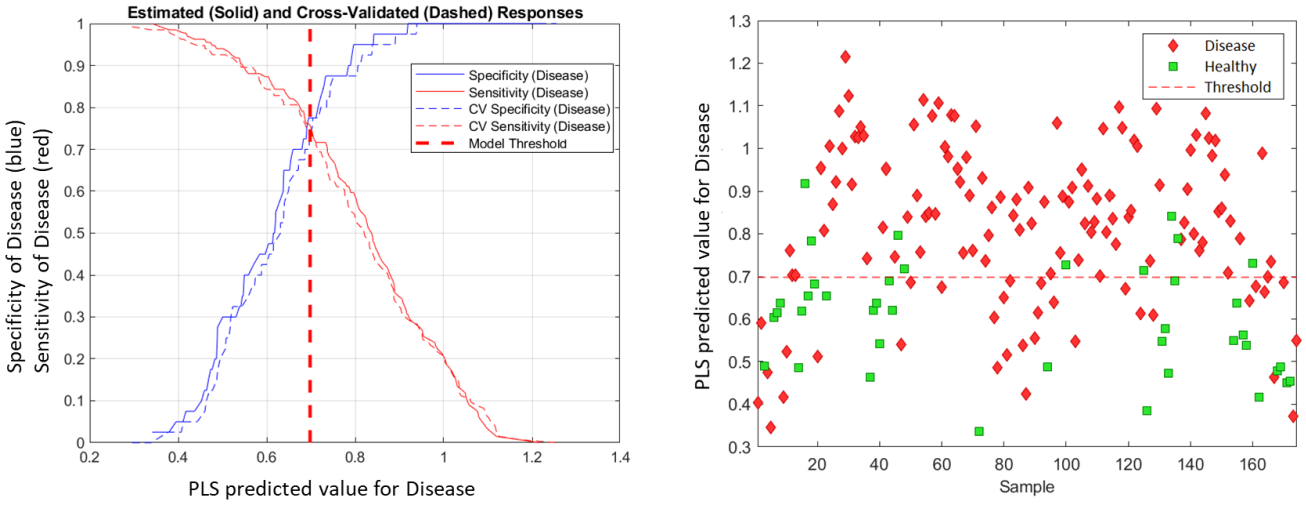

(**a**) (**b**)

Figure 3. PLS-DA threshold determination. (**a**) ROC curve for disease class; (**b**) plot of PLS predicted value for disease class for Chardonnay in March 2021. The threshold was 0.698 in this model.

3. Results

3.1. Virus Test Results

The laboratory test results showed that all of the virus-infected vines were co-infected with two viruses, GLRaV-1 and GVA, for which 206 out of 347 samples tested positive. All vines tested negative for GLRaV-3 and -4. In addition, 141 vines tested negative for each of the viruses (GLRaV-1, -3, -4, and GVA). The sample sizes of each group for Chardonnay and Pinot Noir are shown in Table 1.

Table 1. ELISA test results for both cultivars.

	Diseased (GLRaV-1 + GVA)	Healthy	Total
Chardonnay	134	40	174
Pinot Noir	72	101	173

3.2. Disease Symptomology

The disease symptoms for Chardonnay were difficult to visualise. There was no visual difference between healthy and diseased vines at the early flowering stage (EL-23; Figure 4a) and pea-size berry stage (EL-31; Figure 4b). Leaves of the diseased vines started to show mild yellowing before harvest (Figure 4c). Approx. 5% of leaves in the GLD-infected canopy showed leaf-rolling symptoms (Figure 4d). In Pinot Noir, disease symptoms did not appear before the flowering stage (Figure 4e). A few reddening spots appeared on mature leaves after the fruit setting stage (EL-27; Figure 4f). The red leaf and green veins became obvious at the veraison stage (EL-35; Figure 4g). The red leaf disease symptoms were most evident from harvest through post-harvest (Figure 4h).

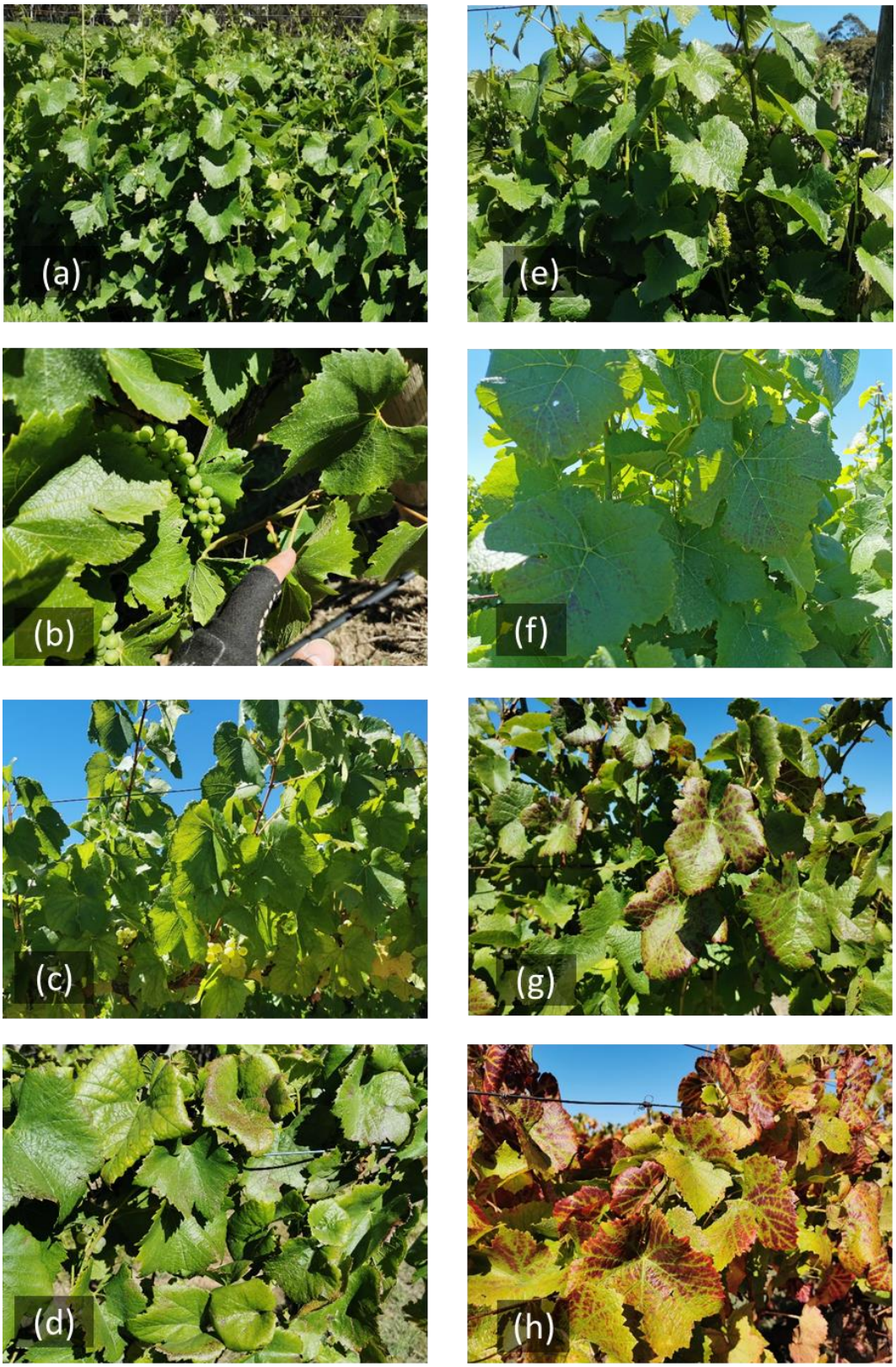

Figure 4. The GLD-infected vines at different development stages. Chardonnay in (**a**) November—flowering stage (EL-17); (**b**) December— pea-size berries; (**c**) February—veraison; (**d**) April—post-harvest. Pinot Noir in (**e**) November—flowering; (**f**) December—pea-size berries; (**g**) February—veraison; (**h**) April—post-harvest.

3.3. Critical Spectral Regions for Disease Classification

The difference between normalised average spectra of diseased and healthy vines was compared at each timepoint for the two cultivars as shown in Figure 5. An overall increase in reflectance difference over time in the diseased vines was observed in Chardonnay, which had the highest relative reflectance in March 2021. However, the difference decreased between the diseased and healthy vines in April. Between 690 to 730 nm in the red-edge region had a higher difference, and between 530 to 630 nm in the visible region showed a small increased reflectance in diseased Chardonnay. This matched the visual symptoms that diseased leaves were slightly yellower than healthy leaves, especially at later growth stages.

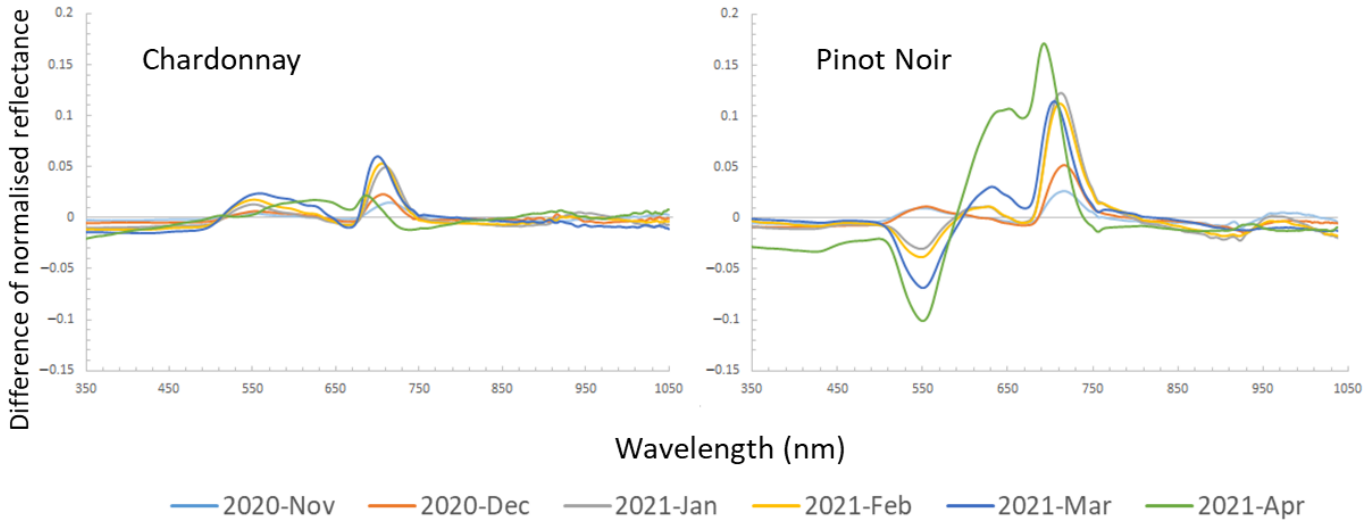

Figure 5. The difference of normalised averaged spectral reflectance of diseased to healthy vines (value at 0) for each timepoint.

In Pinot Noir, the diseased vines showed a similar pattern as Chardonnay in the early season (November and December). However, beginning in January (around the veraison stage), the diseased vine showed a significantly lower reflectance at a peak around 550 nm. Similar to Chardonnay, the red-edge region in Pinot Noir had much higher reflectance compared to healthy vines. In April, the spectral reflectance of diseased vines showed the highest difference to healthy vines compared to other timepoints, which had a higher reflectance at around 650 nm and between 690–730 nm, and lower reflectance at 550 nm.

3.4. The Model Results

The comprehensive results, including the confusion matrix, sensitivity, F1-score, accuracy, and MCC for each model, are shown in Table 2 (Chardonnay) and Table 3 (Pinot Noir). In Chardonnay, the model built at the earliest timepoint had the lowest accuracy but gradually improved over time. The best model result was in March, with a sensitivity of 0.76 and F1-score of 0.83 for the disease class; an accuracy of 0.76 and an MCC of 0.47 in the calibration set; and sensitivity and F1-score for the disease class of 0.74 and 0.81, an accuracy of 0.74, and an MCC of 0.41 in the validation set.

In Pinot Noir, the models did not well perform in the early season (November and December). However, the model improved dramatically beginning in January. The accuracy of the model was 0.89 and MCC was 0.78 as the diseased leaf started showing reddening symptoms. The best model was after harvest in April. The sensitivity and F1-score for the disease class were 0.92 and 0.95, respectively, the accuracy was 0.96, and MCC was 0.92 in the calibration set; the sensitivity and F1 score for the disease class were 0.92 and 0.94, respectively, the accuracy was 0.95, and MCC was 0.89 in the validation set.

Table 2. PLS-DA results for Chardonnay. Sample number: Disease = 134, Healthy = 40.

			Calibration Model Results						Cross-Validation Results					
Time	**LVs**	**Predicted**	**Confusion Matrix** **Actual Disease**	**Actual Healthy**	**Sensitivity**	**F1-Score**	**Accuracy**	**MCC**	**Confusion Matrix** **Actual Disease**	**Actual Healthy**	**Sensitivity**	**F1-Score**	**Accuracy**	**MCC**
Nov	2	Disease	80	15	0.60	0.70	0.60	0.19	77	14	0.57	0.68	0.59	0.19
		Healthy	54	25	0.63	0.42			57	26	0.65	0.42		
Dec	3	Disease	95	12	0.71	0.79	0.71	0.35	92	13	0.69	0.77	0.68	0.31
		Healthy	39	28	0.70	0.52			42	27	0.68	0.50		
Jan	3	Disease	96	10	0.72	0.80	0.72	0.40	91	15	0.68	0.76	0.67	0.26
		Healthy	38	30	0.75	0.56			43	25	0.63	0.46		
Feb	3	Disease	98	11	0.73	0.81	0.73	0.40	96	16	0.72	0.78	0.69	0.28
		Healthy	36	29	0.73	0.55			38	24	0.60	0.47		
Mar	4	Disease	102	9	0.76	0.83	0.76	0.47	99	11	0.74	0.81	0.74	0.41
		Healthy	32	31	0.78	0.60			35	29	0.73	0.56		
Apr	4	Disease	88	11	0.66	0.76	0.67	0.32	86	15	0.64	0.73	0.64	0.22
		Healthy	46	28	0.72	0.50			48	24	0.62	0.43		

Table 3. PLS-DA results for Pinot Noir. Sample number: Disease = 72, Healthy = 101.

			Calibration Model Results						Cross-Validation Results					
Time	**LVs**	**Predicted**	**Confusion Matrix** **Actual Disease**	**Actual Healthy**	**Sensitivity**	**F1-Score**	**Accuracy**	**MCC**	**Confusion Matrix** **Actual Disease**	**Actual Healthy**	**Sensitivity**	**F1-Score**	**Accuracy**	**MCC**
Nov	1	Disease	43	40	0.60	0.55	0.60	0.20	43	46	0.60	0.53	0.57	0.14
		Healthy	29	61	0.60	0.64			29	55	0.54	0.59		
Dec	3	Disease	48	33	0.68	0.63	0.67	0.35	45	34	0.63	0.60	0.65	0.29
		Healthy	23	68	0.67	0.71			26	67	0.66	0.69		
Jan	2	Disease	63	10	0.88	0.87	0.89	0.78	64	12	0.89	0.86	0.88	0.77
		Healthy	9	91	0.90	0.91			8	89	0.88	0.90		
Feb	2	Disease	61	3	0.85	0.90	0.92	0.84	58	2	0.81	0.88	0.91	0.81
		Healthy	11	98	0.97	0.93			14	99	0.98	0.93		
Mar	3	Disease	54	9	0.75	0.80	0.84	0.68	56	12	0.78	0.80	0.84	0.67
		Healthy	18	92	0.91	0.87			16	89	0.88	0.86		
Apr	5	Disease	66	1	0.92	0.95	0.96	0.92	66	3	0.92	0.94	0.95	0.89
		Healthy	6	100	0.99	0.97			6	98	0.97	0.96		

Due to the unbalanced samples, the F1 score was different between disease and healthy classes in Chardonnay. A low sample number in the healthy class resulted in a low F1 score because it did not count TN.

One advantage of the PLS-DA model is the explainable linear relationship between classes [34]. As the spectral signal changes over time, the evidence shows in the PLS predicted value in the combined violin and box plots (Figure 6). The vertical histograms show the sample distribution of both classes in the predicted value axis. Increased separation between healthy and disease classes can be observed over time in the plots. In the Chardonnay plot (Figure 6a), the samples in disease and healthy were close to each other in November and started to separate in December, and the largest separation was in March. In Pinot Noir, two classes overlapped in the first two timepoints; however, a noticeably higher PLS predicted value could be observed in disease samples from January, with the largest difference in April (Figure 6b). This plot matched the visual symptoms and the model results (Tables 1 and 2) that provide a visual and subjective basis for the model performance.

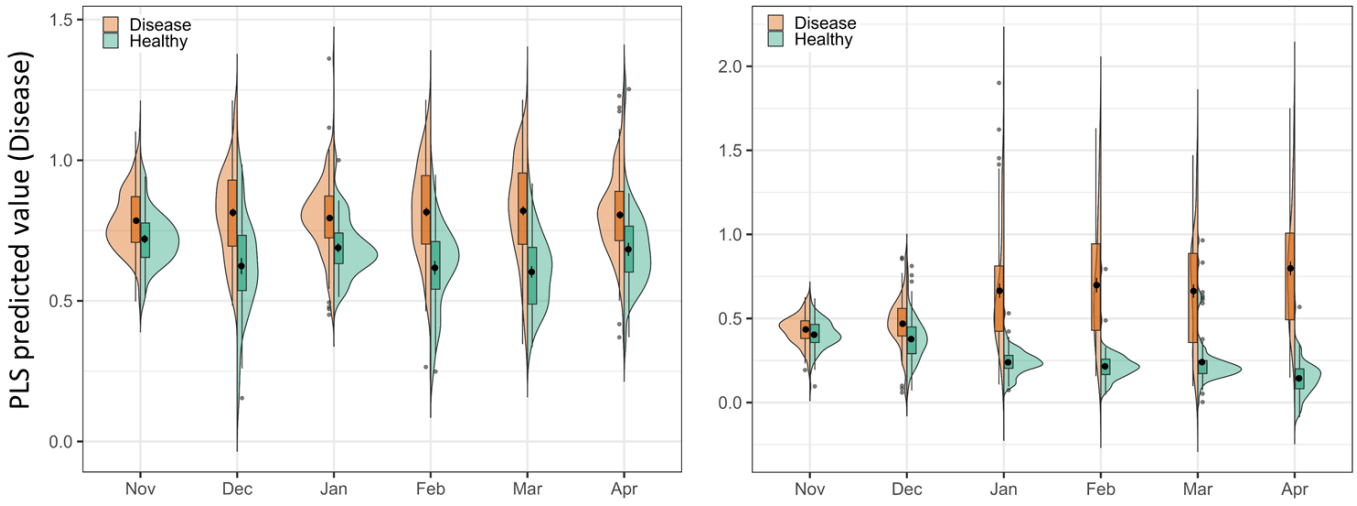

(**a**) (**b**)

Figure 6. The combined violin plot and box plot of the predicted value of disease from the PLS-DA model for (**a**) Chardonnay, and (**b**) Pinot Noir at each timepoint. The larger the value, the higher the probability of a sample belonging to a diseased vine, and the smaller the value, the lower the probability of a diseased vine. In this binary model, a low value means the sample more likely belongs to a healthy vine. The greater the separation between actual disease and healthy samples, the better the performance of the classification model.

3.5. Model Prediction Matrix

The model built at each timepoint was used to predict the data at other times for each cultivar, and MCC was used to assess the prediction performance. MCC can overcome the issue of the imbalanced data set in binary classifications (disease or healthy), which made a better comparison for model performance in both cultivars at the same scale compared to other parameters (accurate, F1-score, and sensitivity) [54]. The matrices of MCC results of the model at each timepoint that were used to predict all other times are presented in Figure 7. In Chardonnay (Figure 7a), only the January model could reasonably predict the data in February; no other models were useful for predictions at different times. In Pinot Noir (Figure 7b), the model built from January data can forward predict February, and February can backward predict January very well. The March model backward predicted both January and February data. The April model had the best forward prediction overall; however, this model did poorly in predicting earlier timepoints.

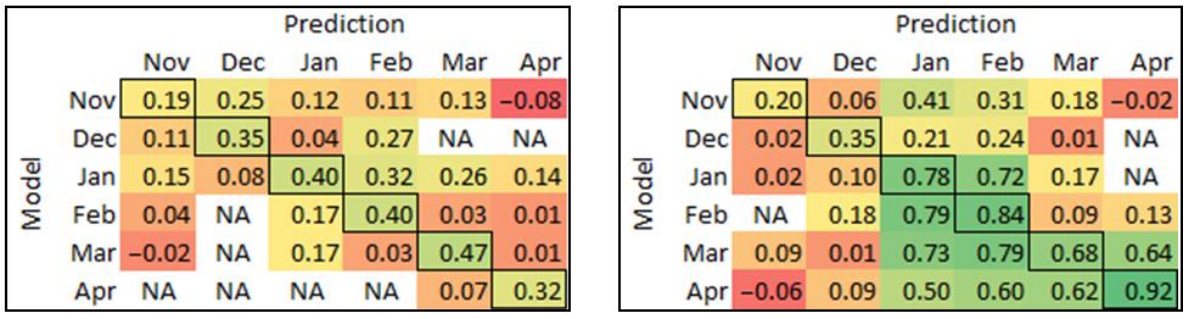

(**a**) (**b**)

Figure 7. The matrix of MCC from each model prediction of other timepoints for (**a**) Chardonnay, and (**b**) Pinot Noir. The bold cells are the self-predicted results, which are equal to the calibration results. The colour score ranges from red (low value) to yellow (medium) to green (high value). NA means $\sqrt{((TP + FP)\cdot(TP + FN)\cdot(TN + FP)\cdot(TN + FN))}$ equal to zero that cannot be divided.

4. Discussion

The current study systematically assessed virus-infected (GLRaV-1 + GVA) vines in both red (Pinot Noir) and white (Chardonnay) winegrape cultivars from flowering to post-harvest stages, both visually as well as with a proximal spectroradiometer, under field conditions. Visual assessments did not allow us to distinguish between virus-infected and healthy vines in the early season (before January in either cultivar). Typical GLD symptoms manifested as reddening on leaves in Pinot Noir and leaf edge rolling in Chardonnay and commenced in the virus-infected vines around late December. The severity of symptoms gradually increased and became visually more evident over time. This indicates that the virus may be multiplying in the vines and increasing the virus concentration or titre level during the growing season [55]. Another study also found there was a higher virus titre in symptomatic vines than in asymptomatic vines [56]. However, the symptomatology of virus infection is complicated and depends on various factors including environment, growth stage, virus isolate, cultivars, and infection ages [15,57]. It is therefore challenging to detect viral diseases with only visual symptomology, especially for the white cultivars, as their symptoms are less visually obvious compared to red cultivars. Montero et al. [58] found the GLRaV-3-infected Malvasia de Banyalbufar grapevine (white cultivar) did not show visual symptoms; however, the leaf net carbon dioxide assimilation and electron transport rates of infected vines were lower compared to healthy vines. This indicates the virus could affect plant growth and physiology even if it is asymptomatic. A systematic investigation of the symptomology of virus-inoculated vines over a period of time for white cultivars should be conducted, similar to the study done on GLRaV-3 infected red cultivars in New Zealand [16,59].

Our study showed that the average spectral reflectance of GLRaV-1 + GVA-infected vines was different to healthy vines in certain spectral regions. In the visible spectrum region (400–700 nm) in Pinot Noir, the green (550 nm) and red regions (630–650 nm) showed a large difference between virus-infected and healthy vines at the later stage, consistent with the findings by Naidu et al. [19], who measured the GLRaV-3-infected leaves in Cabernet Sauvignon and Merlot (both red cultivars) with leaf contact-based spectroradiometer. Gutha et al. [60] demonstrated that the red leaf symptom in GLRaV-3-infected Merlot (red cultivar) was largely caused by the accumulation of anthocyanin in leaves as a response to the stress. The authors also found that infected vines' leaves contained approx. 20% less chlorophyll and carotenoids than healthy leaves. As anthocyanins mainly absorb green and yellow light, the leaves appear red when anthocyanin content is high [61]. Anthocyanins absorb the spectral wavelength between 500 and 600 nm and especially at 550 nm [62]. This can be observed from January to April in Pinot Noir (Figure 5), a peak low reflectance was around the 550 nm spectral region. As anthocyanin pigments appear red in colour, the red spectral region (620–650 nm) in the virus-infected Pinot Noir had a higher reflectance compared to the healthy vines. In comparison, the virus-infected Chardonnay had poor expression of visual symptoms due to the lack of anthocyanin biosynthesis in white cultivars [63,64]. Thus, it was expected that there would be less difference between healthy and diseased vines in the blue and red spectral regions. We found that virus-infected Chardonnay had a higher average reflectance in the 530–630 nm region, which may be due to lower chlorophyll content in the leaves. In the red-edge region, both virus-infected red and white cultivars showed a high reflectance between 690 and 730 nm, indicating that the plant was under stress. Various studies have shown that the red-edge spectrum has a linear relationship with the chlorophyll content in leaves and is sensitive to stress [65–68]. This was clearly observed in our study (Figure 5) and suggests that the red-edge spectrum is useful for virus infection detection in both red- and white-berried grapevines. Based on the spectral difference between healthy and diseased vines, a multispectral sensor offers a simpler solution compared to hyperspectral sensing with a red-edge and green bands; e.g., MicaSense RedEdge P and Sentera 6X multispectral cameras could be used for viral disease detection in grapevines.

From the PLS-DA-predicted value plots and the model results, we observed increasing model accuracy over time for both red and white cultivars, which can be related to the development of disease symptoms in grapevines and the associated changes in spectral reflectance. The model prediction results (MCC) matrix (Figure 7b) showed that Pinot Noir models in both January and February could reliably predict each other's data, indicating that the spectral signatures of virus-infected vines are similar during this period. The best model for Pinot Noir was in April with an accuracy of 0.96 and an MCC of 0.92. This result indicates that the later part of the growing season (post-harvest) is the best time for viral disease detection in red cultivars if using the current proximal sensing method. However, if the vines are machine-harvested, resulting in considerable damage to the canopy, the current method may be unreliable, as the physical damage could change the spectral reflectance of the leaves. In our study, the grapes were hand-harvested with minimum alteration to the canopy, i.e., virtually no damage to the leaves. The accuracy of Chardonnay was low in April; this may be due to the onset of leaf senescence that creates gaps and holes in the canopies, which results in some background noise during the measurement. The best model for virus-infection prediction in Chardonnay was in March (at harvest time) with an accuracy of 0.76 and MCC of 0.47. The result was not considered high compared to Pinot Noir. Future studies could use sensors with different spectral ranges, e.g., shortwave infrared (SWIR). Bendel et al. [25] used a SWIR (1000–2500 nm) hyperspectral sensor to detect viral diseases in grapevines. The authors achieved an accuracy between 0.82 to 0.89 for GLRaV-1 detection, and 0.82 to 1.00 accuracy for GLRaV-3 detection on symptomatic white cultivars (Aligoté, Gewürztraminer, and Silvaner) in the vineyard.

In the present study, only the PLS-DA algorithm was used for modelling, as the purpose of this study was not to compare different statistical and machine learning algorithms, but rather to assess the temporal spectral difference and changes for reliable detection of virus-infected vines. PLS-DA is computationally efficient, relatively fast, and provides easy-to-interpret results that can quickly compare the model results from each timepoint. The model results showed high accuracy in the classification of virus-infected and healthy vines in Pinot Noir and moderate accuracy for Chardonnay. However, various other classification techniques can be used for high dimensional datasets, including linear discriminant analysis, k-nearest neighbours, support vector machine, and artificial neural networks [69]. Many studies compared different modelling techniques for plant disease detection [25,27,70,71]. It is worth testing other discrimination techniques in future studies to improve the accuracy for white cultivars, such as the deep learning method, which has been shown to reliably classify plant species and diseases with both proximal and remote sensing hyperspectral data [72,73].

Our study demonstrated that the proximal spectroradiometer in the field with a solar radiation source is a practical method for predicting viral disease in grapevines. The spectral difference of diseased Pinot Noir showed a similar pattern to other GLD-infected red cultivars that were measured with an active sensor (leaf contacted), which demonstrated the reliability of the proximal sensing. The proximal sensing method collected data relatively simply and rapidly compared to on-leaf, contact-based sensors. The method developed from the present study could be readily applicable to different sensing platforms for future studies, such as a land vehicle platform for fast disease detection in vineyards [74], or using remote sensing platforms such as UAV or airplane platform for large-scale disease surveillance in vineyards. For example, MacDonald et al. [75] used remote-sensing hyperspectral images from an airplane platform for GLRaV-3 detection in Cabernet Sauvignon in the vineyards.

5. Conclusions

Detecting viral diseases in grapevines is achievable using a proximal hyperspectral sensor. The current study used a hand-held spectroradiometer to assess spectral differences between virus-infected and healthy vines under field conditions. The PLS-DA model was used to classify the diseased and healthy vines; this model proved to be a suitable method for viral disease detection in grapevines. The model result showed an optimal time window for detecting viruses in Pinot Noir and Chardonnay. Comparing the spectral reflectance between healthy and diseased vines, the red-edge spectral region was found to be an important region for GLD symptom detection in both Pinot Noir and Chardonnay. The 550 nm spectral region is important, particularly in red cultivars. This indicates that a multispectral sensor with green and red-edge bands could be used for viral disease detection in red cultivars. The proximal sensing method used in this study applies to other platforms such as ground-based vehicles or low-altitude remote-sensing platforms. Although the detection of viral diseases in white-berried grape cultivars remains challenging, this may be addressed in future studies through advances in sensing technology with a wider range of spectra and data processing methods and algorithms.

Author Contributions: Conceptualization, Y.M.W., B.O. and V.P.; methodology, Y.M.W.; formal analysis, Y.M.W.; resources, V.P.; data curation, Y.M.W.; writing—original draft preparation, Y.M.W.; writing—review and editing, B.O. and V.P.; supervision, B.O. and V.P.; project administration, V.P.; funding acquisition, Y.M.W. and V.P. All authors have read and agreed to the published version of the manuscript.

Funding: This research was funded by the South Australian Vine Improvement Association, Riverland Wine Industry Development Council, and a top-up scholarship for Y.M.W. from Wine Australia (Project Number: WA Ph2008).

Institutional Review Board Statement: Not applicable.

Informed Consent Statement: Not applicable.

Data Availability Statement: Not applicable.

Acknowledgments: We acknowledge the funding bodies: South Australian Vine Improvement Association, Riverland Wine, and Wine Australia. Special thanks to the industry collaborators: K1 Wines.

Conflicts of Interest: The authors declare no conflict of interest.

References

1. Naidu, R.; Rowhani, A.; Fuchs, M.; Golino, D.; Martelli, G.P. Grapevine leafroll: A complex viral disease affecting a high-value fruit crop. *Plant Dis.* **2014**, *98*, 1172–1185. [CrossRef]
2. Lee, J.; Keller, K.E.; Rennaker, C.; Martin, R.R. Influence of grapevine leafroll associated viruses (GLRaV-2 and -3) on the fruit composition of Oregon *Vitis vinifera* L. cv. Pinot noir: Free amino acids, sugars, and organic acids. *Food Chem.* **2009**, *117*, 99–105. [CrossRef]
3. Wolpert, J.A.; Vilas, E.P. Effect of mild leafroll disease on growth, yield, and fruit maturity indices of Riesling and Zinfandel. *Am. J. Enol. Vitic.* **1992**, *43*, 367. [CrossRef]
4. Alabi, O.J.; Casassa, L.F.; Gutha, L.R.; Larsen, R.C.; Henick-Kling, T.; Harbertson, J.F.; Naidu, R.A. Impacts of Grapevine leafroll disease on fruit yield and grape and wine chemistry in a wine grape (*Vitis vinifera* L.) cultivar. *PLoS ONE* **2016**, *11*, e0149666. [CrossRef]
5. Douglas, N.; Krüger, K. Transmission efficiency of Grapevine leafroll-associated virus 3 (GLRaV-3) by the mealybugs Planococcus ficus and Pseudococcus longispinus (*Hemiptera*: *Pseudococcidae*). *Eur. J. Plant Pathol.* **2008**, *122*, 207–212. [CrossRef]
6. Charles, J.; Froud, K.; Van den Brink, R.; Allan, D. Mealybugs and the spread of grapevine leafroll-associated virus 3 (GLRaV-3) in a New Zealand vineyard. *Australas. Plant Pathol.* **2009**, *38*, 576–583. [CrossRef]
7. Atallah, S.; Gomez, M.; Fuchs, M.; Martinson, T. Economic impact of grapevine leafroll disease on Vitis viniferacv. Cabernet franc in Finger Lakes vineyards of New York. *Am. J. Enol. Vitic.* **2012**, *63*, 73–79. [CrossRef]
8. Zorloni, A.; Prati, S.; Bianco, P.A.; Belli, G. Transmission of Grapevine virus A and Grapevine leafroll-associated virus 3 by *Heliococcus bohemicus*. *J. Plant Pathol.* **2006**, *88*, 325–328.

9. Martelli, G.P.; Ghanem-Sabanadzovic, N.A.; Agranovsky, A.A.; Rwahnih, M.A.; Dolja, V.V.; Dovas, C.I.; Fuchs, M.; Gugerli, P.; Hu, J.S.; Jelkmann, W.; et al. Taxonomic revision of the family *Closteroviridae* with special reference to the grapevine leafroll-associated members of the genus *Ampelovirus* and the putative species unassigned to the family. *J. Plant Pathol.* **2012**, *94*, 7–19.
10. Constable, F.E.; Rodoni, B.C. *Grapevine Leafroll-Associated Viruses*; Wine Australia: Adelaide, Australia, 2014.
11. Fortusini, A.; Scattini, G.; Prati, S.; Cinquanta, S.; Belli, G. Transmission of grapevine leafroll virus 1 (GLRaV-1) and grapevine virus A (GVA) by scale insects. In Proceedings of the 12th Meeting of ICVG, Lisbon, Portugal, 29 September 1997; pp. 121–122.
12. Wu, Q.; Habili, N.; Constable, F.; Al Rwahnih, M.A.; Goszczynski, D.E.; Wang, Y.; Pagay, V. Virus pathogens in Australian vineyards with an emphasis on Shiraz Disease. *Viruses* **2020**, *12*, 818. [CrossRef]
13. Bell, V.A.; Lester, P.J.; Pietersen, G.; Hall, A.J. The management and financial implications of variable responses to grapevine leafroll disease. *J. Plant Pathol.* **2021**, *103*, 5–15. [CrossRef]
14. Rubio, L.; Galipienso, L.; Ferriol, I. Detection of plant viruses and disease management: Relevance of genetic diversity and evolution. *Front. Plant Sci.* **2020**, *11*, 1092. [CrossRef]
15. Maree, H.J.; Almeida, R.P.; Bester, R.; Chooi, K.M.; Cohen, D.; Dolja, V.V.; Fuchs, M.F.; Golino, D.A.; Jooste, A.E.; Martelli, G.P.; et al. Grapevine leafroll-associated virus 3. *Front. Microbiol.* **2013**, *4*, 82. [CrossRef]
16. Bell, V.A.; Blouin, A.G.; Cohen, D.; Hedderley, D.I.; Oosthuizen, T.; Spreeth, N.; Lester, P.J.; Pietersen, G. Visual symptom identification of grapevine leafroll-associated virus 3 in red berry cultivars supports virus management by roguing. *J. Plant Pathol.* **2017**, *99*, 477–482.
17. Legrand, P. Biological assays for plant viruses and other graft-transmissible pathogens diagnoses: A review. *EPPO Bull.* **2015**, *45*, 240–251. [CrossRef]
18. Thomas, S.; Kuska, M.T.; Bohnenkamp, D.; Brugger, A.; Alisaac, E.; Wahabzada, M.; Behmann, J.; Mahlein, A.-K. Benefits of hyperspectral imaging for plant disease detection and plant protection: A technical perspective. *J. Plant Dis. Prot.* **2018**, *125*, 5–20. [CrossRef]
19. Naidu, R.A.; Perry, E.M.; Pierce, F.J.; Mekuria, T. The potential of spectral reflectance technique for the detection of Grapevine leafroll-associated virus-3 in two red-berried wine grape cultivars. *Comput. Electron. Agric.* **2009**, *66*, 38–45. [CrossRef]
20. Sinha, R.; Khot, L.R.; Rathnayake, A.P.; Gao, Z.; Naidu, R.A. Visible-near infrared spectroradiometry-based detection of grapevine leafroll-associated virus 3 in a red-fruited wine grape cultivar. *Comput. Electron. Agric.* **2019**, *162*, 165–173. [CrossRef]
21. Pagay, V.; Habili, N.; Wu, Q.; Coleman, D. Rapid and non-destructive detection of Shiraz disease and grapevine leafroll disease on asymptomatic grapevines in Australian vineyards. In Proceedings of the 19th Congress of the International Council for the study of Virus and Virus-like Diseases of Grapevine, Santiago, Chile, 9–12 April 2018.
22. Junges, A.H.; Almança, M.A.K.; Fajardo, T.V.M.; Ducati, J.R. Leaf hyperspectral reflectance as a potential tool to detect diseases associated with vineyard decline. *Trop. Plant Pathol.* **2020**, *45*, 522–533. [CrossRef]
23. Gao, Z.; Khot, L.R.; Naidu, R.A.; Zhang, Q. Early detection of grapevine leafroll disease in a red-berried wine grape cultivar using hyperspectral imaging. *Comput. Electron. Agric.* **2020**, *179*, 105807. [CrossRef]
24. Fahey, T.; Pham, H.; Gardi, A.; Sabatini, R.; Stefanelli, D.; Goodwin, I.; Lamb, D.W. Active and passive electro-optical sensors for health assessment in food crops. *Sensors* **2021**, *21*, 171. [CrossRef]
25. Bendel, N.; Kicherer, A.; Backhaus, A.; Köckerling, J.; Maixner, M.; Bleser, E.; Klück, H.-C.; Seiffert, U.; Voegele, R.T.; Töpfer, R. Detection of Grapevine leafroll-associated virus 1 and 3 in white and red grapevine cultivars using hyperspectral imaging. *Remote Sens.* **2020**, *12*, 1693. [CrossRef]
26. Pinheiro, F.; Gusmo dos Anjos, W.d.P. Optical Sensors Applied in Agricultural Crops. In *Optical Sensors—New Developments and Practical Applications*; InTech: Rang-Du-Fliers, France, 2014. [CrossRef]
27. Nguyen, C.; Sagan, V.; Maimaitiyiming, M.; Maimaitijiang, M.; Bhadra, S.; Kwasniewski, M.T. Early detection of plant viral disease using hyperspectral imaging and deep learning. *Sensors* **2021**, *21*, 742. [CrossRef] [PubMed]
28. Lowe, A.; Harrison, N.; French, A.P. Hyperspectral image analysis techniques for the detection and classification of the early onset of plant disease and stress. *Plant Methods* **2017**, *13*, 80. [CrossRef]
29. Wang, Y.M.; Ostendorf, B.; Gautam, D.; Habili, N.; Pagay, V. Plant viral disease detection: From molecular diagnosis to optical sensing technology—A multidisciplinary review. *Remote Sens.* **2022**, *14*, 1542. [CrossRef]
30. Mendez, K.M.; Reinke, S.N.; Broadhurst, D.I. A comparative evaluation of the generalised predictive ability of eight machine learning algorithms across ten clinical metabolomics data sets for binary classification. *Metabolomics* **2019**, *15*, 150. [CrossRef]
31. Barker, M.; Rayens, W. Partial least squares for discrimination. *J. Chemom.* **2003**, *17*, 166–173. [CrossRef]
32. Höskuldsson, A. PLS regression methods. *J. Chemom.* **1988**, *2*, 211–228. [CrossRef]
33. Wold, S.; Sjöström, M.; Eriksson, L. PLS-regression: A basic tool of chemometrics. *Chemom. Intell. Lab. Syst.* **2001**, *58*, 109–130. [CrossRef]
34. Ballabio, D.; Consonni, V. Classification tools in chemistry. Part 1: Linear models. PLS-DA. *Anal. Methods* **2013**, *5*, 3790–3798. [CrossRef]
35. Copley, T.; Aliferis, K.; Jabaji, S. Maple bark biochar affects rhizoctonia solani Metabolism and increases damping-off severity. *Phytopathology* **2015**, *105*, 1334–1346. [CrossRef] [PubMed]
36. Yu, K.; Anderegg, J.; Mikaberidze, A.; Karisto, P.; Mascher, F.; McDonald, B.A.; Walter, A.; Hund, A. Hyperspectral canopy sensing of Wheat Septoria Tritici Blotch Disease. *Front. Plant Sci.* **2018**, *9*, 1195. [CrossRef] [PubMed]

37. Zhou, R.-Q.; Jin, J.-J.; Li, Q.-M.; Su, Z.-Z.; Yu, X.-J.; Tang, Y.; Luo, S.-M.; He, Y.; Li, X.-L. Early detection of magnaporthe oryzae-infected barley leaves and lesion visualization based on hyperspectral imaging. *Front. Plant Sci.* **2018**, *9*, 1962. [CrossRef]
38. Deng, H.; He, R.; Xia, H.; Xu, N.; Deng, Q.; Liang, D.; Lin, L.; Liao, L.; Xiong, B.; Xie, X.; et al. Ultra-HPLC-MS pseudo-targeted metabolomic profiling reveals metabolites and associated metabolic pathway alterations in Asian plum (*Prunus salicina*) fruits in response to gummosis disease. *Funct. Plant Biol.* **2022**, *49*, 936–945. [CrossRef] [PubMed]
39. Zhu, H.; Chu, B.; Zhang, C.; Liu, F.; Jiang, L.; He, L. Hyperspectral imaging for presymptomatic detection of tobacco disease with successive projections algorithm and machine-learning classifiers. *Sci. Rep.* **2017**, *7*, 4125. [CrossRef]
40. Monis, J.; Bestwick, R.K. Detection and localization of Grapevine Leafroll Associated Closteroviruses in greenhouse and tissue culture grown plants. *Am. J. Enol. Vitic.* **1996**, *47*, 199. [CrossRef]
41. Bioreba, A.G. Double Antibody Sandwich Enzyme-Linked Immunosorbent Assay (DAS-ELISA): Test Specifications. Available online: https://www.bioreba.ch/saas/CustomUpload/374O357O340O370O356O369O350O321O360O366O369O356O353O352O350O320O326O/ELISA_Test_procedure_efd_and_es.pdf (accessed on 7 February 2023).
42. Engel, J.; Gerretzen, J.; Szymańska, E.; Jansen, J.J.; Downey, G.; Blanchet, L.; Buydens, L.M.C. Breaking with trends in pre-processing? *TrAC Trends Anal. Chem.* **2013**, *50*, 96–106. [CrossRef]
43. Rinnan, Å.; Nørgaard, L.; Berg, F.v.d.; Thygesen, J.; Bro, R.; Engelsen, S.B. Chapter 2—Data Pre-processing. In *Infrared Spectroscopy for Food Quality Analysis and Control*; Sun, D.-W., Ed.; Academic Press: San Diego, CA, USA, 2009; pp. 29–50. [CrossRef]
44. Savitzky, A.; Golay, M.J.E. Smoothing and Differentiation of Data by Simplified Least Squares Procedures. *Anal. Chem.* **1964**, *36*, 1627–1639. [CrossRef]
45. Barnes, R.J.; Dhanoa, M.S.; Lister, S.J. Standard normal variate transformation and de-trending of near-infrared diffuse reflectance spectra. *Appl. Spectrosc.* **1989**, *43*, 772–777. [CrossRef]
46. Hofer, M. Mean centering. In *The International Encyclopedia of Communication Research Methods*; John Wiley & Sons, Inc.: Hoboken, NJ, USA, 2017; pp. 1–3. [CrossRef]
47. Miller, C.E. Chemometrics in Process Analytical Technology (PAT). In *Process Analytical Technology*; John Wiley & Sons, Inc.: Hoboken, NJ, USA, 2010; pp. 353–438. [CrossRef]
48. Kuligowski, J.; Pérez-Guaita, D.; Quintás, G. Application of discriminant analysis and cross-validation on proteomics data. In *Statistical Analysis in Proteomics*; Jung, K., Ed.; Springer New York: New York, NY, USA, 2016; pp. 175–184. [CrossRef]
49. Rácz, A.; Bajusz, D.; Héberger, K. Modelling methods and cross-validation variants in QSAR: A multi-level analysis$. *SAR QSAR Environ. Res.* **2018**, *29*, 661–674. [CrossRef]
50. Götz, O.; Liehr-Gobbers, K.; Krafft, M. Evaluation of structural equation models using the Partial Least Squares (PLS) approach. In *Handbook of Partial Least Squares: Concepts, Methods and Applications*; Esposito Vinzi, V., Chin, W.W., Henseler, J., Wang, H., Eds.; Springer: Berlin/Heidelberg, Germany, 2010; pp. 691–711. [CrossRef]
51. Lê Cao, K.-A.; Welham, Z.M. PLS-Discriminant Aalysis (PLS-DA). In *Multivariate Data Integration Using R: Methods and Applications with the MixOmics Package*; Routledge: Oxford, UK, 2021; pp. 201–231. [CrossRef]
52. Wold, S. Cross-validatory estimation of the number of components in factor and principal components models. *Technometrics* **1978**, *20*, 397–405. [CrossRef]
53. Matthews, B.W. Comparison of the predicted and observed secondary structure of T4 phage lysozyme. *Biochim. Biophys. Acta (BBA) Protein Struct.* **1975**, *405*, 442–451. [CrossRef]
54. Chicco, D.; Jurman, G. The advantages of the Matthews correlation coefficient (MCC) over F1 score and accuracy in binary classification evaluation. *BMC Genom.* **2020**, *21*, 6. [CrossRef]
55. Shabanian, M.; Xiao, H.; Meng, B. Seasonal dynamics and tissue distribution of two major viruses associated with grapevine Leafroll under cool climate condition. *Eur. J. Plant Pathol.* **2020**, *158*, 1017–1031. [CrossRef]
56. Bertazzon, N.; Forte, V.; Filippin, L.; Causin, R.; Maixner, M.; Angelini, E. Association between genetic variability and titre of Grapevine Pinot gris virus with disease symptoms. *Plant Pathol.* **2017**, *66*, 949–959. [CrossRef]
57. Martelli, G.P. Grapevine virology highlights 2006–2009. In Proceedings of the 16th Meeting of the International Council for the Study of Virus and Virus-like Diseases of the Grapevine, Dijon, France, 31 August–4 September 2009; pp. 15–23.
58. Montero, R.; El aou ouad, H.; Pacifico, D.; Marzachì, C.; Castillo, N.; García, E.; Del Saz, N.F.; Florez-Sarasa, I.; Flexas, J.; Bota, J. Effects of Grapevine leafroll-associated virus 3 on the physiology in asymptomatic plants of Vitis vinifera. *Ann. Appl. Biol.* **2017**, *171*, 155–171. [CrossRef]
59. Chooi, K.M.; Bell, V.A.; Blouin, A.G.; Cohen, D.; Mundy, D.; Henshall, W.; MacDiarmid, R.M. Grapevine leafroll-associated virus 3 genotype influences foliar symptom development in New Zealand vineyards. *Viruses* **2022**, *14*, 1348. [CrossRef]
60. Gutha, L.R.; Casassa, L.F.; Harbertson, J.F.; Naidu, R.A. Modulation of flavonoid biosynthetic pathway genes and anthocyanins due to virus infection in grapevine (*Vitis vinifera* L.) leaves. *BMC Plant Biol.* **2010**, *10*, 187. [CrossRef]
61. Gould, K.S. Nature's Swiss army knife: The diverse protective roles of anthocyanins in leaves. *J. Biomed. Biotechnol.* **2004**, *2004*, 314–320. [CrossRef]
62. Merzlyak, M.N.; Chivkunova, O.B.; Solovchenko, A.E.; Naqvi, K.R. Light absorption by anthocyanins in juvenile, stressed, and senescing leaves. *J. Exp. Bot.* **2008**, *59*, 3903–3911. [CrossRef]
63. Ivanova, V.; Stefova, M.; Vojnoski, B.; Dörnyei, Á.; Márk, L.; Dimovska, V.; Stafilov, T.; Kilár, F. Identification of polyphenolic compounds in red and white grape varieties grown in R. Macedonia and changes of their content during ripening. *Food Res. Int.* **2011**, *44*, 2851–2860. [CrossRef]

64. Rustioni, L.; Rocchi, L.; Failla, O. Effect of anthocyanin absence on white berry grape (*Vitis vinifera* L.). *Vitis* **2015**, *54*, 239–242.
65. Eitel, J.U.H.; Vierling, L.A.; Litvak, M.E.; Long, D.S.; Schulthess, U.; Ager, A.A.; Krofcheck, D.J.; Stoscheck, L. Broadband, red-edge information from satellites improves early stress detection in a New Mexico conifer woodland. *Remote Sens. Environ.* **2011**, *115*, 3640–3646. [CrossRef]
66. Asmaryan, S.; Warner, T.A.; Muradyan, V.; Nersisyan, G. Mapping tree stress associated with urban pollution using the WorldView-2 Red Edge band. *Remote Sens. Lett.* **2013**, *4*, 200–209. [CrossRef]
67. Horler, D.N.H.; Dockray, M.; Barber, J. The red edge of plant leaf reflectance. *Int. J. Remote Sens.* **1983**, *4*, 273–288. [CrossRef]
68. Smith, K.L.; Steven, M.D.; Colls, J.J. Use of hyperspectral derivative ratios in the red-edge region to identify plant stress responses to gas leaks. *Remote Sens. Environ.* **2004**, *92*, 207–217. [CrossRef]
69. Borràs, E.; Ferré, J.; Boqué, R.; Mestres, M.; Aceña, L.; Busto, O. Data fusion methodologies for food and beverage authentication and quality assessment—A review. *Anal. Chim. Acta* **2015**, *891*, 1–14. [CrossRef]
70. Feng, Z.; Song, L.; Duan, J.; He, L.; Zhang, Y.; Wei, Y.; Feng, W. Monitoring wheat powdery mildew based on hyperspectral, thermal infrared, and rgb image data fusion. *Sensors* **2021**, *22*, 31. [CrossRef] [PubMed]
71. Owomugisha, G.; Nuwamanya, E.; Quinn, J.A.; Biehl, M.; Mwebaze, E. Early detection of plant diseases using spectral data. In Proceedings of the 3rd International Conference on Applications of Intelligent Systems, Las Palmas de Gran Canaria, Spain, 7–9 January 2020; pp. 1–6. [CrossRef]
72. Golhani, K.; Balasundram, S.K.; Vadamalai, G.; Pradhan, B. A review of neural networks in plant disease detection using hyperspectral data. *Inf. Process. Agric.* **2018**, *5*, 354–371. [CrossRef]
73. Li, S.; Song, W.; Fang, L.; Chen, Y.; Ghamisi, P.; Benediktsson, J.A. Deep learning for hyperspectral image classification: An overview. *IEEE Trans. Geosci. Remote Sens.* **2019**, *57*, 6690–6709. [CrossRef]
74. Mishra, P.; Polder, G.; Vilfan, N. Close range spectral imaging for disease detection in plants using autonomous platforms: A review on recent studies. *Curr. Robot. Rep.* **2020**, *1*, 43–48. [CrossRef]
75. MacDonald, S.L.; Staid, M.; Staid, M.; Cooper, M.L. Remote hyperspectral imaging of grapevine leafroll-associated virus 3 in Cabernet Sauvignon vineyards. *Comput. Electron. Agric.* **2016**, *130*, 109–117. [CrossRef]

Chapter 5

Seeing the unseen: Detecting plant viral diseases using high-resolution hyperspectral imagery

Wang, Y.M.; Ostendorf, B.; Pagay, V.

Preamble:

Proximal hyperspectral sensing offers the capability to detect disease symptoms that are challenging to visualise. However, compared to remote sensing methods, it is relatively slow, making it difficult to efficiently detect diseases in large vineyards. To overcome this limitation, low-altitude flying UAVs can be equipped with small hyperspectral cameras to conduct vineyard-scale scanning. This technology provides distinct advantages, including high spatial and spectral resolution hyperspectral images, which enable the rapid detection of unnoticeable grapevine viral disease symptoms on a large scale. This chapter presents a study that leveraged UAV-based hyperspectral remote sensing data to detect GLD and SD in three Australian vineyards. This chapter has been submitted for publication on 5 May 2023 and is currently under review for publication in the journal - *ISPRS Open Journal of Photogrammetry and Remote Sensing*.

Statement of Authorship

Title of Paper	*Seeing the unseen:* Detecting plant viral diseases using high-resolution hyperspectral imagery
Publication Status	☐ Published ☐ Accepted for Publication ☑ Submitted for Publication ☐ Unpublished and Unsubmitted work written in manuscript style
Publication Details	Submitted for publication in ISPRS Open Journal of Photogrammetry and Remote Sensing on 05 May 2023

Principal Author

Name of Principal Author (Candidate)	Yeniu (Mickey) Wang		
Contribution to the Paper	Designed the experiments Carried out the field and lab works to gather data Conducted data processing and analysis Drafted the manuscript and revision		
Overall percentage (%)	80%		
Certification:	This paper reports on original research I conducted during the period of my Higher Degree by Research candidature and is not subject to any obligations or contractual agreements with a third party that would constrain its inclusion in this thesis. I am the primary author of this paper.		
Signature		Date	13/06/2023

Co-Author Contributions

By signing the Statement of Authorship, each author certifies that:

i. the candidate's stated contribution to the publication is accurate (as detailed above);
ii. permission is granted for the candidate in include the publication in the thesis; and
iii. the sum of all co-author contributions is equal to 100% less the candidate's stated contribution.

Name of Co-Author	Bertram Ostendorf		
Contribution to the Paper	Conceptualisation Reviewed and edited the manuscript		
Signature		Date	20/06/2023

Name of Co-Author	Vinay Pagay		
Contribution to the Paper	Conceptualisation Reviewed and edited the manuscript Corresponding author		
Signature		Date	27/06/2023

Seeing the unseen: Detecting plant viral diseases using high-resolution hyperspectral imagery from UAV

Yeniu Mickey Wang [a, b], Bertram Ostendorf [c] and Vinay Pagay [a,*]

[a] School of Agriculture, Food & Wine, Waite Research Institute, University of Adelaide, PMB 1, Glen Osmond, Adelaide 5064, SA, Australia

[b] CSIRO, Manufacturing, Autonomous Sensors Future Science Platform, 13 Kintore Ave, Adelaide, SA, 5000, Australia

[c] School of Biological Sciences, The University of Adelaide, Molecular Life Sciences Building, North Terrace Campus, Adelaide 5005, SA, Australia

*Corresponding author.
E-mail: vinay.pagay@adelaide.edu.au (V. Pagay)

Abstract

Plant viral diseases cause substantial productivity and economic losses to crops globally. Current disease detection methods are expensive and labour-intensive. Low-altitude hyperspectral remote sensing provides high spectral and spatial resolutions required for precise disease detection of crops, and is particularly useful in cropping systems that have inter-row vegetation such as orchards and vineyards. However, no studies to date have applied this method for the detection of viral diseases in grapevine (*Vitis* spp.). The present study evaluates the feasibility of unmanned aerial vehicle (UAV)-based hyperspectral sensing in the visible and near-infrared (VNIR) spectral bands to detect two economically significant viral diseases – Grapevine Leafroll Disease (GLD) and Shiraz Disease (SD) – in four popular wine grapevine cultivars in Australian vineyards. The partial least squares discriminant analysis (PLS-DA) method was used to discriminate between diseased and healthy pixels from the hyperspectral image. The diseased vines were classified with Receiver Operating Characteristics (ROC) curve using the disease pixel ratio. The model predictions for red- and white-berried grapevine cultivars achieved an accuracy of 98% and 75%, respectively. For each viral disease, unique spectral regions and optimal detection times during the growing season were identified. Our work demonstrates the value of hyperspectral remote sensing for the detection of viral disease infection patterns in vineyards within both red and white grape cultivars.

Keywords: Grapevine Leafroll Disease; Shiraz Disease; low-altitude remote sensing; GLRaVs; GVA; PLS-DA; virus surveillance

1. Introduction

Grapevine viral diseases cause substantial productivity and economic losses in the viticulture industry globally (Basso et al., 2017; Martelli, 2017). Virus infections alter the physiology of the vines, which affects carbohydrate metabolism, unbalances plant hormones, reduces chlorophyll content, and accumulates soluble sugar in the leaves thereby reducing the sugar translocated to the fruit (Hull, 2014b; Naidu et al., 2015). The latter leads to lower total soluble solids in berries, decreased anthocyanin in berry skin, and reduced yield of the grapes (Alabi et al., 2016; Lee et al., 2009; Naidu et al., 2014). Long-term economic losses have been reported in vineyards if viral diseases are neglected (Atallah et al., 2012). Grapevine Leafroll Disease (GLD) is an economically significant viral disease in Australia (Habili et al., 2007). GLD can affect many grapevines including both red and white cultivars (Chooi et al., 2022; Pietersen et al., 2013). Several grapevine leafroll-associated viruses (GLRaVs) have been linked with GLD (Habili et al., 2007; Naidu et al., 2015). GLRaV-1, -3, and -4 strains were more frequently detected than other GLRaV strains in Australian vineyards (Constable and Rodoni, 2014). Shiraz Disease (SD) is another debilitating viral disease that delays bud burst, restricts the spring growth of shoots, and delays the lignification of canes as well as leaf senescence (Goszczynski and Habili, 2012; Habili, 2013). SD symptoms have been observed in only a few sensitive grapevine cultivars including Shiraz, Merlot, and Malbec (Goszczynski et al., 2008). Grapevine virus A (GVA) is associated with SD (Habili et al., 2016; Wu et al., 2020), particularly the GVA Group II variants (Goszczynski and Habili, 2012; Goszczynski and Jooste, 2003). In a recent survey of Australian vineyards, Wu et al. (2023) found that all three variants (Group I, II, and III) of GVA were present and that Group II variants were the only ones that were symptomatic. Co-infection of GVA and GLRaVs are commonly found in grapevines (Blaisdell et al., 2020; Credi, 1997; Digiaro et al., 1994; Hommay, 2008).

Unlike bacterial or fungal diseases that can be controlled by chemical applications, no such methods are available for the treatment of virus infections (Hull, 2014a; Rubio et al., 2020). Thus, the management of grapevine viral diseases is predominantly preventive, such as planting certified (virus-free) material, controlling the spread of vectors such as mealybugs and soft scale insects, and roguing (removing) infected vines from vineyards (Bell et al., 2017; Douglas and Krüger, 2008; Hommay et al., 2022). Roguing relies on accurate disease detection, which presently includes the visual assessment of symptoms, and laboratory-based tissue testing using the serological method, such as enzyme-linked immunosorbent assay (ELISA) and nucleic acid-based method, such as Reverse-transcription polymerase chain reaction (RT-PCR) (Naidu and Hughes, 2003; Zherdev et al., 2018). However, the visual assessment is labour intensive and can be subjective; the laboratory-based methods are highly costly therefore limiting the test rate. The cost of different detection methods was compared by Wang et al. (2022).

Advanced optical sensing technology, such as hyperspectral sensors, has shown potential for non-destructive plant disease detection (Zhang et al., 2020). Hyperspectral sensors can measure a continuous narrow range of spectral wavelengths from visible and near-infrared (VNIR) to short-wave infrared (SWIR) that can provide detailed spectral signal changes related to leaf health and potentially caused by plant diseases (Thenkabail et al., 2011; Thomas et al., 2018). Various studies have used hyperspectral sensing for plant disease detection (Nguyen et al., 2021; Wang et al., 2019; Zhang et al., 2019; Zhu et al., 2017). For GLD detection, a direct leaf contact spectroradiometer (spectral range 350 – 2500 nm) was used to measure GLRaV-3 infection in Cabernet Sauvignon (Sinha et al., 2019); classification accuracy of 93-98% was achieved. The proximal sensing with a handheld hyperspectral sensor (spectral range 325-1075 nm) was used to detect GLD in Pinot Noir and Chardonnay with 96% and 76% prediction accuracies respectively (Wang et al., 2023a). An over-the-row grape harvester-mounted hyperspectral camera (spectral range 400-2500 nm) was used to detect GLD in four grape

cultivars (Bendel et al., 2020). The authors achieved classification accuracies of 84-96% in red cultivars and 76-93% in white cultivars. These direct contact and proximal sensing method can give relatively high spatial resolution, however, are time-consuming, labourious, and therefore expensive compared to remote sensing methods making them impractical for large vineyards (Wang et al., 2022).

Remote sensing can provide information over large areas rapidly and there has been much recent development, but there is little information about the necessary spatial and spectral detail needed for viral disease detection in grapevines. An aircraft-mounted hyperspectral camera (with a spectral range of 400-1000 nm and 0.25-0.50 m spatial resolution) was used to detect GLRaV-3 infection in Cabernet Sauvignon with 94% disease detection sensitivity (MacDonald et al., 2016). An accuracy of 87% was achieved when distinguishing between noninfected and asymptomatic GLRaV-3 infected vines using a hyperspectral camera mounted on an airplane (Galvan et al., 2023), the camera had a spectral range of 380-2510 nm and a spatial resolution of 3 meters. Multispectral satellite imagery (red, green, blue, and near-infrared bands with 50 m spatial resolution) was used to detect GLD in Merlot and Cabernet Sauvignon with 75-94% classification accuracies (Hou et al., 2016). The high operating altitudes of manned aircraft and satellites result in relatively low spatial resolution compared to unmanned aerial vehicles (UAV), which lowers their accuracy of disease detection. The low spatial resolution limitation has been overcome recently through the use of UAV with various optical sensors, which are now frequently employed for grapevine disease detection (Albetis et al., 2017; Vanegas et al., 2018; Wang et al., 2023b; Zia-Khan et al., 2022). However, there is little information about how transferrable findings are in space, time, and for different varieties, and the benefit of combining high spectral detail with high spatial resolution is unknown.

In this study, we assess the potential of a UAV-based hyperspectral camera in the VNIR spectral range to detect GLD- and SD-infected grapevines in four popular winegrape (*Vitis vinifera* L.) cultivars, including both red and white cultivars, from three viticulture regions in South Australia. The specific objectives of this study are: (1) develop a workflow to classify healthy and diseased vines from high-resolution hyperspectral remote sensing images; (2) investigate spectral reflectance differences between the healthy and virus-infected vines across different cultivars and locations; (3) build a prediction model to classify diseased vines from healthy vines using PLS-DA method; (4) assess the prediction accuracy to determine the optimal growing stage for disease detection; and, (5) evaluate the robustness of model with data from different seasons and locations. To the best of our knowledge, this study is the first to use a UAV-based hyperspectral sensor for grapevine viral disease detection.

2. Materials and Methods

2.1. Study sites and weather

Three virus-infected vineyards in South Australia were selected for this study (Fig. 1). The first vineyard was in Adelaide Hills wine region, located in Kuitpo, SA (35°13'31"S, 138°39'40"E). Three blocks in this vineyard were selected for the study, including 0.8 ha of Chardonnay, 1.6 ha of Pinot Noir, and 1.4 ha of Cabernet Sauvignon. The Chardonnay and Pinot Noir were planted in 1987, and Cabernet Sauvignon was planted in 1988. All vines were own-rooted and planted at 3.0 x 1.5 m (row x vine) spacing. The soil type of the vineyard was podsol over sandstone. The vineyard was drip-irrigated at approx. 0.8 ML ha^{-1} annually. Ryegrass and clover were planted inter-rows as the cover crop. Integrated pest management (IPM) was as per convention in this region. The vines were sprayed two to three times with sulphur and copper-based chemical to prevent pest and fungi disease.

The second vineyard was in the Barossa wine region, located in Lyndoch, SA (34°35'28"S, 138°53'01"E). A 3 ha block was chosen for the study with 24 rows of own-rooted Cabernet Sauvignon grapevines planted in 1997. Half of the block (12 rows) was top-worked (grafted) with Shiraz in 2015. The block had 3.0 x 1.5 m (row x vine) spacing that sits on a deep red clay loam soil. It was drip-irrigated at approx. 1.5 ML ha^{-1} per year. Convention regional IPM practices were applied to the vineyard. Sulphur-based fungicide was used to prevent mildew diseases. Barley was planted in winter as a cover crop in the middle rows.

The third vineyard was located in the Riverland region, in Monash, SA (34°13'28"S, 140°33'01"E). A block of 1.5 ha of grafted Shiraz grapevines was selected for the study. The Shiraz (on K51-40 rootstock) was planted in 1998 with 3.5 x 3.5 m (row x vine) spacing. The soil type of vineyard is sand soil over limestone. The block was drip-irrigated at approx. 7.5 ML ha^{-1} per year. No cover crop was growing in the vineyard. Generally low disease pressure in this wine region due to the dry and warm climate. Usually, two to three sulphur-based fungicides were sprayed per season.

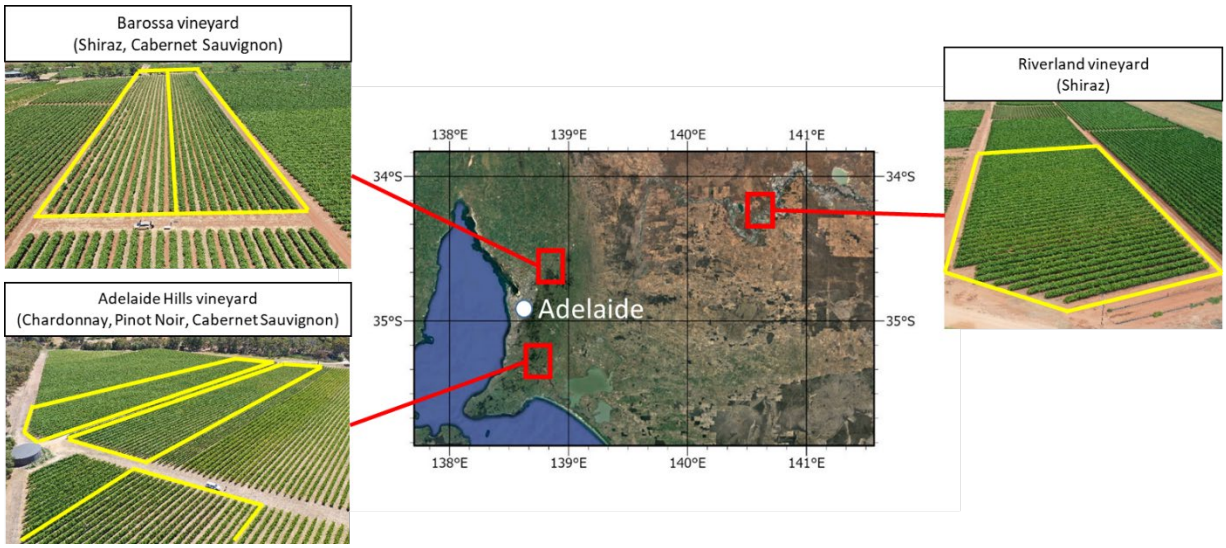

Fig. 1. Location of the study sites in South Australia

Each of the vineyards chosen for the study was in a different climatic region. The Adelaide Hills vineyard had relatively cooler weather (Mean January Temperature (MJT) is 18.9 °C) and higher rainfall (annual rainfall is 835 mm). Barossa vineyard was in a warm weather region (MJT is 22.1 °C) and had lower rainfall (annual rainfall is 438 mm). The Riverland vineyard was in a hot and dry region. The temperature in Riverland was the highest (MJT is 25.9 °C) and rainfall was the lowest (annual rainfall is 269 mm) in the three locations. Seasonal weather data obtained from the closest weather station to each vineyard site is provided in Table 1.

Table 1

Summary of weather data from 1st Oct to 31st Mar in each vineyard in the 2020-21 season (S1), and 2021-22 season (S2) for Adelaide Hills. The data was gathered from the weather stations of the Australian Bureau of Meteorology – Kuitpo Forest Reserve (Bureau of Meteorology (BOM) Station ID 023887) for Adelaide Hills, Nuriootpa PIRSA (BOM Station ID 023373) for Barossa, and Loxton Research Centre (BOM Station ID 024024) for Riverland.

Vineyards	**Barossa**	**Riverland**	**Adelaide Hills**	
Season	S1	S1	S1	S2
Average maximum temperature (°C)	26.4	29.0	22.8	22.4
Average minimum temperature (°C)	8.5	9.5	11.9	12.1

Average maximum relative humidity (%)	93.0	80.0	90.2	91.6
Average minimum relative humidity (%)	24.0	19.0	42.8	44.5
Average solar radiation (MJ m^{-2})	22.6	23.3	21.5	21.6
Accumulated evapotranspiration (mm)	1,009	1,153	864	845
Accumulated rainfall (mm)	129	80	246	190
GDD (°C)[1]	1,633	1,959	1,343	1,319

[1] GDD = growing degree days (base 10°C)

2.2. Visual assessment and lab testing for the viral diseases

A visual assessment was conducted in each block in the 2020-21 season (S1) and 2021-22 season (S2) for the Adelaide Hills vineyard. In the early season, e.g., at the flowering stage (E-L 23), no disease symptoms were observed in Chardonnay, Pinot Noir, and Cabernet Sauvignon in any vineyards. The GLD symptoms (reddening on leaves with green veins) could be observed on some leaves around the veraison stage (E-L 35) in Pinot Noir and Cabernet Sauvignon in both Adelaide Hills and Barossa vineyard. The GLD symptoms gradually became more obvious later in the season (Fig. 2 a, b). In comparison to red cultivars, the disease symptoms of Chardonnay were not as obvious as white cultivars do not produce anthocyanin pigments (Burger et al., 2017; Rustioni et al., 2015). Chardonnay only showed a rolling edge and slight chlorosis on some of the leaves from the veraison stage (Fig. 2 d). For Shiraz vines, SD symptoms (delayed growth with a shorter shoot and smaller canopy) were observed in spring in both Barossa and Riverland vineyards. By mid-summer (approx. fruit set stage, E-L 27), healthy and infected vines had indistinguishable canopy sizes. However, in the virus-infected vines, there were noticeable bright green young leaves developed from the tip of the mature shoot throughout the season even after harvest. Most mature leaves of SD-infected vines became anthocyanic as the season progressed, turning from dark green to a dark red colour, including veins (in contrast to GLD). These changes make the young bright green colour leaves more visually distinct (Fig. 2 d). In comparison, healthy Shiraz grapevines stopped developing the young leave after the veraison stage. The estimated disease incidence rate for each block is summarised in Table 2.

Table 2. Virus infection status in each block used in this study. Disease incidence was estimated by visual assessment. Positive test results of any combination of GLRaVs and GVA virus were categorised as 'diseased' while negative results for all GLRaV-1, -3, -4 strains and GVA were categorised as 'healthy'.

Vineyard and cultivars	Total number of vines per block	Estimated disease incidence at harvest	Number of vines tested	Number of positive tests	Number of negative tests
Adelaide Hills - Chardonnay	2,640	50%	194	144	50
Adelaide Hills – Pinot Noir	4,302	20%	192	84	108
Adelaide Hills – Cabernet Sauvignon	3,664	5%	80	39	41

Barossa - Cabernet Sauvignon	2,700	10%	72	36	36
Barossa - Shiraz	2666	15%	72	38	34
Riverland - Shiraz	1185	5%	42	19	23

Fig. 2. Grapevine viral disease symptoms at harvest stage (E-L 38). GLD symptoms on (a) Cabernet Sauvignon, (b) Pinot Noir, and (c) Chardonnay; (d) SD symptoms on Shiraz (the red arrow shows young leaves still developing at the harvest time).

For ground-truthing, the laboratory-based tissue testing was conducted in S1 in each vineyard and 20% of the random sample was resampled for confirmation test in S2 in Adelaide Hills vineyard. The sampling was based on visual symptoms. Even numbers of symptomatic and asymptomatic vines were randomly and scatteredly collected across each block. Each sampled vine had an ID with row and vine number. Leaf petioles were sampled near harvest time for virus testing as the virus titre level is usually high in petiole tissues in the later season (Monis and Bestwick, 1996). The leaves were selected from shoots located near the trunk of the vine to ensure that neighbouring vines were not inadvertently sampled. Four petioles near the base of the shoots were sampled for testing.

All samples were virus-tested in the lab using the ELISA test kits produced by Bioreba (Reinach, Switzerland). GVA, GLRaV-1, GLRaV-3, and GLRaV-4 strains were conducted for each sample. The

GLRaV-4 strains test kit can detect GLRaV-4, and GLRaV-4 strains 5, 6, and 9 (Bioreba_AG, 2017). To validate the ELISA test results, approx. 20% of ELISA-tested samples from each block (125 samples in total) were tested with RT-PCR (Gambino, 2015; Zherdev et al., 2018). The petiole samples were sent to a commercial grapevine virus diagnostics lab (Affinity Labs, Adelaide) for the RT-PCR test. GVA, GLRaV-1, GLRaV-3, GLRaV-4, and GLRaV-4 strains 6 and 9 were tested as these grapevine viruses were most frequently been found than other viruses in Australian vineyards (Constable and Rodoni, 2014). The RT-PCR test results matched 99% of the ELISA results, which confirms the reliability of the ELISA tests. The ELISA test closely correlated with visual assessments in both seasons. In all cases where vines displayed symptoms, the ELISA test yielded positive results, and in 98% of cases where vines were asymptomatic, the ELISA test produced negative results. When comparing the seasonal difference, visual assessments and virus testing results between S1 and S2 in Adelaide Hills were 95% and 100% matching respectively.

The virus test results showed that 95% of virus infections were co-infected with GLRaV-1 and GVA in the Adelaide Hills vineyard, and the rest of the infected vines had mixed infections with GLRaV-1, -4s, or -9 and GVA in this vineyard. In the Barossa vineyard, the majority (90%) of virus infection in Cabernet Sauvignon was the co-infection with GLRaV-1, -4s or -9, and GVA, and about 10% of vines were co-infected with GLRaV-4s or -9 and GVA. For Shiraz, most of the virus-infected vines were GLRaV-1, -4s or -9, and GVA, except two vines were co-infected with GLRaV-1, -3, -4s and GVA in Barossa. The infection in the Riverland vineyard was mostly GLRaV-4s or -9 with GVA, except for three vines infected with only GVA. The detailed test result shows in Appendix A (Table 1). Since these GLRaV strains are associated with GLD symptoms in Chardonnay, Pinot Noir, and Cabernet Sauvignon (Naidu et al., 2014), and GVA were associated with SD symptoms in Shiraz (Goszczynski and Habili, 2012), the vines that were infected with any combination of GLRaVs or GVA infection (single or co-infection) were treated as the diseased vine. The vines that tested negative for all these viruses were considered healthy vines. The summarised virus test results for each block are shown in Table 2.

2.3. UAV data collection

The hyperspectral images were collected by Resonon airborne hyperspectral system (Resonon Inc. Bozeman, USA). The system includes the Resonon Pika L camera, an IMU/GPS unit, and an onboard computer. The system was mounted on a three-axis gimbal carried by DJI Matrice 600 UAV (SZ DJI Technology Co., Ltd, Shenzhen, China). The hyperspectral camera was a push-broom type sensor (Fowler, 2014). The sensor detects spectral wavelengths between 400 – 1000 nm at a 3.3 nm spectral resolution with 12-bit colour depths and 900 spatial pixels swath. The focal length of the lens was 17 mm and the f-number was 2.4 which gives a 17.6-degree field of view. The framerate was set at 150 fps. To avoid over-exposure, the exposure time was set before each flight by auto-exposure of the camera to the 21% flat reflectance panel. The exposure time was usually between 4 to 6 ms with zero gain under full sunlight conditions. A geo-fence with three meters buffer around each block was set for the camera system that triggered the recording when the system entered the geofenced region. The flying missions were operated using the DJI GS Pro app (SZ DJI Technology Co., Ltd, Shenzhen, China). The missions used lawnmower patterns aligned to vine rows and covered whole blocks with ten meters buffers. The altitude of the flights was 60 m above ground level (AGL). The flying speed was 3 m s^{-1}, which was calculated using the Resonon airborne calculator based on the framerate, altitude, and field of view to produce the images with an aspect ratio close to one. The resulting spatial resolution of the hyperspectral image was approx. 4 cm px^{-1}. The side overlap was 50% to avoid gaps between flight paths. The airborne system wrote the data and generate one hyperspectral data cube every ten seconds. Each flight captured between 32 to 48 hyperspectral data cubes depending on the

block size. There were between 6 to 12 flying paths per block depending on the width of the block. Each UAV path contained 4 to 9 hyperspectral data cubes depending on row length.

For hyperspectral radiometric correction, custom-made grey-scale flat reflectance calibration panels (at 19% and 21% reflectances) were used (Sanches et al., 2009). The spectral reflectance of the calibration panel was measured proximally with an ASD Handheld 2 spectroradiometer (Malvern Panalytical Ltd, Malvern, UK) that was calibrated with the white Spectralon® diffuse reflectance material (>99% reflectance). The grayscale panel was included in the scenes of the hyperspectral image as the known spectral reflectance target in each flight.

Concurrently with each hyperspectral data collection mission, UAV-based high-resolution RGB imagery was also collected for geo-referencing the hyperspectral images. DJI Mavic 2 Pro UAV (SZ DJI Technology Co., Ltd, Shenzhen, China) was used for RGB image collection. The camera had a 77-degree field of view with 5472 × 3648 pixels in image size. The flight path was automated by Pix4Dcapture (Pix4D, Prilly, Switzerland). The side and forward overlap was set at 80 %, and an altitude of 45 m AGL. The calculated spatial resolution or ground sample distance (GSD) of the images was approx. 1 cm.

UAV data was collected at three phenological stages of grapevine development: flowering (November), veraison or onset of fruit ripening (January), and harvest (March) in Adelaide Hills and Barossa vineyards in S1. In the Riverland vineyard, data were collected at two time points, November 2020 and March 2021, in the same season. In S2, data were collected at only one time point in the Adelaide Hills vineyard in March 2022 (harvest). All UAV data was collected under sunny and cloudless conditions between 11:00 to 15:00 h.

2.4. UAV image processing

2.4.1. Geo-locating individual vines with RGB UAV images

All the vineyards in this study were planted in rows. When the canopy of the vine fully developed, it was difficult to determine the individual vine from the projected remote sensing image. In order to accurately confirm the canopy of the virus-tested vines from the remote sensing images, precise relative geolocation of each vine was required. A high-resolution orthomosaic RGB UAV image was generated for each block using Agisoft Metashape Professional, Version 1.6.2. (Agisoft LLC, St. Petersburg, Russia). The geo-referenced orthomosaic image from the dormancy period (when trunk shadows can be clearly observed) was used as the reference map. A shape file of a fishnet grid with centre label points was created for each block in ArcGIS Pro V2.8 (Esri, Redlands, California, US). The centre points were manually adjusted to the starting point of the trunk shadow, which represented the base of the vine trunk (Fig. 3a). A square bounding box was created from each centre point to cover the individual vine. The box size was set at about 90 % of vine spacing to avoid potentially overlapping regions between neighbouring vines within a row. In the Adelaide Hills and Barossa vineyards (with 1.5 m vine spacing), the box size was 1.4 x 1.4 m. The box size of Riverland vineyard (with 3.5 m vine spacing) was 3 x 3 m.

For each time point, a high-resolution orthomosaic image from the RGB UAV images was created and manually geo-referenced to the dormancy image (Fig. 3b) by using the end post from each corner of the block as the ground control points (GCP). The hyperspectral could then be registered to the orthomosaic image in order to accurately align individual vines for an accurate data process.

(a) **(b)**

Fig. 3. Geo-locating individual vines using high-resolution RGB UAV images. **(a)** Top view of the vineyard at dormancy that the shadow of the trunk is clearly showing. Red dots highlight the trunk location (base), which was the starting point of the shadow of the trunk. The 1.4 x 1.4 m bounding box (shape file) was created for each vine; **(b)** bounding boxes were used to delineate individual grapevine canopies in the hyperspectral orthomosaic.

2.4.2. Hyperspectral image processing

The hyperspectral image processing was conducted in Spectronon software (Resonon Inc. Bozeman, USA). The raw hyperspectral data were radiometrically corrected using the average spectral radiance of the grey scale calibration panel in the scene. The radiometric correction process transformed the digital number (DN) into a reflectance value (range 0-1). The hyperspectral data was then geo-rectified using the IMU/GPS data with a digital elevation model that was created from the point cloud from the high-resolution UAV RGB images in Agisoft Metashape. Each georectified hyperspectral image covered

296 an area of approx. 50 x 16 m (L x W) with a GSD of 4 cm. The hyperspectral images were then
297 mosaicked using the 'Seamless Mosaic' tool in ENVI (L3Harris Geospatial, Colorado, US) to create a
298 single strip hyperspectral image per each UAV path. Then the registration for each hyperspectral strip
299 image was conducted using the 'Image to Map Registration' tool in ENVI. The end posts of vine rows
300 were used as the GCPs for manually registering the hyperspectral strips to the geo-referenced
301 orthomosaic UAV RGB image that was collected on the same day. The resampling method for the
302 registration process was the nearest neighbour (Olivier and Hanqiang, 2012). Finally, all strips were
303 mosaicked to generate a single hyperspectral image for the whole block with the geo-location of
304 individual vines that could be accurately identified.

305 The raw hyperspectral image had 150 bands from 380 – 1015 nm. However, spectral bands below 400
306 nm and above 920 nm were removed due to the high noise caused by low camera sensitivity in these
307 regions, which resulted in 123 useful bands from 400 – 920 nm (Fig. 4b).

308 In this study, the grape canopy is the region of interest. A mask was created to eliminate the non-
309 grapevine canopy regions, e.g. inter-row areas, by using the classification tool in ENVI. The spectral
310 angle mapper algorithm (Yuhas et al., 1992) was used in the supervised classification tool to classify
311 grapevine canopy from the non-canopy area (soil, shadow, and grass). A final clean-up step used a
312 smooth kernel (three kernel sizes) and an aggregation method (nine aggregate minimum sizes) to
313 refine the pixel-level classification.

314 The canopy of virus-tested vines was manually labelled in a bounding box in the classified image based
315 on vine ID (Fig. 4c). Twenty healthy and twenty diseased vines (refer to section 2.8) was randomly
316 selected from each block for the calibration model except Riverland vineyard (ten healthy and ten
317 diseased vines due to fewer samples).

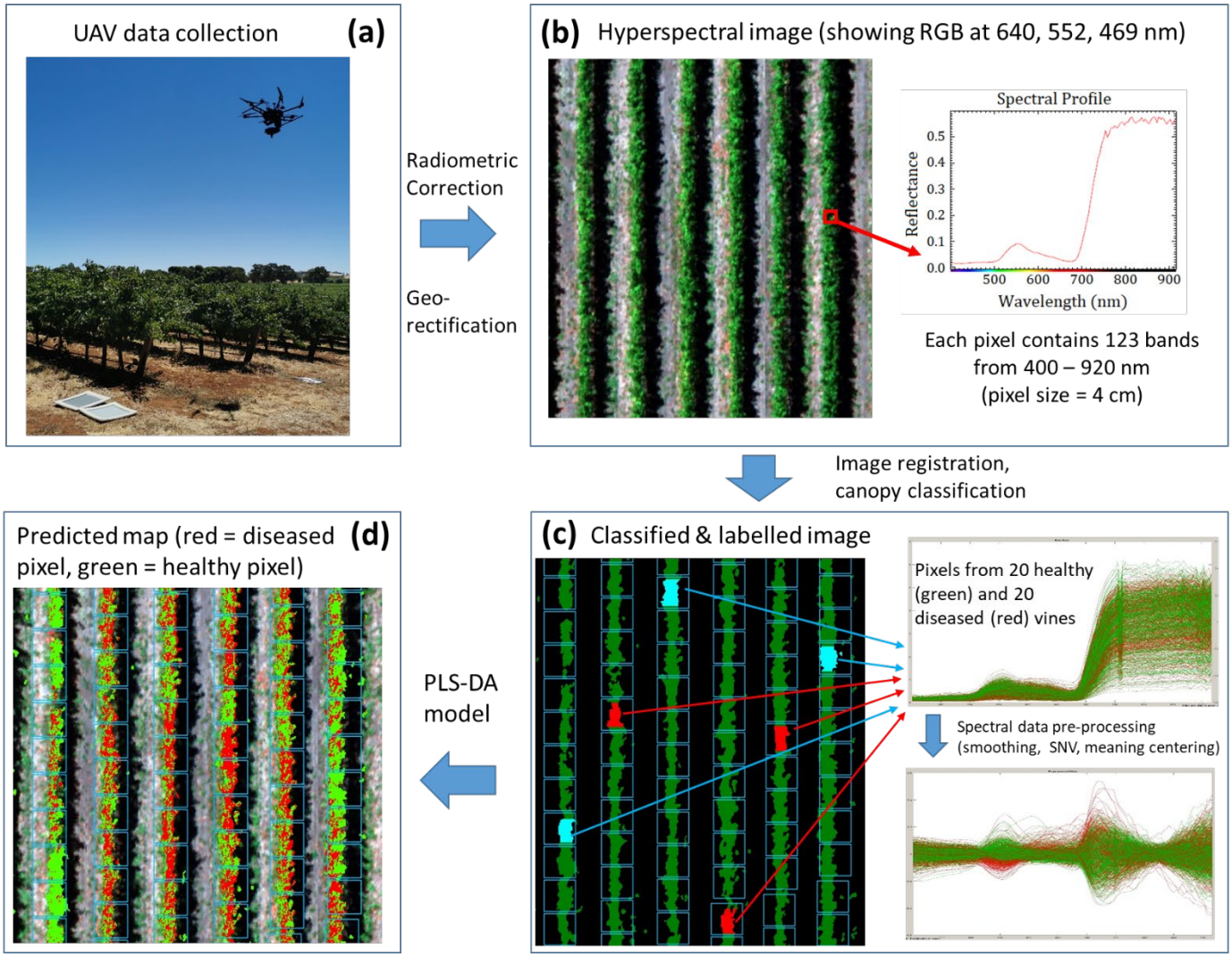

Fig. 4. Workflow for hyperspectral image processing. **(a)** UAV data collection in the vineyard; **(b)** pre-processed hyperspectral image; **(c)** registered and classified image, pixels of 40 virus-tested vines were selected to train the PLS-DA model; **(d)** the prediction result - canopy pixels in the block predicted as either 'disease' (red pixels) or 'healthy' (green pixels).

2.5. Pixel level classification

Classification modelling was conducted in the PLS Toolbox plugin (v.9.0, Eigenvector Research, Inc., Manson, WA USA) in the MATLAB R2021b (The MathWorks Inc., Natick, MA, USA) environment.

The hyperspectral image was loaded into PLS Toolbox with class names for each pixel (Healthy, Disease, Grape canopy, or unclassified = 0). Each pixel was treated as one spectral sample in the PLS-DA model. On average per vine, the Adelaide Hill and Barossa vineyards (1.4 x 1.4 m bounding box) contained approx. 300 – 700 canopy pixels and Riverland vineyard (3 x 3 m bounding box) contained 1,500- 2,400 canopy pixels depending on the development stage of the vine, cultivar, and the canopy training system. For Adelaide Hill and Barossa vineyards, 40 vines resulted in 3,000-7,000 spectral samples (pixels) for the calibration model. There were 15,000-24,000 spectral samples for the Riverland vineyard.

The spectral data were firstly pre-processed with smoothing, normalisation, and scaling steps. Savitzky-Golay Filter (Savitzky and Golay, 1964) with five filter widths was used to reduce the noise in the spectral data. Then, Standard Normal Variate (SNV) (Barnes et al., 1989) was used to normalise the spectral data in order to compensate for the difference in leaf angles and the vine position in the field of view (centre or edge in the image). Lastly, the data was brought to the same magnitude by mean centering (Hofer, 2017) for modelling.

PLS-DA (Barker and Rayens, 2003) classification model was used to classify disease and healthy pixels. The spectral information was set in the X matrix and the disease and healthy classes were set in the Y matrix within PLS Toolbox's PLS-DA model. Cross-validation (CV) was used to avoid overfitting the model. The contiguous block method was selected for the CV method with a number of data split = 20 (Valavi et al., 2019), which means the data set was spatially split into 20 contiguous divisions and one division was left out as the test set. A plot of the cumulative CV error rate was used for latent variable (LV) number selection in the PLS-DA model (Ballabio and Consonni, 2013). The point at which CV errors decreased significantly was the optimum number of LVs selected for the model. The disease discrimination threshold was then set in based on the Receiver Operating Characteristics (ROC) curve to discriminate between diseased and healthy samples from PLS predicted value (Ballabio and Consonni, 2013).

2.6. Vine level classification

The pixel classifications were not 100 % accurate. As shown in Fig. 4d, some vines had mixed 'healthy' and 'disease' pixels in the same boundary box. To evaluate whether a whole vine belongs to a healthy or diseased vine, the ratio of classified 'disease' pixels per bounding box was used. The higher ratio the more likely a diseased vine. The sum of diseased and healthy pixels in each bounding box was calculated by the 'Zonal Statistics' tool in ArcGIS Pro. The ratio of diseased pixels from the 40 vines for modelling was used for the evaluation. An optimal threshold to discriminate healthy and diseased vine was calculated based on the balance between sensitivity (Eqn. 1) and specificity (Eqn. 2) which is the nearest point to the top-left corner of the ROC curve (Hoo et al., 2017). Fig.5 shows the threshold calculated from the ROC curve for Pinot Noir in Adelaide Hills at the harvest stage in Season 1. The threshold is 0.178 based on a sensitivity of 0.895 and a specificity of 0.943. Therefore, based on the threshold, if the diseased pixel ratio was higher than 17.8%, the vine would be predicted as a 'diseased' vine, whereas if it was lower than this ratio, it would be predicted as a 'healthy' vine.

$$Sensitivity = \frac{TP_{vine}}{TP_{vine} + FN_{vine}} \quad (1)$$

$$Specificity = \frac{TN_{vine}}{TN_{vine} + FP_{vine}} \quad (2)$$

where TP_{vine} is the number of diseased vines correctly predicted, FN_{vine} is the number of diseased vines incorrectly predicted, TN_{vine} is the number of healthy vines correctly predicted, and FP_{vine} is the number of healthy vines incorrectly predicted.

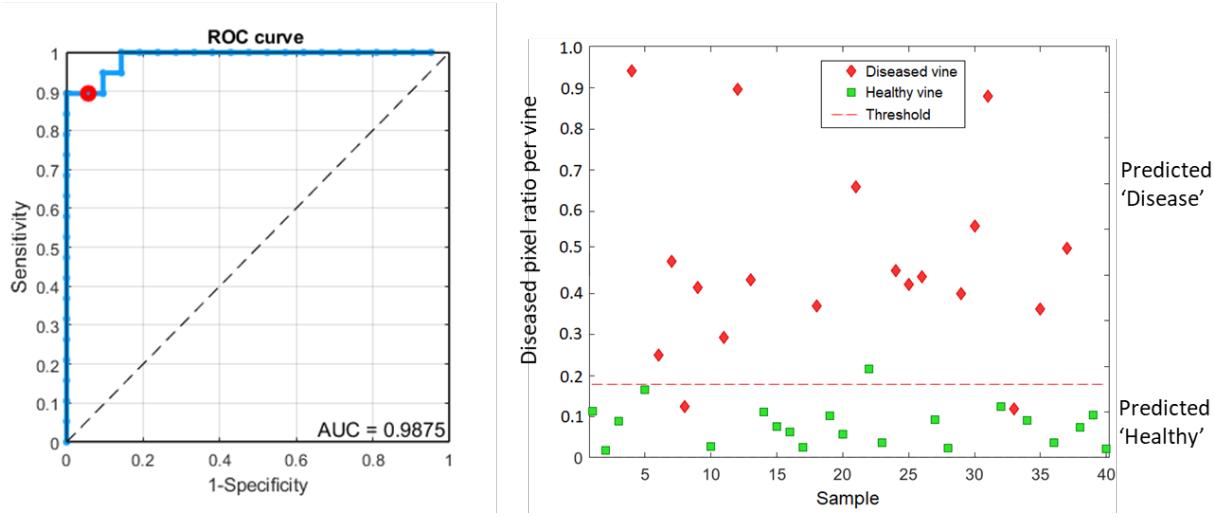

(a) **(b)**

Fig. 5. Vine-level prediction results for Adelaide Hills Pinot Noir at the harvest stage in Season 1. **(a)** ROC curve, the red dot shows the optimal threshold, AUC stand for 'Area under the ROC curve'; **(b)** diseased pixel ratio results for the training data, the threshold is calculated from the ROC curve. In this example, the percentage of predicted diseased pixels higher than the threshold (17.8%) are predicted to be a 'diseased' vine, and pixels lower than the threshold are predicted to be a 'healthy' vine.

2.8. Assessing the minimum number of vines needed for the calibration model

The minimal number of vines needed for the calibration model was evaluated using Pinot Noir at harvest in S1. The different number of vines (balanced number in classes) were selected for the calibration model, and the rest of the virus test vines were used as the validation data. Fig. 5 shows the model became stable and no significant improvement in prediction accuracy for more than 40 vines (20 healthy and 20 diseased vines) selected for the training data. For the other blocks in the study, 20 diseased and 20 healthy vines were selected for modelling for consistency.

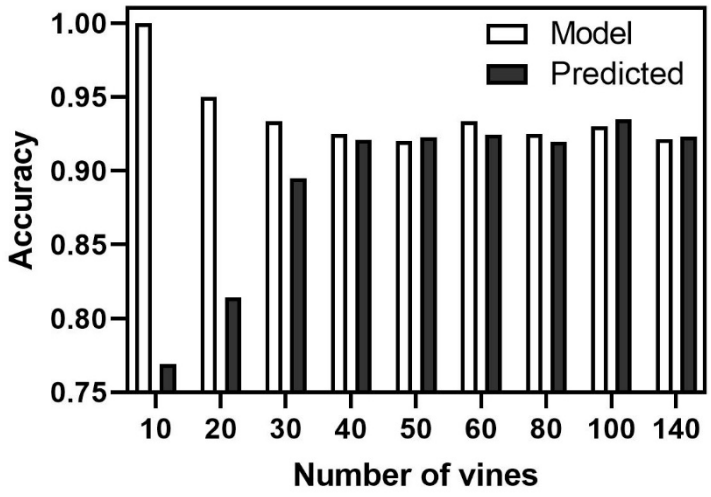

Fig. 6. Accuracy at vine level for the different number of vines selected for modelling. The model became stable and the prediction accuracy did not increase if more than 40 vines (half disease and half healthy) were selected for modelling.

2.7. Accuracy Assessment

A comprehensive result included the confusion matrix accuracy (Eqn. 3), F1 score (Eqn. 4), and Matthews correlation coefficient (MCC; Eqn. 5) (Baldi et al., 2000). Eqn. 3 was used to assess the performance of the model at pixel and vine level. Accuracy and F1 score are commonly used metrics to assess the performance of the classification model (Goutte and Gaussier, 2005; Sokolova et al., 2006). MCC only evaluate binary classifications, but it provides a reliable assessment of an imbalanced data set (Boughorbel et al., 2017; Chicco and Jurman, 2020). In our case, the Adelaide Hills Chardonnay block was a relatively imbalanced data set that had 144 diseased and 50 healthy vines.

$$Accuracy = \frac{TP + TN}{TP + TN + FP + FN} \quad (3)$$

$$F1\ score = \frac{TP}{TP + \frac{1}{2}(FP + FN)} \quad (4)$$

$$MCC = \frac{TP \cdot TN - FP \cdot FN}{\sqrt{(TP + FP) \cdot (TP + FN) \cdot (TN + FP) \cdot (TN + FN)}} \quad (5)$$

where the TP is true positive - diseased pixels correctly predicted; TN is true negative - healthy pixels correctly predicted; FP is false positive - healthy pixels incorrectly predicted as diseased; FN is false negative - diseased pixels incorrectly predicted as healthy.

3. Results

3.1. Spectral difference between healthy and diseased vines

The normalised average spectrum of the diseased vines (relative to healthy vines) for each block and time point is plotted in Fig. 6. The majority of spectral differences between healthy and diseased vines were in the red edge region (700-740 nm), green region (~ 550 nm), and red region (620-640 nm).

In contrast to the red cultivars, virus-infected Chardonnay vines had few differences from healthy vines, and the difference was primarily in the red edge region. In Pinot Noir, diseased vines had higher reflectance in the red and red edge region, and lower reflectance in the green region compared to the healthy vines. That had a similar pattern to the Cabernet Sauvignon from two different vineyards. The diseased Shiraz had higher reflectance in the red edge, as well the green and red regions. The Shiraz from two different vineyards also showed a similar pattern. In terms of the difference in the development stage, the spectral difference between diseased and healthy vines was less in the early season (flowering) and gradually increase and become the largest at the end of the season (harvest).

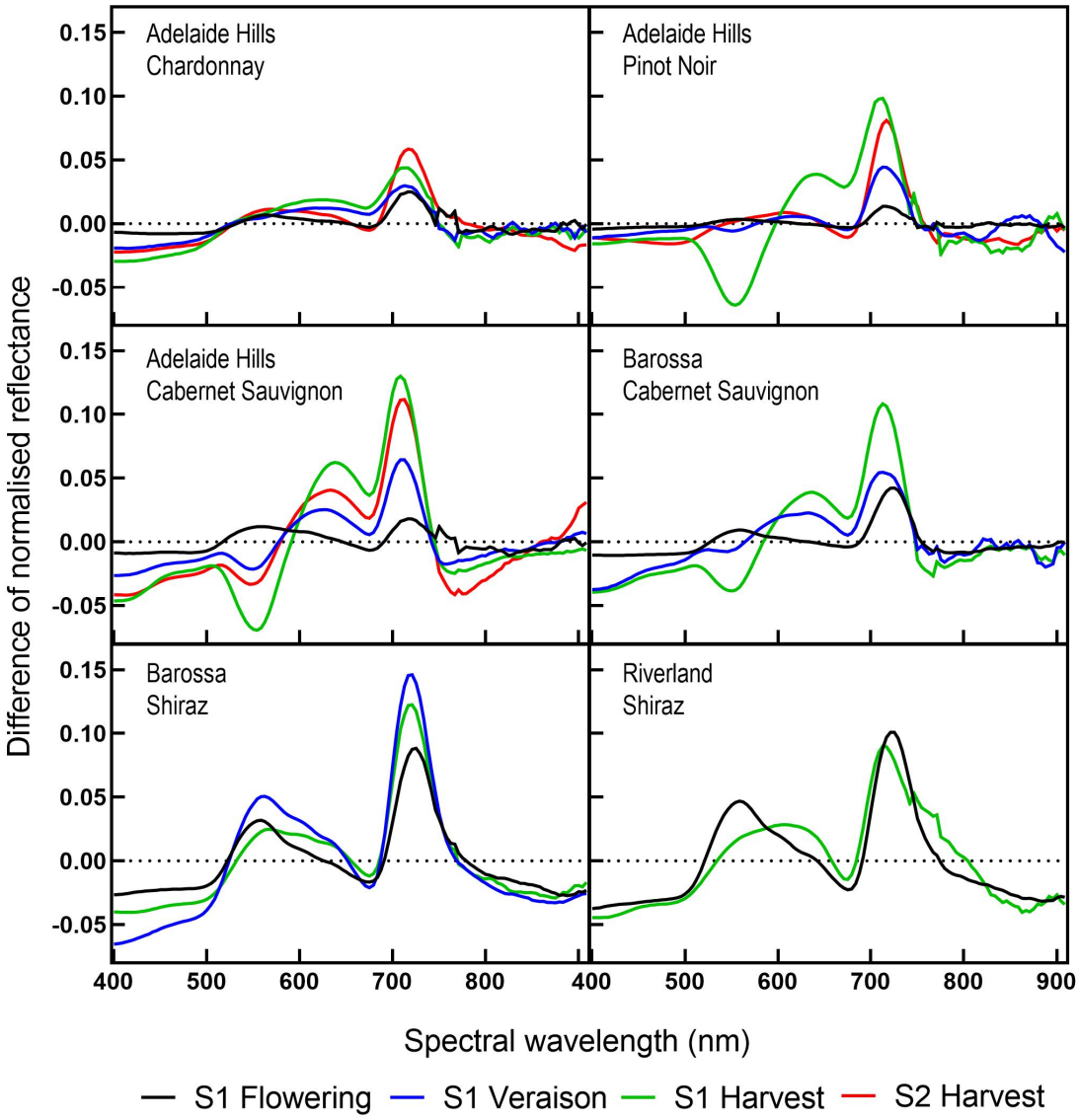

Fig. 7. Difference of normalised average diseased pixels spectral reflectance relative to the healthy. The average spectra were from pixels of 20 diseased and 20 healthy vines at each time point in each block (10 diseased and 10 healthy vines for Riverland Shiraz). Healthy vines at zero line.

3.2. Pixel level classification results

The PLS-DA model performance was assessed at each development stage for each block, and the accuracy of CV for each model is plotted in Fig. 8. In the early development stage (flowering), the accuracy of Chardonnay, Pinot Noir, and Cabernet Sauvignon are low. The accuracy gradually increased and was highest at the harvest stage. In Shiraz, the accuracy at the different stages is relatively close (between 0.76 and 0.83). The highest accuracy was at the veraison stage. Unfortunately, we did not collect the data at the veraison stage for Riverland Shiraz for both seasons.

Compared to the red cultivars, the white cultivar Chardonnay had the lowest accuracy (0.74 at harvest). Pinot Noir and Cabernet Sauvignon in Adelaide Hills had a relatively good performance (accuracy = 0.87). Barossa Cabernet Sauvignon had an accuracy of 0.81 at harvest. The best model for Shiraz was

at the veraison stage (accuracy = 0.83), and accuracy of 0.81 at the harvest stage for both Barossa and Riverland vineyard.

The model built from the second season data at the harvest stage in Adelaide Hills also shows in Fig. 7 (yellow bars). The accuracy was 0.69, 0.70, and 0.84 for Chardonnay, Pinot Noir, and Cabernet Sauvignon, respectively. Detailed model results include the latent variable selected for the model, the confusion matrix, F1 score, accuracy, and MCC for both calibration and CV can be found in Appendix A (Table 2).

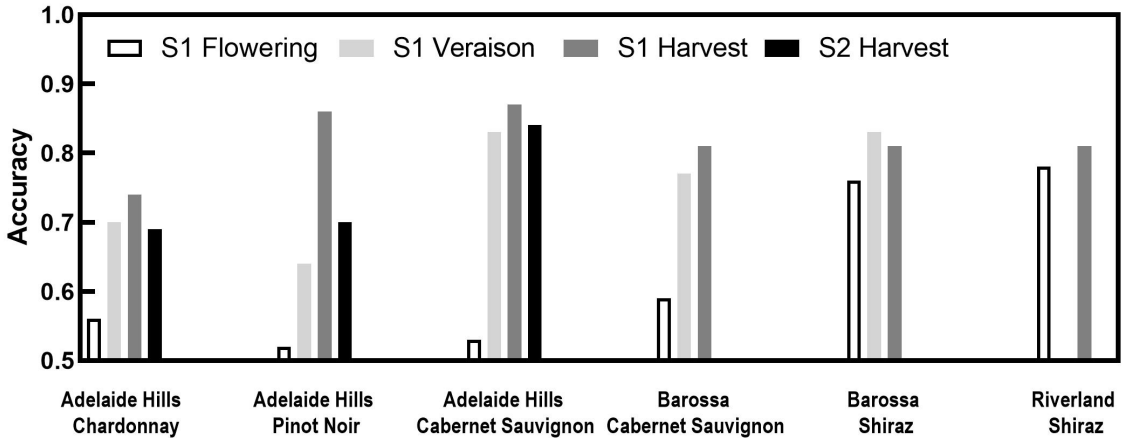

Fig. 8. The accuracy of CV results at the pixel level. Each model is built from the pixel of 20 diseased and 20 healthy vines.

3.3. Vine level classification

At vine level prediction, the diseased pixel ratio for each virus-tested vine (for each block and time point) was assessed. The model and prediction accuracy results at the vine level are presented in Table 3. The more detailed result shows in Appendix A (Table 3).

Table 3. The accuracy at the vine level for each time point for each block.

Block	Season & Time point	Model			Prediction		
		Accuracy	F1 score	Matthews correlation coefficient	Accuracy	F1 score	Matthews correlation coefficient
Ade Hills Chardonnay	S1 Flowering	0.58	0.59	0.15	0.55	0.66	0.08
	S1 Veraison	0.73	0.73	0.45	0.68	0.77	0.26
	S1 Harvest	0.80	0.80	0.60	0.75	0.82	0.47
	S2 Harvest	0.73	0.72	0.45	0.69	0.77	0.39
Ade Hills Pinot Noir	S1 Flowering	0.58	0.56	0.15	0.50	0.40	-0.03
	S1 Veraison	0.68	0.67	0.35	0.68	0.63	0.34
	S1 Harvest	0.93	0.92	0.85	0.91	0.90	0.83
	S2 Harvest	0.78	0.78	0.55	0.76	0.75	0.54
Ade Hills Cab Sav	S1 Flowering	0.60	0.58	0.20	0.48	0.40	-0.06
	S1 Veraison	0.90	0.90	0.80	0.95	0.95	0.90

	S1 Harvest	0.93	0.93	0.85	0.98	0.97	0.95
	S2 Harvest	0.93	0.92	0.85	0.93	0.93	0.86
Barossa Cab Sav	S1 Flowering	0.60	0.62	0.20	0.56	0.56	0.13
	S1 Veraison	0.88	0.88	0.75	0.84	0.86	0.70
	S1 Harvest	0.93	0.93	0.85	0.94	0.94	0.88
Barossa Shiraz	S1 Flowering	0.83	0.82	0.65	0.81	0.83	0.62
	S1 Veraison	0.93	0.92	0.85	0.94	0.94	0.88
	S1 Harvest	0.93	0.93	0.85	0.88	0.89	0.75
Riverland Shiraz	S1 Flowering	0.85	0.86	0.70	0.86	0.84	0.73
	S1 Harvest	0.90	0.90	0.80	0.91	0.90	0.83

3.4. Predict the disease between seasons and locations

To test whether the model could be robust enough to predict between seasons, the models built for S1 and S2 were used to predict the data from each other. At the pixel level, the pixels of 40 vines selected vine from the earlier process was used in the prediction. For vine level, disease pixel ratio based on pixel level prediction and threshold from vine level model was used for all virus-tested vines. Only Adelaide Hills vineyard had two seasons' data at the harvest stage. Table 4 shows the prediction results. The results showed that Chardonnay and Pinot Noir poorly predicted the data between S1 and S2 either at pixel or vine level. The Cabernet Sauvignon model built for S1 could well predict the data in S2 with an accuracy of 0.91, F1 score of 0.90, and MCC of 0.83 at the vine level. Inversely, the model built for S2 could well predict the data from S1.

Table 4. Model prediction results between two seasons in Adelaide Hills vineyard.

		S1 model predict S2 data			**S2 model predict S1 data**		
		Accuracy	F1 score	Matthews correlation coefficient	Accuracy	F1 score	Matthews correlation coefficient
Pixel level	Chardonnay	0.64	0.59	0.27	0.66	0.68	0.33
	Pinot Noir	0.63	0.55	0.26	0.69	0.71	0.39
	Cab Sav	0.84	0.83	0.69	0.82	0.83	0.64
Vine level	Chardonnay	0.58	0.66	0.21	0.64	0.75	0.16
	Pinot Noir	0.61	0.44	0.18	0.62	0.65	0.29
	Cab Sav	0.91	0.90	0.83	0.89	0.89	0.78

Moreover, the models built from the same cultivar from different vineyards were used to predict each other. The results are in Table 5. Shows that the GLD in Cabernet Sauvignon and SD in Shiraz could predict each other between locations with the highest accuracy at 0.85 and 0.88 for Cabernet Sauvignon and Shiraz at vine level respectively.

Table 5. Model prediction results between locations.

Model	**Prediction**	**Accuracy**	**F1 score**	**Matthews correlation coefficient**

Pixel level	Ade Hills - Cab Sav	Barossa - Cab Sav	0.76	0.75	0.53
	Barossa - Cab Sav	Ade Hills - Cab Sav	0.80	0.81	0.60
	Barossa - Shiraz	Riverland - Shiraz	0.82	0.82	0.64
	Riverland - Shiraz	Barossa - Shiraz	0.79	0.80	0.58
Vine level	Ade Hills - Cab Sav	Barossa - Cab Sav	0.82	0.81	0.65
	Barossa - Cab Sav	Ade Hills - Cab Sav	0.85	0.86	0.72
	Barossa - Shiraz	Riverland - Shiraz	0.88	0.88	0.77
	Riverland - Shiraz	Barossa - Shiraz	0.86	0.86	0.73

4. Discussion

The present study assessed the capability of UAV-based high-resolution hyperspectral images for grapevine viral disease detection in Australian vineyards. The advantage of the high spatial and spectral resolution allows us to compare the spectral signals between healthy and diseased vines to better understand the spectral difference in disease symptoms. The spectral signal of the GLD symptomatic Pinot Noir and Cabernet Sauvignon from the airborne hyperspectral data closely matched the ground studies that used the hyperspectral proximal sensing or directed leaf contact sensors for GLD detection (Junges et al., 2020; Naidu et al., 2009; Wang et al., 2023a), which demonstrated the reliability of the hyperspectral remote sensing from the low-altitude UAV system for grapevine viral disease detection. The spectral difference between diseased and healthy vines showed progressively increasing spectral differences from the early development stage (flowering) towards the later season (harvest), which matched the development of the visual disease symptoms over time; the late season had the most intense symptoms. It was noticeable at harvest time that the red-edge region (700-740 nm) had higher reflectance in all cultivars. The red edge spectral region is very sensitive to plant stress (Filella and Penuelas, 1994; Horler et al., 1983; Smith et al., 2004), which, in our case, was most likely the stress from the virus infections. However, the spectral differences in other parts of the spectrum were variable depending on cultivars. The Pinot Noir and Cabernet Sauvignon showed a similar spectral pattern, which had higher reflectance in the red and red-edge regions, and lower reflectance in the green region. This is mainly due to the biosynthesis of anthocyanins in the leaves (Gutha et al., 2010). Anthocyanin reflects red light and has high absorption at 500 to 600 nm spectrums with a peak at 550 nm. In comparison, the diseased Shiraz had higher reflectance at 550 nm. This could be because the SD symptomatic Shiraz had many newly developed young leaves throughout the season. The bright young leaves usually reflect more green light than the healthy mature leaves (Gausman, 1974; Moura et al., 2017). The SD symptomatic mature leaves on Shiraz also showed reddening, which was mixed with the young leaves in the pixels and showed high reflectance between 600-650 nm. The diseased vines also had lower reflectance in the 400-500 nm region in Cabernet Sauvignon and Shiraz, which could be due to the lower chlorophyll and carotenoid contents in the leaves (Gutha et al., 2010). Compared to the red cultivars, the white cultivar Chardonnay had less spectral difference between healthy and diseased vines in all VNIR regions, except the red-edge region. These minimal differences could explain the lack of symptoms in white cultivars as they are beyond human vision, i.e. in the red edge region (Campbell and Gubisch, 1966).

The PLS-DA model performance was closely related to the visual symptom and spectral difference in the study. Comparing different developmental stages for the accuracy of GLD in Chardonnay, Pinot Noir, and Cabernet Sauvignon, higher accuracies were found later season compared to the early season, which is consistent with other studies on GLD detection (Bell, 2015; MacDonald et al., 2016).

In comparison, the accuracy for SD prediction in Shiraz at the early stage had a relatively small difference to the later season, and the highest was in the veraison stage in Barossa. That was because the SD symptoms in Shiraz started at the beginning of the season (Habili, 2013; Wu et al., 2020). In terms of the models' performance between cultivars, the PLS-DA models could well predict the virus infection in the red cultivars including GLD symptoms in Pinot Noir and Cabernet Sauvignon and SD symptoms in Shiraz across different vineyards with best accuracy of 0.91 to 0.98 at vine level. In the white cultivars, even though the vine did not show obvious disease symptoms, we achieved an accuracy of 0.75 to predict the diseased Chardonnay. In the current study, by comparing a different number of vines used for modelling, we found 20 diseased and 20 healthy vines were adequate to build a robust model. However, if the canopy in the vineyard is inconsistent due to various biotic or abiotic stresses, more samples would likely be needed. The models were built from a single block that works well within the same block in the present study, however, the robustness of the model varied between seasons, cultivars, and locations. In the same vineyard, the model built for Chardonnay and Pinot Noir in each season at the same stage (harvest) could not predict each other, despite having similar weather in S1 and S2. However, the model for Cabernet Sauvignon in S1 and S2 could predict each other well with an accuracy of 0.89-0.91. Cabernet Sauvignon also performed well with an accuracy of 0.82-0.85 to predict the disease in a different vineyard. This indicated that our method could predict GLD in Cabernet Sauvignon across seasons and locations. Moreover, the model for SD on Shiraz also had a good accuracy of 0.82-0.88 at the vine level for predicting the disease in different vineyards even though the climate was very different between Barossa and Riverland vineyards.

Although the current study demonstrated the feasibility of high-resolution hyperspectral technology for grapevine viral disease detection, it is worthwhile noting that the method is an indirect method for disease detection. Disease detection is based on the symptom and stress response to the virus. Symptoms of grapevine viral diseases can be influenced by the environment, biotic stress such as other pathogens, and abiotic stress such as water stress (Guță and Buciumeanu, 2020; Perrone et al., 2017). Viral disease symptoms can also be confused with nutrient deficiency and mechanical damage (Budoi, 2003; Charles et al., 2006; Rustioni et al., 2018). The current study selected the vineyards that are all well uniformly managed, including soil, irrigation, fertilization, and canopy management, to minimise potential variation. However, further studies need to include more regions and different locations as well as more seasons for building a reliable and robust model for disease detection. In addition, the viruses in grapevines are very complicated. The infection ages, viral strains, and co-infection of different viruses, and cultivars could alter the symptoms (Maliogka et al., 2015; Naidu et al., 2015; Wu et al., 2023). The virus testing in the current study only included the most commonly seen grapevine viruses in an Australian vineyard, which does not guarantee other viruses can exist in the vineyard. Ideally, a full scan of viruses with next-generation sequencing to detect all viruses in the sample can help to understand the symptomology, however high cost will be associated.

Another challenge of the detection is that the shoot of the grapevine is very long that could grow to the neighbouring vines' space, which could influence the prediction results. The diseased pixel ratio could help compensate for the issue to some degree, however, different size bounding boxes could be used to minimize the impact. MacDonald et al, (MacDonald et al., 2016) used remote sensing images for GLD detection. They used a round buffer for individual vines. By comparing different buffer sizes, the authors got different prediction results.

The average spectral difference between diseased healthy vines indicated that a multi-spectral camera with the critical spectral region could use for viral disease detection. Multispectral cameras are usually cheaper and easier to operate compared to hyperspectral cameras. Many companies make small UAVs with multispectral cameras, which can easily and quickly be used by grape growers. The method

552 developed from the current study could also apply to other crops and stress detections for precision
553 agriculture applications.

554 The current study only used PLS-DA for pixel level modelling due to its advantage in high-dimensional
555 data processing and computational efficiency. However, there are many other machine learning
556 algorithms that can be used to improve the model performance at the pixel level. For example,
557 support vector machine, random forest, and neural networks. Especially, many recent studies used
558 deep learning algorithms for remote sensing hyperspectral images (Audebert et al., 2019; Li et al.,
559 2019). The model accuracy could be improved with 3-D deep learning algorithms (Zhong et al., 2018).

560 While the current study showed good prediction results in red cultivars, there remain opportunities
561 for improvement in white cultivars. Other spectral regions such as SWIR (900-1700 nm) or longwave
562 infrared (thermal; 8-13 µm) wavelengths can be investigated in future studies. The SWIR hyperspectral
563 camera has demonstrated a better performance in detecting GLD in white grapevines compared to a
564 VNIR camera with a proximal sensing method (Bendel et al., 2020).

565 ## 5. Conclusions

566 High spatial and spectral resolution hyperspectral imagery is a powerful tool for grapevine viral disease
567 detection. The results demonstrate that this remote sensing method provides a realistic pattern of
568 virus infection, allowing the targeting of grapevines for laboratory testing with associated cost savings.
569 Furthermore, the difference in spectral reflectance between diseased and healthy grapevine varieties
570 is consistent across regions, which demonstrates that the technology provides the opportunity to
571 rapidly and reliably detect viral diseases at the vineyard scale without prior empirical ground-based
572 data. However, the results also show that detectability varies with the growth stage; timing of imaging
573 is critical for detection success. Clearly, larger datasets that span multiple seasons, locations, and
574 especially white cultivars will undoubtedly result in a more robust virus detection model in the future.
575 The results indicate that remote sensing has the potential to become a reliable alternative to
576 traditional methods such as visual assessment and random sampling for laboratory tests, saving time
577 and cost for grape growers to help them to make prudent disease management decisions.

578

579

580

581 **Declaration of competing Interest:**

582 The authors declare that they have no known competing financial interests or personal relationships
583 that could have appeared to influence the work reported in this paper.

584

585 **Acknowledgments:**

586 We acknowledge the funding bodies: South Australian Vine Improvement Association, Riverland Wine,
587 and Wine Australia. We also appreciate the growers and vineyard managers for collaboration.

588

589 **Appendix A. Supplementary data**

590

References

Alabi, O.J., Casassa, L.F., Gutha, L.R., Larsen, R.C., Henick-Kling, T., Harbertson, J.F., Naidu, R.A., 2016. Impacts of Grapevine leafroll disease on fruit yield and grape and wine chemistry in a wine grape (*Vitis vinifera L.*) cultivar. PLoS One 11, e0149666.

Albetis, J., Duthoit, S., Guttler, F., Jacquin, A., Goulard, M., Poilvé, H., Féret, J.-B., Dedieu, G., 2017. Detection of Flavescence dorée Grapevine Disease using unmanned aerial vehicle (UAV) multispectral imagery. Remote Sensing 9, 308-328.

Atallah, S., Gomez, M., Fuchs, M., Martinson, T., 2012. Economic impact of grapevine leafroll disease on *Vitis vinifera cv.* Cabernet franc in Finger Lakes vineyards of New York. American Journal of Enology and Viticulture 63, 73-79.

Audebert, N., Le Saux, B., Lefevre, S., 2019. Deep learning for classification of hyperspectral data: A comparative review. IEEE Geoscience and Remote Sensing Magazine 7, 159-173.

Baldi, P., Brunak, S., Chauvin, Y., Andersen, C.A.F., Nielsen, H., 2000. Assessing the accuracy of prediction algorithms for classification: an overview. Bioinformatics 16, 412-424.

Ballabio, D., Consonni, V., 2013. Classification tools in chemistry. Part 1: linear models. PLS-DA. Analytical Methods 5, 3790-3798.

Barker, M., Rayens, W., 2003. Partial least squares for discrimination. Journal of Chemometrics 17, 166-173.

Barnes, R.J., Dhanoa, M.S., Lister, S.J., 1989. Standard normal variate transformation and de-trending of near-infrared diffuse reflectance spectra. Applied Spectroscopy 43, 772-777.

Basso, M.F., Fajardo, T.V.M., Saldarelli, P., 2017. Grapevine virus diseases: Economic impact and current advances in viral prospection and management. Revista Brasileira de Fruticultura 39.

Bell, V.A., 2015. An integrated strategy for managing Grapevine leafroll-associated virus 3 in red berry cultivars in New Zealand vineyards. Open Access Te Herenga Waka-Victoria University of Wellington.

Bell, V.A., Blouin, A.G., Cohen, D., Hedderley, D.I., Oosthuizen, T., Spreeth, N., Lester, P.J., Pietersen, G., 2017. Visual symptom identification of grapevine leafroll-associated virus 3 in red berry cultivars supports virus management by roguing. Journal of Plant Pathology 99, 477-482.

Bendel, N., Kicherer, A., Backhaus, A., Köckerling, J., Maixner, M., Bleser, E., Klück, H.-C., Seiffert, U., Voegele, R.T., Töpfer, R., 2020. Detection of Grapevine leafroll-associated virus 1 and 3 in white and red grapevine cultivars using hyperspectral imaging. Remote Sensing 12.

Bioreba_AG, 2017. Product Information: DAS-ELISA - Grapevine leafroll-associated virus generic 4 strains (GLRaV-4 strains).

Blaisdell, G.K., Zhang, S., Rowhani, A., Klaassen, V., Cooper, M.L., Daane, K.M., Almeida, R.P.P., 2020. Trends in vector-borne transmission efficiency from coinfected hosts: Grapevine leafroll-associated virus-3 and Grapevine virus A. European Journal of Plant Pathology 156, 1163-1167.

Boughorbel, S., Jarray, F., El-Anbari, M., 2017. Optimal classifier for imbalanced data using Matthews Correlation Coefficient metric. PLOS ONE 12, e0177678.

Budoi, G., Berca, M., Penescu, A., Soare, M. , Gavriluta, I., Dana, D., Bireescu, L., Alexandru, D., 2003. Similarities and differences between visual symptoms of nutrient disorders and plant diseases– criteria to avoid confusions. ESNA UIR, 108-113.

Burger, J.T., Maree, H.J., Gouveia, P., Naidu, R.A., 2017. Grapevine leafroll-associated virus3, in: Meng, B., Martelli, G.P., Golino, D.A., Fuchs, M. (Eds.), Grapevine viruses: Molecular biology, diagnostics and management. Springer International Publishing, Germany, pp. 167-195.

Campbell, F.W., Gubisch, R.W., 1966. Optical quality of the human eye. The Journal of Physiology 186, 558-578.

Charles, J.G., Cohen, D., Walker, J.T.S., Forgie, S.A., Bell, V.A., Breen, K.C., 2006. A review of the ecology of grapevine leafroll associated virus type 3 (GLRaV3). New Zealand Plant Protection 59, 330-337.

Chicco, D., Jurman, G., 2020. The advantages of the Matthews correlation coefficient (MCC) over F1 score and accuracy in binary classification evaluation. BMC Genomics 21, 6.

Chooi, K.M., Bell, V.A., Blouin, A.G., Cohen, D., Mundy, D., Henshall, W., MacDiarmid, R.M., 2022. Grapevine leafroll-associated virus 3 genotype influences foliar symptom development in New Zealand vineyards. Viruses 14.

Constable, F.E., Rodoni, B.C., 2014. Grapevine leafroll-associated viruses. Wine Australia, Adelaide, Australia.

Credi, R., 1997. Characterization of Grapevine Rugose Wood Disease sources from Italy. Plant Dis. 81, 1288-1292.

Digiaro, M., Bedzrob, M.P., D'Onghia, A.M., Boscia, D., Savino, V.N., 1994. On the correlation between grapevine virus A and rugose wood. Phytopathologia Mediterranea 33, 187-193.

Douglas, N., Krüger, K., 2008. Transmission efficiency of Grapevine leafroll-associated virus 3 (GLRaV-3) by the mealybugs *Planococcus ficus* and *Pseudococcus longispinus* (Hemiptera: *Pseudococcidae*). European Journal of Plant Pathology 122, 207-212.

Filella, I., Penuelas, J., 1994. The red edge position and shape as indicators of plant chlorophyll content, biomass and hydric status. International Journal of Remote Sensing 15, 1459-1470.

Fowler, J.E., 2014. Compressive pushbroom and whiskbroom sensing for hyperspectral remote-sensing imaging, 2014 IEEE International Conference on Image Processing (ICIP), pp. 684-688.

Galvan, F.E.R., Pavlick, R., Trolley, G., Aggarwal, S., Sousa, D., Starr, C., Forrestel, E., Bolton, S., Alsina, M.d.M., Dokoozlian, N., Gold, K.M., 2023. Scalable Early Detection of Grapevine Viral Infection with Airborne Imaging Spectroscopy. Phytopathology®, PHYTO-01-23-0030-R.

Gambino, G., 2015. Multiplex RT-PCR method for the simultaneous detection of nine grapevine viruses. Methods in Molecular Biology 1236, 39-47.

Gausman, H.W., 1974. Leaf reflectance of near-infrared. Photogrammetric Engineering 40, 183-191.

Goszczynski, D.E., du Preez, J., Burger, J.T., 2008. Molecular divergence of Grapevine virus A (GVA) variants associated with Shiraz disease in South Africa. Virus Res. 138, 105-110.

Goszczynski, D.E., Habili, N., 2012. Grapevine virus A variants of group II associated with Shiraz disease in South Africa are present in plants affected by Australian Shiraz disease, and have also been detected in the USA. Plant Pathology 61, 205-214.

Goszczynski, D.E., Jooste, A.E.C., 2003. Identification of divergent variants of Grapevine virus A. European Journal of Plant Pathology 109, 397-403.

Goutte, C., Gaussier, E., 2005. A Probabilistic Interpretation of Precision, Recall and F-Score, with Implication for Evaluation, in: Losada, D.E., Fernández-Luna, J.M. (Eds.), Advances in Information Retrieval. Springer Berlin Heidelberg, Berlin, Heidelberg, pp. 345-359.

Guță, I.C., Buciumeanu, E.C., 2020. The behaviour of grapevine under virus infection and drought stress combination. AgroLife Scientific Journal 9.

Gutha, L.R., Casassa, L.F., Harbertson, J.F., Naidu, R.A., 2010. Modulation of flavonoid biosynthetic pathway genes and anthocyanins due to virus infection in grapevine (*Vitis vinifera L.*) leaves. BMC Plant Biology 10, 187.

Habili, N., 2013. Australian Shiraz Disease: an emerging virus disease of *Vitis vinifera* cv. Shiraz. Wine and Viticulture Journal 28, 59-61.

Habili, N., Komínek, P., Little, A., 2007. Grapevine leafroll-associated virus 1 as a common grapevine pathogen. Plant Viruses 1.

Habili, N., Wu, Q., Pagay, V., 2016. Virus-associated Shiraz Disease may lead Shiraz to become an endangered variety in Australia. Wine and Viticulture Journal V31N1, 47-50.

Hofer, M., 2017. Mean centering, The International Encyclopedia of Communication Research Methods, pp. 1-3.

Hommay, G., 2008. Grapevine virus A transmission by larvae of *Parthenolecanium corni*. European journal of plant pathology 121, pp. 185-188-2008 v.2121 no.2002.

Hommay, G., Beuve, M., Herrbach, E., 2022. Transmission of grapevine leafroll-associated viruses and grapevine virus A by vineyard-sampled soft scales (*Parthenolecanium corni*, Hemiptera: *Coccidae*). Viruses 14.

Hoo, Z.H., Candlish, J., Teare, D., 2017. What is an ROC curve? Emergency Medicine Journal 34, 357-359.

Horler, D.N.H., Dockray, M., Barber, J., 1983. The red edge of plant leaf reflectance. International Journal of Remote Sensing 4, 273-288.

Hou, J., Li, L., He, J., 2016. Detection of grapevine leafroll disease based on 11-index imagery and ant colony clustering algorithm. Precision Agriculture 17, 488-505.

Hull, R., 2014a. Ecology, epidemiology, and control of plant viruses, Plant Virology, pp. 809-876.

Hull, R., 2014b. Virus–plant interactions in non-permissive and permissive hosts, Plant Virology, pp. 605-668.

Junges, A.H., Almança, M.A.K., Fajardo, T.V.M., Ducati, J.R., 2020. Leaf hyperspectral reflectance as a potential tool to detect diseases associated with vineyard decline. Trop. Plant Pathol. 45, 522-533.

Lee, J., Keller, K.E., Rennaker, C., Martin, R.R., 2009. Influence of grapevine leafroll associated viruses (GLRaV-2 and -3) on the fruit composition of Oregon *Vitis vinifera L. cv.* Pinot noir: Free amino acids, sugars, and organic acids. Food Chemistry 117, 99-105.

Li, S., Song, W., Fang, L., Chen, Y., Ghamisi, P., Benediktsson, J.A., 2019. Deep learning for hyperspectral image classification: An overview. IEEE Transactions on Geoscience and Remote Sensing 57, 6690-6709.

MacDonald, S.L., Staid, M., Staid, M., Cooper, M.L., 2016. Remote hyperspectral imaging of grapevine leafroll-associated virus 3 in Cabernet Sauvignon vineyards. Computers and Electronics in Agriculture 130, 109-117.

Maliogka, V.I., Martelli, G.P., Fuchs, M., Katis, N.I., 2015. Chapter Six - Control of Viruses Infecting Grapevine, in: Loebenstein, G., Katis, N.I. (Eds.), Advances in Virus Research. Academic Press, pp. 175-227.

Martelli, G.P., 2017. An overview on grapevine viruses, viroids, and the diseases they cause, in: Meng, B., Martelli, G.P., Golino, D.A., Fuchs, M. (Eds.), Grapevine Viruses: Molecular Biology, Diagnostics and Management. Springer International Publishing, Cham, pp. 31-46.

Monis, J., Bestwick, R.K., 1996. Detection and localization of Grapevine Leafroll Associated Closteroviruses in greenhouse and tissue culture grown plants. American Journal of Enology and Viticulture 47, 199.

Moura, Y., Galvão, L., Hilker, T., Wu, J., Saleska, S., Amaral, C., Nelson, B., Lopes, A., Wiedemann, K., Prohaska, N., Oliveira Junior, R., Bueno Machado, C., Aragão, L., Paulson, J., 2017. Spectral analysis of amazon canopy phenology during the dry season using a tower hyperspectral camera and modis observations. ISPRS Journal of Photogrammetry and Remote Sensing 131, 52-64.

Naidu, R., Rowhani, A., Fuchs, M., Golino, D., Martelli, G.P., 2014. Grapevine leafroll: A complex viral disease affecting a high-value fruit crop. Plant Dis. 98, 1172-1185.

Naidu, R.A., Hughes, J.D.A., 2003. Methods for the detection of plant virus diseases, Plant Virology in Sub-Saharan Africa: Proceedings of a Conference Organized by IITA: 4-8 June 2001, International Institute of Tropical Agriculture, Ibadan, Nigeria. IITA, p. 233.

Naidu, R.A., Maree, H.J., Burger, J.T., 2015. Grapevine leafroll disease and associated viruses: a unique pathosystem. Annual review of phytopathology 53, 613-634.

Naidu, R.A., Perry, E.M., Pierce, F.J., Mekuria, T., 2009. The potential of spectral reflectance technique for the detection of Grapevine leafroll-associated virus-3 in two red-berried wine grape cultivars. Computers and Electronics in Agriculture 66, 38-45.

Nguyen, C., Sagan, V., Maimaitiyiming, M., Maimaitijiang, M., Bhadra, S., Kwasniewski, M.T., 2021. Early detection of plant viral disease using hyperspectral imaging and deep learning. Sensors 21.

Olivier, R., Hanqiang, C., 2012. Nearest neighbor value interpolation. International Journal of Advanced Computer Science and Applications 3.

Perrone, I., Chitarra, W., Boccacci, P., Gambino, G., 2017. Grapevine–virus–environment interactions: an intriguing puzzle to solve. New Phytologist 213, 983--987.

Pietersen, G., Spreeth, N., Oosthuizen, T., van Rensburg, A., van Rensburg, M., Lottering, D., Rossouw, N., Tooth, D., 2013. Control of grapevine leafroll disease spread at a commercial wine estate in South Africa: A case study. American Journal of Enology and Viticulture 64, 296.

Rubio, L., Galipienso, L., Ferriol, I., 2020. Detection of plant viruses and disease management: Relevance of genetic diversity and evolution. Frontiers in Plant Science 11.

Rustioni, L., Grossi, D., Brancadoro, L., Failla, O., 2018. Iron, magnesium, nitrogen and potassium deficiency symptom discrimination by reflectance spectroscopy in grapevine leaves. Scientia Horticulturae 241, 152-159.

Rustioni, L., Rocchi, L., Failla, O., 2015. Effect of anthocyanin absence on white berry grape (*Vitis vinifera L.*). 54, 239-242.

Sanches, I.D., Tuohy, M.P., Hedley, M.J., Bretherton, M.R., 2009. Large, durable and low‐cost reflectance standard for field remote sensing applications. International Journal of Remote Sensing 30, 2309-2319.

Savitzky, A., Golay, M.J.E., 1964. Smoothing and Differentiation of Data by Simplified Least Squares Procedures. Analytical Chemistry 36, 1627-1639.

Sinha, R., Khot, L.R., Rathnayake, A.P., Gao, Z., Naidu, R.A., 2019. Visible-near infrared spectroradiometry-based detection of grapevine leafroll-associated virus 3 in a red-fruited wine grape cultivar. Computers and Electronics in Agriculture 162, 165-173.

Smith, K.L., Steven, M.D., Colls, J.J., 2004. Use of hyperspectral derivative ratios in the red-edge region to identify plant stress responses to gas leaks. Remote Sensing of Environment 92, 207-217.

Sokolova, M., Japkowicz, N., Szpakowicz, S., 2006. Beyond accuracy, F-score and ROC: a family of discriminant measures for performance evaluation, Australasian joint conference on artificial intelligence. Springer, pp. 1015-1021.

Thenkabail, P.S., Lyon, J.G., Huete, A., 2011. Advances in hyperspectral remote sensing of vegetation and agricultural croplands, in: Thenkabail, P.S., Lyon, J.G., Huete, A. (Eds.), Hyperspectral remote sensing of vegetation. CRC Press, Boca Raton, FL, pp. 3-35.

Thomas, S., Kuska, M.T., Bohnenkamp, D., Brugger, A., Alisaac, E., Wahabzada, M., Behmann, J., Mahlein, A.-K., 2018. Benefits of hyperspectral imaging for plant disease detection and plant protection: a technical perspective. Journal of Plant Diseases and Protection 125, 5-20.

Valavi, R., Elith, J., Lahoz-Monfort, J.J., Guillera-Arroita, G., 2019. blockCV: An r package for generating spatially or environmentally separated folds for k-fold cross-validation of species distribution models. Methods in Ecology and Evolution 10, 225-232.

Vanegas, F., Bratanov, D., Powell, K., Weiss, J., Gonzalez, F., 2018. A novel methodology for improving plant pest surveillance in vineyards and crops using UAV-based hyperspectral and spatial data. Sensors 18.

Wang, D., Vinson, R., Holmes, M., Seibel, G., Bechar, A., Nof, S., Tao, Y., 2019. Early detection of Tomato Spotted Wilt Virus by hyperspectral imaging and outlier removal auxiliary classifier generative adversarial nets (OR-AC-GAN). Sci Rep 9, 4377.

Wang, Y.M., Ostendorf, B., Gautam, D., Habili, N., Pagay, V., 2022. Plant viral disease detection: from molecular diagnosis to optical sensing technology—A multidisciplinary review. Remote Sensing 14.

Wang, Y.M., Ostendorf, B., Pagay, V., 2023a. Detecting grapevine virus infections in red and white winegrape canopies using proximal hyperspectral sensing. Sensors 23.

Wang, Y.M., Ostendorf, B., Pagay, V., 2023b. Evaluating the potential of high-resolution visible remote sensing to detect Shiraz Disease in grapevines. Australian Journal of Grape and Wine Research 2023, 7376153.

Wu, Q., Habili, N., Constable, F., Al Rwahnih, M.A., Goszczynski, D.E., Wang, Y., Pagay, V., 2020. Virus pathogens in Australian vineyards with an emphasis on Shiraz Disease. Viruses 12.

Wu, Q., Habili, N., Kinoti, W.M., Tyerman, S.D., Rinaldo, A., Zheng, L., Constable, F.E., 2023. A metagenomic investigation of the viruses associated with Shiraz Disease in Australia. Viruses 15.

Yuhas, R.H., Goetz, A.F., Boardman, J.W., 1992. Discrimination among semi-arid landscape endmembers using the spectral angle mapper (SAM) algorithm, JPL, Summaries of the Third Annual JPL Airborne Geoscience Workshop. Volume 1: AVIRIS Workshop.

Zhang, N., Yang, G., Pan, Y., Yang, X., Chen, L., Zhao, C., 2020. A review of advanced technologies and development for hyperspectral-based plant disease detection in the past three decades. Remote Sensing 12.

Zhang, X., Han, L., Dong, Y., Shi, Y., Huang, W., Han, L., González-Moreno, P., Ma, H., Ye, H., Sobeih, T., 2019. A deep learning-based approach for automated Yellow Rust Disease detection from high-resolution hyperspectral UAV images. Remote Sensing 11.

Zherdev, A.V., Vinogradova, S.V., Byzova, N.A., Porotikova, E.V., Kamionskaya, A.M., Dzantiev, B.B., 2018. Methods for the diagnosis of grapevine viral infections: A review. Agriculture 8, 195.

Zhong, Z., Li, J., Luo, Z., Chapman, M., 2018. Spectral–Spatial Residual Network for Hyperspectral Image Classification: A 3-D Deep Learning Framework. IEEE Transactions on Geoscience and Remote Sensing 56, 847-858.

Zhu, H., Chu, B., Zhang, C., Liu, F., Jiang, L., He, L., 2017. Hyperspectral imaging for presymptomatic detection of tobacco disease with successive projections algorithm and machine-learning classifiers. Scientific Reports 7.

Zia-Khan, S., Kleb, M., Merkt, N., Schock, S., Müller, J., 2022. Application of infrared imaging for early detection of Downy Mildew (*Plasmopara viticola*) in grapevine. Agriculture 12.

Chapter 6

Conclusions and future perspectives

6.1. Concluding remarks

This PhD research focused on developing rapid detection methods for two grapevine viral diseases – SD and GLD – on a large scale using optical sensors and remote sensing technology. Below, several key results and findings from the research are highlighted.

Firstly, a rapid detection method for SD in Shiraz vineyards was developed based on high-resolution RGB imagery. This imagery allowed for the rapid identification of diseased grapevines using the delayed budburst symptom of SD. This study found that the difference in canopy size between diseased and healthy vines at optimal times (pre-flowering and veraison stages) is closely related to SD infection in the vineyards. The proposed method is practical and easily adopted by growers. With the increasing affordability and user-friendliness of small UAVs and mapping applications, growers can capture high-resolution remote sensing images with minimal training. The timely data from growers can effectively estimate disease incidence in the vineyard, reduce the cost of disease detection, and aid in disease management strategies.

Secondly, a successful demonstration showed the efficacy of passive hyperspectral proximal sensing for the detection of GLD in both red and white cultivars. This approach offers a significant advantage in identifying subtle disease symptoms,

particularly in white cultivars. By using a handheld spectroradiometer in the VNIR spectrum range, an impressive detection accuracy of 96% was achieved for Pinot Noir and 76% for Chardonnay. Furthermore, the spectral reflectance differences observed between GLD-infected and healthy red cultivars closely aligned with previous studies that employed leaf-contact hyperspectral sensors to detect GLD in red grapevines. These results strongly affirm the reliability of hyperspectral proximal sensing for the detection of viral diseases in grapevines. Additionally, the chemometrics analytical method (PLS-DA) used in this study for spectral data modelling is computationally effective and can be used for further comparative studies, such as a quick comparison of the spectral difference between diseases and cultivars, and also benchmarking different algorithms when other modelling methods are used.

Thirdly, using the advantage of both low-altitude remote sensing and hyperspectral imagery technology, a new detection method for GLD and SD at the vineyard scale was developed based on my two previous findings. The utilisation of UAV-based hyperspectral imagery provided high-resolution images encompassing both spectral and spatial domains. The PhD research successfully demonstrated the feasibility of employing high-resolution hyperspectral imagery within the VNIR spectral range to detect GLD and SD in both red and white grapevine cultivars within Australian vineyards. The differences in spectral wavelength regions between healthy and GLD-infected vines were consistent with the proximal sensing method utilised previously. This study further solidified the reliability of the low-altitude remote sensor UAV hyperspectral sensing method for grapevine viral disease detection. While the detection of SD in Shiraz can be accomplished through canopy size measurements employing RGB UAV methods, as mentioned in Chapter 3, the inclusion of spectral

differences provides supplementary information for disease identification during various developmental stages. For instance, the spectral disparities facilitate the detection of variations in both canopy colour and size throughout the growing season, which may not be perceptible to an RGB sensor alone. Consequently, this augmentation in data enhances the overall confidence in the results obtained. The conclusive outcomes yielded disease maps containing precise geo-locations, defining the position of diseased vines within rows and vine numbers in blocks. Such specific geo-information serves as an invaluable tool for growers, enabling precise disease management by facilitating the identification and removal of infected vines.

More importantly, the processed hyperspectral data obtained from both proximal and low-altitude remote sensing methods consistently revealed significant spectral differences between virus-infected and healthy vines. These findings underscore the relevance of specific spectral regions for effective viral disease detection, with particular emphasis on the red-edge band, which proves valuable in discriminating disease presence in both red and white grapevine cultivars.

Additionally, acquiring all the necessary data for this PhD research was a significant endeavour. This encompassed a wide range of data, including virus test results, visual assessments, handheld spectroradiometer data, and UAV remote sensing data collected over multiple seasons and viticultural regions. These data, and also the know-how in data acquisition and processing obtained during this research, can greatly benefit future students and researchers undertaking similar investigations.

Nevertheless, several challenges persist in this research endeavour. The subsequent section will delve into these challenges and explore potential solutions to address them.

6.2. Remaining challenges

6.2.1. The complexity of grapevine virus diseases

Fundamentally, the optical sensing technology used in disease detection is an indirect method that relies on measuring the plant's physiological response to viral infections. However, it is important to note that other stresses, such as nutrient deficiency and mechanical damage, can trigger similar responses in grape leaves. When viral diseases and other biotic or abiotic stresses occur simultaneously in a vine, it becomes more challenging to accurately detect the specific disease using these indirect methods.

Despite decades of research in plant virology, there are still many mysteries that remain to be understood. For instance, the symptoms of grapevine viral diseases can be influenced by environmental factors (Perrone et al. 2017), leading to confusion in disease detection. In this PhD study, the intensity of disease symptoms varied across different seasons, which resulted in lower prediction accuracy based on spectral reflectance between seasons.

Besides, the variants of viruses have a significant impact on the observed symptoms. For example, only GVA phylogroup II variants are associated with the SD symptom in Shiraz, while other variants such as those in GVA phylogroups I and III do not cause SD symptoms (Wu et al. 2023). Unfortunately, distinguishing between virus variants can only be confirmed through costly processes like RT-PCR.

Furthermore, it is common for multiple viruses and virus variants to co-infect the same vine (Blaisdell et al. 2020; Credi 1997; Hommay 2008). The mixture of virus infections can further complicate symptom expression. In some study vineyards, the vines with

multiple virus infections generally exhibited more severe symptoms. For instance, a Shiraz vine infected with GLRaV-1, GLRaV-3, strain 9 of GLRaV-4, and GVA showed more severe SD symptoms compared to a vine infected with only GLRaV-1 and GVA in the same vineyard block. Additionally, older vines, such as those in the Barossa Valley, tend to have a higher prevalence of mixed virus infections compared to newly established blocks in my study sites. The presence of mixed multiple virus infections within the same block poses challenges for modelling and prediction.

Moreover, disease symptoms can vary widely among different grapevine cultivars. It is well-known that GLD in white grapevine cultivars does not exhibit the same obvious symptoms as in red cultivars due to the lack of anthocyanins in the latter, leading to lower accuracy in disease detection (Gutha et al. 2010; Rustioni et al. 2015). However, the tolerance to certain virus infections in different cultivars also adds to the complexity and difficulty of detection. For example, in the Barossa vineyard, a few Shiraz vines grafted onto Cabernet Sauvignon rootstock exhibited two different disease symptoms on the same vine. The Shiraz portion displayed typical SD symptoms, while the water shoots (suckers) from the Cabernet Sauvignon rootstock exhibited GLD symptoms, despite virus testing indicating the presence of GVA and GLRaV-1 in both cultivars on the same vine. The presence of mixed symptoms can affect the accuracy of remote sensing detection for the disease. Although previous studies have stated that SD only appears in sensitive cultivars like Shiraz and Merlot, but not in Cabernet Sauvignon (Goszczynski et al. 2008), the underlying reasons for the cultivar specificity of the disease remain unclear.

6.2.2. Lack of abundant reliable ground-truthing data

A common challenge in remote sensing studies is the lack of adequate ground-truth data, which is essential for ensuring the reliability and accuracy of the model and its results. The most reliable ground-truthing method in this study is RT-PCR testing; however, its high cost limits the number of samples that can be used for modelling. The ELISA test method, although relatively cheaper, still incurs a considerable cost, allowing for a larger number of samples to be used for modelling and validation. On the other hand, visual assessment can provide a wealth of ground-truthing data. For instance, visual assessment has been successfully employed for GLRaV-3 detection in red cultivars such as Cabernet Sauvignon, Merlot, and Shiraz in New Zealand and South Africa, showing a high degree of correlation with ELISA test results (Bell et al. 2017). However, the reliability of visual assessment for other viruses and cultivars, particularly white cultivars, remains uncertain. Striking the right balance between reliability and a higher number of samples for ground-truthing is a challenging task.

Moreover, it is important to acknowledge that lab testing results are not infallible. The virus titer level can vary at different development stages and locations within the vine, leading to potential false negative results. Sampling at different times and parts of the vine may produce varying outcomes (Blouin et al. 2017). For instance, the ELISA testing results from the PhD study for GLRaV-1 infected vines sampled during early development stages (e.g., flowering) are less reliable (could result in false negatives) compared to later stages such as veraison and harvest. Additionally, cane samples taken from the tip of the shoot were found to be less reliable than those taken from the base of the shoots in ELISA testing. Furthermore, human error is an unavoidable factor. Leaves may be mistakenly sampled from the wrong vine as grapevine shoots can grow extensively and enter neighbouring spaces. Cross-contamination could happen during

sample handling and processing. Even a simple mistake, such as incorrectly recording the sample ID, can significantly alter the test results. The incorrect ground-truth data can significantly impact the performance of the model, particularly when working with a limited number of samples.

6.2.3. Technical limitations

Each sensor offers distinct advantages and drawbacks. For instance, RGB sensors provide cost-effective solutions for disease detection, but are limited to detecting symptomatic diseases. On the other hand, multispectral and hyperspectral sensors can detect the spectrum beyond human vision, enabling the detection of asymptomatic diseases. However, these sensors entail higher costs, demand greater expertise, and involve longer data processing times.

Despite the growing popularity of UAV-based hyperspectral technology in agricultural applications (Adão et al. 2017), the development of a user-friendly airborne hyperspectral system is still in progress. Unlike UAVs equipped with RGB cameras, which typically have simple interfaces and are easy to use, hyperspectral UAV systems are more complex. The collection and processing of hyperspectral data require careful attention to factors such as sensor calibration, data acquisition parameters, and spectral calibration targets. These complexities necessitate a higher level of expertise and attention to detail when operating hyperspectral UAV systems. In my study, the RGB-based UAV I used was a plug-and-play device that could be easily adopted by anyone for data collection. In contrast, the airborne hyperspectral system I employed involved a more intricate setup process and was susceptible to operational mistakes and technical issues. During the first year of the research, the study encountered several technical issues with the hyperspectral airborne system.

For instance, interference from the onboard computer affected the GPS cables, resulting in a failure to georeference the data. These issues resulted in missed data capture opportunities during the 2019/20 season.

However, with the increasing demand for high-resolution hyperspectral technology, companies such as Headwall Photonics, Specim, Cubert GmbH, and Resonon are competing to manufacture simpler hyperspectral systems for UAV applications. I am optimistic that airborne hyperspectral systems will become more user-friendly and reliable in the near future.

There are other common challenges associated with UAV operations. These include the limited flying time due to battery constraints, the impact of extreme weather on flights, and restrictions imposed by regulatory bodies such as Civil Aviation Safety Authority (CASA) on the UAV's operating height, distance, and location. These factors need to be considered when planning and conducting UAV-based hyperspectral data collection for disease detection in vineyards.

6.2.4. The economic challenge

This PhD research aims to assist growers in reducing the costs associated with detecting viral diseases, thereby optimising disease management. However, managing these diseases is a significant expense. As previously mentioned, there is currently no effective treatment for virus-infected vines, so the only option is to remove the infected vines and replant with clean materials. This process is both labour-intensive and costly. Additionally, some virus infections, such as GLRaV-1 in white cultivars or GVA in Cabernet Sauvignon, typically do not cause noticeable yield loss. As a result, growers are often hesitant to take action and remove infected vines unless the disease clearly affects vine health and productivity, as observed with SD in Shiraz.

Throughout this research, only two growers opted to replant a few rows of Shiraz due to the persistently low productivity caused by SD over several years.

The overall cost of managing viral diseases significantly influences growers' attitudes and actions. After speaking with several growers, it became clear that replanting is viewed as an expensive undertaking. If the vines are still productive, the process of removing infected vines may not be prioritised. Consequently, growers question the need to spend money on expensive virus testing. However, if this research could provide a cost-effective and rapid assessment of the viral infection status across the entire vineyard, they would be more inclined to invest in such technology. Nevertheless, the optical sensing method is not yet economically viable due to the high costs associated with equipment, logistics, and skilled labour. There is still work to be done in commercialising this service for growers.

6.3. Suggestions for further research

Future research could aim to address the above challenges that are suggested as follow:

Firstly, fundamental studies should continue to improve the understanding of viral diseases. Obtaining a deeper understanding of the interaction between symptomology and different environments, as well as the effects of different combinations of viruses or viral strains, can significantly enhance virus detection capabilities. The challenge of reliably detecting single or multiple viruses in a grapevine is complicated by various factors, including environment, cultivar, age, and phenological stage, amongst others, which can change the spectral responses. This challenge can be addressed by higher dimensionality in experimental designs, for example, considering the impacts of

environmental factors and nutrient deficiencies in conjunction with various combinations of virus infections within a single experiment.

Secondly, it is crucial to enhance the reliability of virus testing by improving ground-truthing. The growers should follow sampling protocols from the diagnostic laboratory (e.g. determining when and where to sample and the sample rate and frequency). Recording visual symptoms during sampling is recommended. It can provide confidence in testing results. If the test results are questionable, conducting additional confirmatory tests or testing the vines using multiple methods, such as ELISA and RT-PCR is advisable. Providing more training to vineyard source block inspectors to ensure accurate visual assessments is also important. Paying attention to unique characters, such as non-lignified canes and rolling leaf edges rather than only looking for colour changes can provide more confidence to identify the diseases. These suggestions also apply to the industry who regularly conducts virus testing using lab testing and visual assessment methods.

Further research should encompass greater diversity, including different locations, various grapevine varieties, vine ages, and different mixtures of virus infections. Investigating the important spectral signals for each situation is necessary. While the preliminary research blocks chosen for the studies were well-managed and uniformly controlled to minimise the impact of other factors on the symptomology of viral diseases, future studies can focus on more complex scenarios. As an example, simultaneously detecting virus infections alongside other stress factors—be they biotic or abiotic, such as leaf nutrient levels, fungal presence, and leaf moisture—can further enhance the robustness of the sensing methods.

The sensing technology used for disease detection should not be limited to RGB and VNIR hyperspectral sensors. Other types of sensors, such as SWIR (shortwave infrared) and far-infrared thermal sensors, should be considered. For instance, SWIR sensors have shown high accuracy in detecting GLD in white cultivars using active proximal sensing methods (Bendel et al. 2020). Since important spectral bands like

the red-edge region have been found crucial for disease detection in my study, using a multi-spectral camera that includes these spectral regions can be beneficial in terms of cost reduction and simplifying data processing for effective viral disease detection. Thermal cameras and chlorophyll fluorescence cameras have also demonstrated capabilities in early disease detection and water stress detection (Chaerle et al. 2004; Gautam et al. 2020; Ishimwe et al. 2014). It would be worthwhile to test these technologies in grapevine viral disease detection under remote sensing in field conditions.

Regarding remote sensing data processing, it is suggested to explore alternative image processing methods to improve efficiency. One specific issue is the misclassification between weeds and grapevines during the initial stages of image processing. While under-vine weeds were effectively managed in the vineyards during the current study, the promotion of under-vine cover crops in recent years (Marks et al. 2022) can pose challenges to the classification process. Some cover crops may exhibit similar spectral reflectance to grapevine leaves. In such cases, utilising the height of the canopy obtained from the digital elevation model (DEM) and digital surface model (DSM) can serve as a mask to eliminate non-canopy areas (Gautam et al. 2021). This approach can help improve the accuracy of classification. In addition to

data processing, various statistical and machine learning algorithms mentioned in Chapter 2 of the review paper can be employed for disease classification and modelling. Future studies can leverage these algorithms to enhance the classification model, thereby improving disease detection and identification.

Educating growers about grapevine viral diseases is essential to raise awareness of their significance. It is crucial to remind growers that diseases can spread from asymptomatic vines to other sensitive cultivars. Therefore, minor virus infections in vineyards should not be disregarded.

Conducting comprehensive virus disease inspections in all cultivars across major wine regions in Australia is highly recommended to gain a comprehensive understanding of the virus infection status. To achieve this goal, implementing larger-scale disease detection platforms is advisable. For example, utilising long-duration and long-distance solar-powered fixed-wing UAVs (such as the SolarXOne UAV from XSUN) or manned surveillance airplanes (Galvan et al. 2023) can significantly enhance coverage capabilities. Machine learning algorithms can be applied to analyse similar spectral signals from hyperspectral images obtained from high-resolution, low-altitude remote sensing platforms and lower-resolution satellite imagery. By leveraging these algorithms, it is possible to facilitate broader area disease detection throughout a wine region using satellite images. Ultimately, the integration of surveillance data with precise laboratory test results will facilitate the swift and thorough delivery of information to growers, assisting them in effectively eliminating viruses from their vineyards.

Reference

Adão, T, Hruška, J, Pádua, L, Bessa, J, Peres, E, Morais, R & Sousa, J 2017, 'Hyperspectral Imaging: A review on UAV-based sensors, data processing and applications for agriculture and forestry', *Remote Sensing*, vol. 9, no. 11.

Alabi, OJ, Casassa, LF, Gutha, LR, Larsen, RC, Henick-Kling, T, Harbertson, JF & Naidu, RA 2016, 'Impacts of Grapevine leafroll disease on fruit yield and grape and wine chemistry in a wine grape (*Vitis vinifera L.*) cultivar', *PLoS One*, vol. 11, no. 2, p. e0149666.

Almeida, R, Daane, K, Bell, V, Blaisdell, GK, Cooper, M, Herrbach, E & Pietersen, G 2013, 'Ecology and management of grapevine leafroll disease', *Frontiers in Microbiology*, vol. 4, 2013-April-24, pp. 1-13.

Atallah, S, Gomez, M, Fuchs, M & Martinson, T 2012, 'Economic impact of grapevine leafroll disease on *Vitis vinifera cv.* Cabernet franc in Finger Lakes vineyards of New York', *American Journal of Enology and Viticulture*, vol. 63, 03/01, pp. 73-79.

Bell, VA, Blouin, AG, Cohen, D, Hedderley, DI, Oosthuizen, T, Spreeth, N, Lester, PJ & Pietersen, G 2017, 'Visual symptom identification of grapevine leafroll-associated virus 3 in red berry cultivars supports virus management by roguing', *Journal of Plant Pathology*, vol. 99, no. 2, pp. 477-482.

Bendel, N, Kicherer, A, Backhaus, A, Köckerling, J, Maixner, M, Bleser, E, Klück, H-C, Seiffert, U, Voegele, RT & Töpfer, R 2020, 'Detection of Grapevine leafroll-associated virus 1 and 3 in white and red grapevine cultivars using hyperspectral imaging', *Remote Sensing*, vol. 12, no. 10.

Blaisdell, GK, Zhang, S, Rowhani, A, Klaassen, V, Cooper, ML, Daane, KM & Almeida, RPP 2020, 'Trends in vector-borne transmission efficiency from coinfected hosts: Grapevine leafroll-associated virus-3 and Grapevine virus A', *European Journal of Plant Pathology*, vol. 156, no. 4, 2020/04/01, pp. 1163-1167.

Blouin, AG, Chooi, KM, Cohen, D & MacDiarmid, RM 2017, 'Serological methods for the detection of major grapevine viruses', in B Meng, GP Martelli, DA Golino & M Fuchs (eds), *Grapevine Viruses: Molecular Biology, Diagnostics and Management*, Springer International Publishing, Cham, pp. 409-429.

Chaerle, L, Hagenbeek, D, De Bruyne, E, Valcke, R & Van Der Straeten, D 2004, 'Thermal and chlorophyll-fluorescence imaging distinguish plant-pathogen interactions at an early stage', *Plant and Cell Physiology*, vol. 45, no. 7, pp. 887-896.

Chooi, KM, Bell, VA, Blouin, AG, Cohen, D, Mundy, D, Henshall, W & MacDiarmid, RM 2022, 'Grapevine leafroll-associated virus 3 genotype influences foliar symptom development in New Zealand vineyards', *Viruses*, vol. 14, no. 7.

Constable, FE & Rodoni, BC 2014, *Grapevine leafroll-associated viruses*, Wine Australia, Adelaide, Australia.

Credi, R 1997, 'Characterization of Grapevine Rugose Wood Disease sources from Italy', *Plant Disease*, vol. 81, no. 11, Nov, pp. 1288-1292.

Digiaro, M, Bedzrob, MP, D'Onghia, AM, Boscia, D & Savino, VN 1994, 'On the correlation between grapevine virus A and rugose wood', *Phytopathologia Mediterranea*, vol. 33, pp. 187-193.

Douglas, N & Krüger, K 2008, 'Transmission efficiency of Grapevine leafroll-associated virus 3 (GLRaV-3) by the mealybugs *Planococcus ficus* and *Pseudococcus longispinus* (Hemiptera: *Pseudococcidae*)', *European Journal of Plant Pathology*, vol. 122, no. 2, 2008/10/01, pp. 207-212.

Fortusini, A, Scattini, G, Prati, S, Cinquanta, S & Belli, G 1997, 'Transmission of grapevine leafroll virus 1 (GLRaV-1) and grapevine virus A (GVA) by scale insects', paper presented at Proceedings of 12th Meeting of ICVG, Lisbon.

Galvan, FER, Pavlick, R, Trolley, G, Aggarwal, S, Sousa, D, Starr, C, Forrestel, E, Bolton, S, Alsina, MdM, Dokoozlian, N & Gold, KM 2023, 'Scalable Early Detection of Grapevine Viral Infection with Airborne Imaging Spectroscopy', *Phytopathology®*, pp. PHYTO-01-23-0030-R.

Gautam, D, Ostendorf, B & Pagay, V 2021, 'Estimation of Grapevine Crop Coefficient Using a Multispectral Camera on an Unmanned Aerial Vehicle', *Remote Sensing*, vol. 13, no. 13, p. 2639.

Gautam, D & Pagay, V 2020, 'A review of current and potential applications of remote sensing to study the water status of horticultural crops', *Agronomy*, vol. 10, no. 1.

Goszczynski, DE 2007, 'Single-strand conformation polymorphism (SSCP), cloning and sequencing reveal a close association between related molecular variants of Grapevine virus A (GVA) and Shiraz disease in South Africa', *Plant Pathology*, vol. 56, no. 5, pp. 755-762.

Goszczynski, DE, du Preez, J & Burger, JT 2008, 'Molecular divergence of Grapevine virus A (GVA) variants associated with Shiraz disease in South Africa', *Virus Research*, vol. 138, no. 1-2, Dec, pp. 105-110.

Goszczynski, DE & Habili, N 2012, 'Grapevine virus A variants of group II associated with Shiraz disease in South Africa are present in plants affected by Australian Shiraz disease, and have also been detected in the USA', *Plant Pathology*, vol. 61, no. 1, pp. 205-214.

Goszczynski, DE & Jooste, AEC 2003, 'Identification of divergent variants of Grapevine virus A', *European Journal of Plant Pathology*, vol. 109, no. 4, pp. 397-403.

Gutha, LR, Casassa, LF, Harbertson, JF & Naidu, RA 2010, 'Modulation of flavonoid biosynthetic pathway genes and anthocyanins due to virus infection in grapevine (*Vitis vinifera L.*) leaves', *BMC Plant Biology*, vol. 10, no. 1, p. 187.

Habili, N 2013, 'Australian Shiraz Disease: an emerging virus disease of *Vitis vinifera* cv. Shiraz', *Wine and Viticulture Journal*, vol. 28, no. 1, pp. 59-61.

Habili, N, Komínek, P & Little, A 2007, 'Grapevine leafroll-associated virus 1 as a common grapevine pathogen', *Plant Viruses*, vol. 1, no. 1.

Habili, N, Wu, Q & Pagay, V 2016, 'Virus-associated Shiraz Disease may lead Shiraz to become an endangered variety in Australia', *Wine and Viticulture Journal*, vol. V31N1, no. 1, 02/02, pp. 47-50.

Hommay, G 2008, 'Grapevine virus A transmission by larvae of *Parthenolecanium corni*', *European Journal of Plant Pathology*, vol. 121, no. 2, 2008-06, pp. pp. 185-188-2008 v.2121 no.2002.

Hull, R 2014, 'Ecology, epidemiology, and control of plant viruses', in *Plant Virology*, pp. 809-876.

Ishimwe, R, Abutaleb, K & Ahmed, F 2014, 'Applications of thermal imaging in agriculture—A review', *Advances in Remote Sensing*, vol. 03, no. 03, pp. 128-140.

Jones, RA 2014, 'Trends in plant virus epidemiology: opportunities from new or improved technologies', *Virus Res*, vol. 186, Jun 24, pp. 3-19.

MacDonald, SL, Staid, M, Staid, M & Cooper, ML 2016, 'Remote hyperspectral imaging of grapevine leafroll-associated virus 3 in Cabernet Sauvignon vineyards', *Computers and Electronics in Agriculture*, vol. 130, pp. 109-117.

Maree, HJ, Almeida, RP, Bester, R, Chooi, KM, Cohen, D, Dolja, VV, Fuchs, MF, Golino, DA, Jooste, AE, Martelli, GP, Naidu, RA, Rowhani, A, Saldarelli, P & Burger, JT 2013, 'Grapevine leafroll-associated virus 3', *Front Microbiol*, vol. 4, p. 82.

Marks, JNJ, Lines, TEP, Penfold, C & Cavagnaro, TR 2022, 'Cover crops and carbon stocks: How under-vine management influences SOC inputs and turnover in two vineyards', *Science of The Total Environment*, vol. 831, 2022/07/20/, p. 154800.

Meng, B, Martelli, GP, Golino, DA & Fuchs, M 2017, *Grapevine Viruses: Molecular Biology, Diagnostics and Management*, 1st ed. edn, Springer International Publishing : Imprint: Springer.

Naidu, R, Rowhani, A, Fuchs, M, Golino, D & Martelli, GP 2014, 'Grapevine leafroll: A complex viral disease affecting a high-value fruit crop', *Plant Disease*, vol. 98, no. 9, 2014/09/01, pp. 1172-1185.

Naidu, RA, Perry, EM, Pierce, FJ & Mekuria, T 2009, 'The potential of spectral reflectance technique for the detection of Grapevine leafroll-associated virus-3 in two red-berried wine grape cultivars', *Computers and Electronics in Agriculture*, vol. 66, no. 1, pp. 38-45.

Nutter, FW 1997, 'Quantifying the temporal dynamics of plant virus epidemics: a review', *Crop Protection*, vol. 16, no. 7, 1997/11/01/, pp. 603-618.

Olmos, A, Capote, N, Bertolini, E & Cambra, M 2007, 'Molecular diagnostic methods for plant viruses', in ZK Punja, Boer, S. H. de, Sanfaçon, H. (ed.), *Biotechnology and plant disease management*, CAB International, pp. 227-249.

Perrone, I, Chitarra, W, Boccacci, P & Gambino, G 2017, 'Grapevine–virus–environment interactions: an intriguing puzzle to solve', *New Phytologist*, vol. 213, no. 3, pp. 983--987.

Pietersen, G, Spreeth, N, Oosthuizen, T, van Rensburg, A, van Rensburg, M, Lottering, D, Rossouw, N & Tooth, D 2013, 'Control of grapevine leafroll disease spread at a commercial wine estate in South Africa: A case study', *American Journal of Enology and Viticulture*, vol. 64, no. 2, p. 296.

Ricketts, KD, Gomez, MI, Atallah, SS, Fuchs, MF, Martinson, TE, Battany, MC, Bettiga, LJ, Cooper, ML, Verdegaal, PS & Smith, RJ 2015, 'Reducing the economic impact of Grapevine leafroll disease in California: Identifying optimal disease management strategies', *American Journal of Enology and Viticulture*, vol. 66, no. 2, p. 138.

Rustioni, L, Rocchi, L & Failla, O 2015, 'Effect of anthocyanin absence on white berry grape (*Vitis vinifera L.*)', vol. 54, 01/01, pp. 239-242.

Sankaran, S, Mishra, A, Ehsani, R & Davis, C 2010, 'A review of advanced techniques for detecting plant diseases', *Computers and Electronics in Agriculture*, vol. 72, no. 1, pp. 1-13.

Vanegas, F, Bratanov, D, Powell, K, Weiss, J & Gonzalez, F 2018, 'A novel methodology for improving plant pest surveillance in vineyards and crops using UAV-based hyperspectral and spatial data', *Sensors*, vol. 18, no. 1.

Walker, J, Charles, J, Froud, K & Connolly, P 2004, 'Leafroll Virus in Vineyards: Modelling the Spread and Economic Impact', *HortResearch Client report*, vol. 12795, 01/01.

Wu, Q, Habili, N, Constable, F, Al Rwahnih, MA, Goszczynski, DE, Wang, Y & Pagay, V 2020, 'Virus pathogens in Australian vineyards with an emphasis on Shiraz Disease', *Viruses*, vol. 12, no. 8, Jul 28.

Wu, Q, Habili, N, Kinoti, WM, Tyerman, SD, Rinaldo, A, Zheng, L & Constable, FE 2023, 'A metagenomic investigation of the viruses associated with Shiraz Disease in Australia', *Viruses*, vol. 15, no. 3.